



POLITECNICO DI MILANO

M.Sc. in Civil Engineering for Risk Mitigation

Prediction of Clear-water Local Scour at Bridge Piers

Supervisor

Dr. Alessio Radice

Thesis by

Javad Mahmoudi

796551

July 2015



POLITECNICO DI MILANO

Prediction of Clear-water Local Scour at Bridge Piers

A Master thesis submitted to Department of Civil and Environmental Engineering in partial fulfillment of the requirements for the degree of Master of Science in Civil Engineering for Risk Mitigation.

Submitted by:

Javad Mahmoudi

Student ID: 796551

Supervised by:

Dr. Alessio Radice

Dept. of Civil and Environmental Engineering
Politecnico di Milano
Piazza L. da Vinci, 32, I-20133 Milan

Abstract (English)

In modern societies, the normal life of people is highly dependent on the operation of the infrastructures. Any disruption to the normal performance of these critical infrastructures can have negative impacts on the economy of the society and the welfare of the citizens.

Bridges at river crossings, being one of the most important and vital infrastructures, are prone to a major damage during floods. Damage can be caused by various reasons; one of the main ones is riverbed scour at bridge foundations. The damage can range from minor erosion to complete failure of the bridge structure which can lead to death casualties and isolation of entire areas.

In spite of the extensive research efforts on this topic, a general equation which can be able to predict the temporal evolution of scour depth is still missing due to the fact that the existing formulae are mainly appropriate for the experiments that they are developed for.

In this work, an extensive data set for long-duration, clear-water pier scour experiments has been considered. Data from several authors were used to fit a novel predictive equation for the temporal development of the maximum scour depth at a circular pier.

Since the mentioned data by different authors were included in different frameworks, it was necessary to make them homogeneous and present them with the same parameters. In this respect, the approach flow velocity was one of the most influential parameters for the scour trend; some authors used a cross-sectional average flow velocity, some others used instead a depth-averaged value at mid-channel. Therefore, values were converted whenever necessary. A dimensionless framework was considered to highlight the most relevant parameters; the final predictive equation was the product of functions of the individual parameters. The most important dimensionless parameters were the flow shallowness, the sediment coarseness, the ratio of the flow velocity to the critical one, and the dimensionless time.

The performance of the estimated scour function was finally compared to that of previous literature equations, documenting a general improvement of prediction capabilities.

Author keywords: Bridge piers; Local scour; Temporal evolution; Scour prediction.

Abstract (Italian)

La funzionalità delle infrastrutture è cruciale per la società moderna e ogni fallanza delle stesse provoca conseguenze negative per l'economia e il benessere dei cittadini. I ponti fluviali non fanno eccezione, dal momento che eventuali danneggiamenti o crolli di queste strutture possono provocare ingenti danni, isolamento di territori e perdite di vite umane. La vulnerabilità dei ponti dipende da diversi fenomeni, tra i quali si possono includere i processi erosivi localizzati.

A dispetto della grande mole di ricerche condotte su questi fenomeni, non sono ancora disponibili equazioni per la previsione dell'evoluzione temporale dell'erosione, che possano ritenersi di validità generale. Molto spesso la validità delle formule disponibili è limitata agli esperimenti condotti per ottenerle.

In questo lavoro è stato analizzato un ampio campione di dati di letteratura, per il caso dell'erosione a una pila circolare in condizioni di acque chiare. È stata stimata una nuova equazione con l'obiettivo di rappresentare il complesso dei dati.

I dati proposti dai singoli autori non sono in generale omogenei, perché ottenuti tramite procedure sperimentali diverse e inquadrati in schemi di riferimento diversi. È stato dunque necessario un lavoro di omogeneizzazione dei parametri. Uno di quelli più importanti è la velocità del flusso, che alcuni autori considerano media sulla sezione trasversale e altri sulla profondità. I valori di velocità sono stati convertiti laddove necessario. Un opportuno inquadramento adimensionale è stato usato per individuare i parametri di maggiore importanza: la snellezza della pila in relazione alla profondità della corrente, la dimensione dell'ostacolo rispetto a quella dei sedimenti, l'intensità del flusso rispetto alle condizioni critiche, e il tempo. La formula finale proposta è costituita da una produttoria di funzioni dei singoli parametri.

La capacità della formula di prevedere i valori di erosione è stata confrontata con quella di analoghi strumenti disponibili in letteratura, riscontrando un generale miglioramento.

Parole chiave: Pila di ponte; Erosione localizzata; Evoluzione temporale; Stima dell'erosione.

Abstract (Persian)

در جوامع مدرن زندگی روزمره مردم به میزان زیادی به عملکرد سازه های زیربنایی وابسته است. هرگونه اختلال در عملکرد طبیعی زیرساخت های مهم می تواند تأثیرات منفی بر روی اقتصاد جامعه و رفاه شهروندان داشته باشد.

پلها بعنوان یکی از زیرساختهای مهم و حیاتی، مستعد آسیب های عمده در زمان وقوع سیل می باشند. آسیب می تواند با دلایل مختلف ایجاد می شود که آبستنگی بستر رودخانه در ناحیه پی از عمده ترین آنها به شمار می آید. شدت خسارت وارده میتواند از آبستنگی جزئی و موضعی تا تخریب کامل پل که منجر به تلفات جانی و جداسازی منطقه میشود متغیر باشد.

به رغم تلاش های تحقیقاتی گسترده در این زمینه، تا به حال یک فرمول کلی که قادر به پیش بینی تکامل زمانی عمق آبستنگی باشد ارائه نشده است و فرمول های موجود اکثرا برای آزمایش هایی که برای آن طراحی شده اند مناسب هستند.

در این پایان نامه، داده های فراوانی از مطالعات و آزمایش های گذشته که با مدت زمان طولانی پدیده آبستنگی در حالت آب زلال بر روی پایه های استوانه ای را مورد تحقیق قرار داده اند در نظر گرفته شده است. از داده های محققان برای بدست آوردن فرمول پیش بینی کننده حداکثر عمق آبستنگی در پایه های استوانه ای استفاده شده است.

از آنجا که داده های ذکر شده توسط محققان مختلف در چارچوب های مختلف ارائه شده اند، همگنسازی و همچنین هم پارامتر سازی داده ها ضروری میباشد. از این روی، سرعت جریان یکی از تأثیر گذار ترین پارامترهای برای روند آبستنگی می باشد. برخی از محققان سرعت جریان متوسط مقطعی و برخی دیگر سرعت جریان در عمق متوسط در وسط کانال را مورد استفاده قرار داده اند. بنابراین، در صورت لزوم مقادیر مربوطه تبدیل شده اند. یک چارچوب بدون بعد به منظور بزرگنمایی پارامترهای مربوطه در نظر گرفته شده است. فرمول نهایی توابعی از پارامترهای منحصر به فرد میباشد. مهمترین پارامترهای بدون بعد، عمق جریان، درستی رسوبات، نسبت سرعت جریان به مقدار بحرانی آن و زمان بدون بعد بوده است.

مقایسه عملکرد فرمول آبستنگی برآورد شده در این پایان نامه با فرمول های موجود حاکی بر این است که قابلیت های پیش بینی در فرمول ارائه شده افزایش پیدا کرده است.

واژه های کلیدی: پایه پل؛ آبستنگی موضعی؛ تکامل زمانی؛ پیش بینی آبستنگی.

Acknowledgments

I would like to express my sincere gratitude to my advisor Prof. Alessio Radice, for the continuous support of my Master thesis, for his patience, motivation, and immense knowledge. His guidance helped me in all the time of research and writing of this thesis. I could not have imagined having a better advisor and mentor for my Master thesis.

I owe more than thanks to my parents. Thank you for encouraging me in all of my pursuits and inspiring me to follow my dreams. I always knew that you believed in me and wanted the best for me.

*Javad Mahmoudi
Politecnico di Milano
July 2015*

List of Tables

Table 1.1: Basic bed forms in alluvial channels (classification by increasing flow velocities) ...	25
Table 2.1: Full trend data sources and number for each source.....	37
Table 2.2: Isolated points sources and number for each source.	38
Table 2.3: Sediment properties used in Ettema experiment	41
Table 2.4: Pier size used in Ettema experiment.....	41
Table 2.5: Ettema (1980) critical shear velocity definition	42
Table 2.6: Flow, sediment and structure parameters summery	45
Table 2.7: The local Scour results summery.....	47
Table 2.8: VAW Pier Data- Test Conditions.....	50
Table 2.9: VAW Pier Data- Summary of Test Conditions	50
Table 2.10: Characteristic controlling variable of Lanca et al.'s (2013) experiment	52
Table 2.11: Summary of Girmaldi (2005) and Simarro et al (2011) experiment used for validation.....	54
Table 2.12: Sediments characteristics.....	54
Table 2.13: Approach flow Characteristics	55
Table 2.14: Chabert, J. and Engeldinger, P. (1956) test characteristic Summary	61
Table 2.15: Mignosa, P. (1980) test characteristic Summary	62
Table 2.16: Franzetti et al (1989) and Azzaroli, D. (1983) tests characteristic Summary.....	63
Table 3.1: Remaining tests (series) for different values of $\lambda\lambda inf$	70
Table 3.2: Remaining tests (series and Isolated) for different values of $\lambda\lambda inf$	71
Table 3.3: Calibrated parameters at $T = 10^5$ and $T=10^6$	79
Table 3.4: Coefficient of variation.....	81
Table 3.5: Comparison of the obtained and the original values of M, P and R.....	85

List of Figures

Figure 1.1: Force acting on a sediment particle (inter-granular forces not shown).....	17
Figure 1.2: Diagram of forces acting on a sediment particle in open channel flow (Yang, 1973)18	
Figure 1.3: Experimental data by shield (1936).....	20
Figure 1.4: Shield diagram for incipient motion (Vanoni, 1975)	21
Figure 1.5: Bed-load motion: (a) Sketch of saltation motion (b) definition sketch of bed-load layer.....	22
Figure 1.6: Suspended-sediment motion by convection and diffusion processes.	23
Figure 1.7: Bed form is movable boundary hydraulics: (a) typical bed forms and (b) bed form motion.	24
Figure 1.8: Total scour and its components	27
Figure 1.9: Schematic representation of scour at a cylindrical pier.....	27
Figure 1.10: Diagrammatic Flow Pattern at Cylindrical Pier	28
Figure 1.11: (a) Time development of clear-water and live-bed scour (b) scour depth as a function of shear velocity (after Chabert & Engeldinger 1956)	29
Figure 2.1: Cross-section of the working section of 1.52 m wide, flow recirculating, flume by Ettema (1980).....	39
Figure 2.2: Cross-section of the working section of the 0.46 m wide flume by Ettema (1980)...	40
Figure 2.3: Schematic drawing of flume used for Sheppard et al.'s (2002) research.....	44
Figure 2.4: Isometric drawing of the flume	44
Figure 2.5: Definition sketch and measurement points for: (a) pier and (b) abutment. Points defining (●) scour or aggradation depths; (+) scour or aggradation area	49
Figure 2.6: Evolution of dimensionless scour depth at pier nose under steady flow (Chang et al. (2005)).....	56
Figure 2.7: Test flume, plan and profile	57
Figure 2.8: Scour data for cylindrical pier	58
Figure 2.9: Uniform sediments size and gradations.....	59
Figure 2.10: Test flume from Chabert and Engeldinger (1956)	60
Figure 2.11: Scour depth with respect to time trend taken from Franzetti et al.'s (1981) experiment.....	63
Figure 2.12: Scour depth with respect to time graph taken from Azzaroli, D.'s (1983) experiment	63
Figure 3.1: Local scour depth variations with respect to flow shallowness	67
Figure 3.2: Position of all the experiments (series) on the Moody diagram.....	69
Figure 3.3: Chosen experiments (series) on the Moody diagram	70
Figure 3.4: Position of all the experiments (series & Isolated) on the Moody diagram	71
Figure 3.5: Chosen experiments (series & Isolated) on the Moody diagram	72
Figure 3.6: Temporal trend of scour depth (Dimensional)	73
Figure 3.7: Temporal trend of scour depth (Dimensionless)	74
Figure 3.8: Calibration of $f_2(D_{50})$ for 10^5 and 10^6 (Series).....	76

Figure 3.9: Calibration of $f_2(D_{50})$ for 10^5 (Series and Isolated)	76
Figure 3.10: Calibration of $f_2(D_{50})$ for 10^6 (Series and Isolated)	77
Figure 3.11: Calibration of $f_3(U)$ for 10^5 and 10^6 (Series).....	77
Figure 3.12: Calibration of $f_3(U)$ for 10^5 (Series and Isolated).....	78
Figure 3.13: Calibration of $f_3(U)$ for 10^6 (Series and Isolated).....	78
Figure 3.14: Dimensionless trend of scour trend considering f_2 and f_3 (Series)	80
Figure 3.15: Comparison of sample statistics	81
Figure 3.16: Comparison of coefficient of variation	82
Figure 3.17: pdf of dimensional scour trend.....	82
Figure 3.18: pdf of dimensionless scour trend.....	83
Figure 3.19: pdf of dimensionless scour trend according to f_2 and f_3	83
Figure 3.20: Global temporal regression	84
Figure 3.21: global temporal function (Series).....	85
Figure 3.22: comparison of measured and computed D_s (series).....	86
Figure 3.23: PDF of measured and computed D_s (series)	87
Figure 3.24: CDF of measured and computed D_s (series)	87
Figure 3.25: global temporal function (Series & Isolated points)	88
Figure 3.26: comparison of measured and computed D_s (Isolated points)	89
Figure 3.27: PDF of measured and computed D_s (Isolated points).....	89
Figure 3.28: CDF of measured and computed D_s (Isolated points)	90
Figure 3.29: Melville & Chiew formula	92
Figure 3.30: Measured vs. Computed value of D_s using Melville & Chiew formula at $T=105$..	93
Figure 3.31: PDF of Melville & Chiew formula at $T=105$	94
Figure 3.32: CDF of Melville & Chiew formula at $T=105$	94
Figure 3.33: Measured vs. Computed value of D_s using Melville & Chiew formula at $T=106$..	95
Figure 3.34: PDF of Melville & Chiew formula at $T=106$	95
Figure 3.35: CDF of Melville & Chiew formula at $T=106$	95
Figure 3.36: Measured vs. Computed value of D_s using Melville & Chiew formula at $ds/dse= -4$	96
Figure 3.37: PDF of Melville & Chiew formula at $ds/dse= -4$	97
Figure 3.38: CDF of Melville & Chiew formula at $ds/dse= -4$	97
Figure 3.39: Measured vs. Computed value of D_s using Melville & Chiew formula at $ds/dse= -1$	98
Figure 3.40: PDF of Melville & Chiew formula at $ds/dse= -1$	98
Figure 3.41: CDF of Melville & Chiew formula at $ds/dse= -1$	98
Figure 3.42: Oliveto and Hager formula.....	100
Figure 3.43: Measured vs. Computed value of D_s using Oliveto & Hager formula at $T=105$..	101
Figure 3.44: PDF of Oliveto & Hager formula at $T=105$	101
Figure 3.45: CDF of Oliveto & Hager formula at $T=105$	102
Figure 3.46: Measured vs. Computed value of D_s using Oliveto & Hager formula at $T=106$..	102

Figure 3.47: PDF of Oliveto & Hager formula at $T=106$	103
Figure 3.48: CDF of Oliveto & Hager formula at $T=106$	103

List of Symbols

ρ : Density of water;

μ : Dynamic viscosity of water;

ν : Kinematic viscosity of water;

γ : Specific weight of water;

g : Acceleration of gravity;

l_c : Width of the channel;

h : Mean approach flow depth;

b : Width of the pier (Diameter of cylindrical pier);

d_s : Local scour depth at time t ;

d_{se} : Local scour depth at equilibrium;

d_{50} : Median grain size;

σ : Standard deviation of sediment particle size distribution;

ρ_s : Sediment density;

t : Time;

u : Mean approach flow velocity;

u_c : Mean approach flow velocity at threshold condition for sediment movement;

u^* : Shear velocity;

u_c^* : Critical shear velocity for sediment movement;

Re : Reynolds number;

Re_p : Particle Reynolds number;

Fr : Froude number;

D_{50} : Sediment coarseness (b/d_{50});

H : Flow shallowness (h/b);

Δ : Relative submerged weight of sediments;

T : Dimensionless time ($t.u/b$);

U : Flow intensity (u/u_c); and

D_s : Dimensionless scour depth (d_s/b).

Contents

Abstract (English)	3
Abstract (Italian)	4
Abstract (Persian).....	5
Acknowledgments.....	6
List of Tables.....	7
List of Figures	8
List of Symbols	11
Introduction	16
1. GENERAL DESCRIPTION & OBJECTIVES.....	17
1.1. Sediment transport in open channels.....	17
1.1.1. Introduction.....	17
1.1.2. Incipient motion of sediments.....	17
1.1.2.1. Forcing action on sediment particle.....	17
1.1.2.2. Threshold of sediment movement	18
1.1.2.3. Dimensional analysis.....	19
1.1.2.4. Shields diagram	19
1.1.3. Sediment transport mechanism.....	22
1.1.3.1. Bed-load transport	22
1.1.3.2. Bed-load transport rate	22
1.1.3.3. Suspended-load transport	23
1.1.4. Bed formation	24
1.2. Scour.....	25
1.2.1. An introduction to scour	25
1.2.2. Contribution to total scour	26
1.2.2.1. Aggradation and Degradation.....	26
1.2.2.2. General Scour (contraction scour & other general scour).....	26
1.2.2.3. Local scour	26
1.2.2.4. Lateral stream migration.....	26
1.3. Local scour	27

1.3.1.	Local scour mechanism.....	27
1.3.2.	Clear-water and Live-bed scour.....	28
1.3.3.	The parameters of local scour at piers:	30
1.3.4.	Dimensionless analysis of local Scour depth.....	31
1.3.5.	Some existing formula for evaluation of local scour	33
1.4.	Objectives.....	36
2.	AVAILABLE DATA AND LITERATURE REVIEW	37
2.1.	Introduction	37
2.2.	Data Characteristics.....	38
2.2.1.	Full trend scour depth data.....	38
2.2.1.1.	Ettema (1980)	38
2.2.1.2.	Sheppard, et al. (2002).....	43
2.2.1.3.	Oliveto and Hager (2002).....	48
2.2.1.4.	Lanca, et al. (2013).....	51
2.2.1.5.	Change et al. (2004).....	54
2.2.1.6.	Yanmaz and Altinbilek (1991)	56
2.2.1.7.	Raikar and Dey (2005)	58
2.2.1.8.	Chabert and Engeldinger (1956).....	59
2.2.1.9.	Mignosa (1980).....	61
2.2.1.10.	Franzetti et al (1989).....	62
2.2.1.11.	Azzaroli (1983).....	63
2.2.2.	Isolated scour depth points.....	64
3.	DATA ANALYSIS	65
3.1.	Introduction	65
3.2.	Selected threshold conditions.....	65
3.3.	Data selection	67
3.3.1.	Introduction.....	67
3.3.2.	Selection Criteria	67
3.3.3.	Flow regime verification.....	68
3.4.	Scour trend	72
3.4.1.	Dimensional scour trend	72

3.4.2.	Dimensionless scour trend	73
3.5.	Strategy for data analysis	74
3.5.1.	Calibration of $f_2(D_{50})$, $f_3(U)$	75
3.6.	Effectiveness of $f_2(D_{50})$ and $f_3(U)$	79
3.7.	Comparison of the point scatter	80
3.8.	Estimation of temporal scour function	84
3.8.1.	Series.....	84
3.8.1.1.	Dispersion of points.....	86
3.8.2.	Series and Isolated points.....	87
3.9.	Model comparison with previous studies.....	90
3.9.1.	Melville & Chiew (1999).....	90
3.9.1.1.	Comparison at the dimensionless times 105 and 106	92
3.9.1.2.	Comparison at the dimensionless scour depth -4 and -1	95
3.9.2.	Oliveto and Hager (2002)	99
3.9.2.1.	Comparison at the dimensionless times 105 and 106	100
	Conclusion.....	104
	Recommendations for further research	105
	References	106

Introduction

Scour is a natural phenomenon caused by the erosive action of the flowing water on the bed and banks of river and channels. It is the removal of sediments around or near structures located in flowing water. Erosion induces lowering of the riverbed level, a tendency to expose the foundations of a bridge. Such scour around pier and pile-supported structures and abutments can result in structural collapse and loss of life and property. The construction of bridges in river and channels can cause contraction in the waterway at the bridge cross section and, as a consequence, gives rise to significant scour at that location. As the scour continuously progresses at the site, it undermines the foundations of the structure leading to possible failure.

The problem of local scour around bridge piers has been studied extensively by several investigators. However, no single analytically derived equation is available because of the difficulties of the problem, such as combined effects of complex turbulent boundary layer, time-dependent flow pattern and sediment transport mechanism in the scour hole. Besides, since many parameters affect the scour development, experimental studies have been conducted by considering only certain aspects of the problem and accepting the other parameters as constants.

In this study, through a dimensionless approach by collecting the relevant experiments data from the different authors the effort is made to refine the formula presented by prof. Silvio Franzetti by applying the calibration of effective parameters.

In chapter 1, some general explanation about fundamental subjects relevant to local scour phenomena can be found. This chapter includes some essential information about sediments transport mechanisms, threshold of incipient grain motion, different types of scour, local scour mechanism due to acceleration of flow and resulting vortices. The chapter finally states the general objectives of the work.

The literature experiments, from different authors, that are used in this thesis are presented in chapter 2. The brief review mostly accounts for experimental procedures used, whose knowledge is important to understand limitations in experiment unification towards a comprehensive analysis.

In chapter 3, first the valid tests are inserted to the moody diagram and the convertible experiments according to the type of the flow condition are selected. Then, the tests for which the velocity was presented in terms of bulk velocity were converted to depth-averaged at mid-channel velocity.

Afterwards, a strategy is developed to calibrate the tests according to f_2 (D50) and f_3 (U). Besides, the efficiency of these two parameters is investigated. Moreover a temporal scour function is estimated taking to the account the mentioned calibration. Finally, the predictive capability of the proposed formula is assessed in comparison with that of some of the existing ones in the literature.

Chapter 1

GENERAL DESCRIPTION & OBJECTIVES

1.1. Sediment transport in open channels

1.1.1. Introduction

Waters flowing in natural streams and rivers have the ability to scour channel beds, to carry particles (heavier than water) and to deposit materials, hence changing the bed topography. This phenomenon is of great economic importance specially to predict the risks of scouring of bridges.

The transported material is called the sediment load. Distinction is made between the bed load and the suspended load. The bed load characterizes grains rolling, sliding or saltation along the bed while suspended load refers to grains maintained in suspension by turbulence.

1.1.2. Incipient motion of sediments

1.1.2.1. Forcing action on sediment particle

For an open channel flow with a movable bed, the forces acting on each sediment particle are (Figure 1.1):

- the gravity force $\rho_s g v_s$
- the buoyancy force $F_b = \rho g v_s$
- the drag force $C_D A_s V^2 / 2$
- the lift force $C_L \rho A_s V^2 / 2$
- the reaction forces of the surrounding grain,

Where v_s is the volume of the particle, A_s is a characteristic particle cross-sectional area, C_D and C_L are the drag and lift coefficients, respectively, and V is a characteristic velocity next to the channel bed. The gravity force and the buoyancy force act both in the vertical direction while the drag force acts in the flow direction and the lift force in the direction perpendicular to the flow direction.

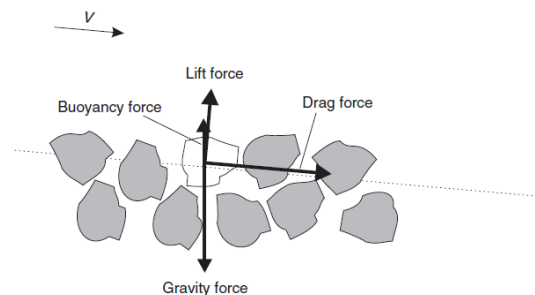


Figure 1.1: Force acting on a sediment particle (inter-granular forces not shown)

1.1.2.2. Threshold of sediment movement

Incipient motion is important in the study of sediment transport, channel degradation, and stable channel design. Due to the stochastic nature of sediment movement along an alluvial bed, it is difficult to define precisely at what flow condition a sediment particle will begin to move. Consequently, it depends more or less on an investigator's definition of incipient motion. They use terms such as "initial motion," "several grain moving," "weak movement," and "critical movement!" In spite of these differences in definition, significant progress has been made on the study of incipient motion, both theoretically and experimentally. Figure 1.2 shows the forces acting on a spherical sediment particle at the bottom of an open channel. For most natural rivers, the channel slopes are small enough that the component of gravitational force in the direction of flow can be neglected compared with other forces acting on a spherical sediment particle. The forces to be considered are the drag force F_D , lift force F_L , submerged weight W_s , and resistance force F_R . A sediment particle is at a state of incipient motion when one of the following conditions is satisfied:

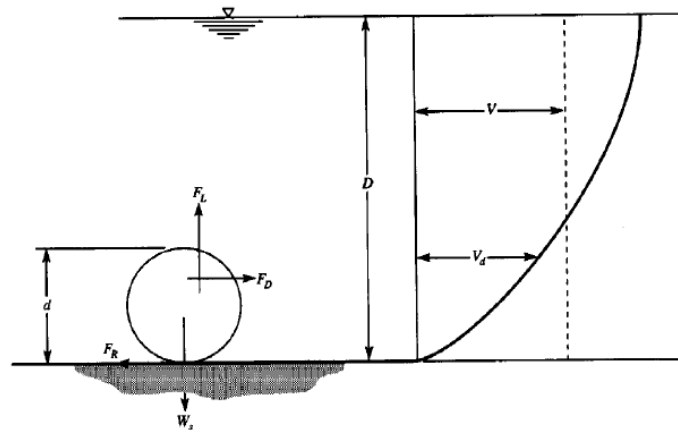


Figure 1.2: Diagram of forces acting on a sediment particle in open channel flow (Yang, 1973)

$$F_L = W_s \quad (1.1)$$

$$F_D = F_R \quad (1.2)$$

$$M_O = M_R \quad (1.3)$$

Where M_O = overturning moment due to F_D and F_L

M_R = resisting moment due to F_L and W_s

1.1.2.3. Dimensional analysis

The relevant parameters for the analysis of sediment transport threshold are the bed shear stress τ_0 , the sediment density ρ_s , the fluid density ρ , the grain diameter d_s , the gravity acceleration g and the fluid viscosity μ ,

$$f_1(\tau_0, \rho, \rho_s, \mu, g, d_s) = 0 \quad (1.4)$$

In dimensionless terms, it yields,

$$f_2\left(\frac{\tau_0}{\rho g d_s}, \frac{\rho_s}{\rho}, \frac{d_s \sqrt{\rho \tau_0}}{\mu}\right) = 0 \quad (1.5)$$

The ratio of the bed shear stress to fluid density is homogeneous (in units) with a velocity squared. Introducing the shear velocity u^* defined as:

$$u^* = \sqrt{\frac{\tau_0}{\rho}} \quad (1.6)$$

In this way we can have an equation in the form of:

$$f_3\left(\frac{u^*}{\sqrt{g d_s}}; \frac{\rho_s}{\rho}; \rho \frac{d_s u^*}{\mu}\right) = 0 \quad (1.7)$$

The first term is a form of Froude number. The second is the relative density (also called specific gravity). The last term is a Reynolds number defined in terms of the grain size and shear velocity. It is often denoted as Re^* and called the shear Reynolds number or particle Reynolds number.

1.1.2.4. Shields diagram

Most incipient motion criteria are derived from either a shear stress or a velocity approach. One of the most prominent and widely used incipient motion criteria is the Shields diagram (1936) based on shear stress. Shields framework is consistent with dimensional analysis in section 1.1.2.3. The mentioned quantities can be grouped into two dimensionless quantities, namely,

$$Re^* = d_s \frac{(\frac{\tau_0}{\rho_f})^{1/2}}{\nu} = \frac{d_s u_*}{\nu} \quad (1.8)$$

and,

$$\tau^* = \frac{\tau_0}{d_s(\rho_s - \rho_f)g} = \frac{\tau_0}{d_s[\left(\frac{\rho_s}{\rho_f}\right) - 1]} = \frac{u_*^2}{g d_s (s - 1)} \quad (1.9)$$

Where:

ρ_s and ρ_f = densities of sediment and fluid, respectively

γ = specific weight of water,

ν =fluid kinematic viscosity,

g =gravity,

u_* =shear velocity, and

τ^* = stability parameter or shields parameter

Re^* = Shear Reynolds number

Critical value of the stability parameter may be defined at the inception of bed motion: i.e.

$$\tau^* = (\tau^*)_c \quad (1.10)$$

Bed load motion occurs for:

$$\tau^* > (\tau^*)_c \quad (1.11)$$

The relationship between these two parameters is then determined experimentally. Figure 1.3 shows the experimental data which was obtained by Shields during the experiment and Figure 1.4 shows the experimental results obtained by Shields and other investigators at incipient motion. Any point in region above the curve indicates the situation of particle movement. In region below the curve, the flow is unable to move the particles.

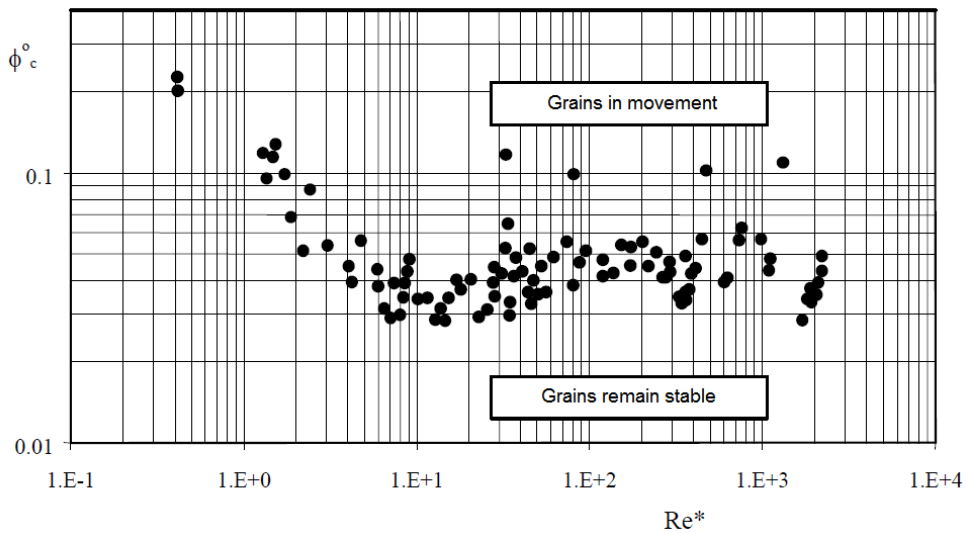


Figure 1.3: Experimental data by shield (1936)

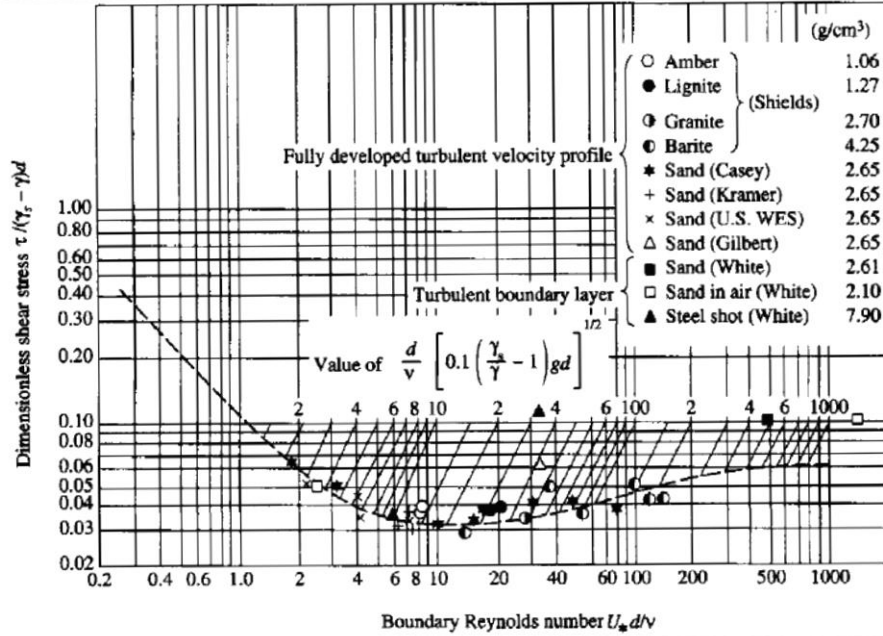


Figure 1.4: Shield diagram for incipient motion (Vanoni, 1975)

Thus the critical shields parameter is:

$$\tau_c^* = \frac{\tau_c}{\rho \Delta g \cdot d_{50}} \quad (1.12)$$

And the critical grain Reynolds number is:

$$R_{*c} \equiv \sqrt{\frac{\tau_c d_{50}^2}{\rho \nu^2}} \quad (1.13)$$

$$\text{Where: } \Delta = \frac{\rho_s}{\rho} - 1 \quad (1.14)$$

On the Shields diagram (Fig. 1.4), the Shields parameter and the particle Reynolds number are both related to the shear velocity and the particle size. Some researchers proposed a modified diagram: τ_c^* as a function of a dimensionless particle parameter d_* . In this way, the above equation can be manipulated and alternatively written as:

$$\tau_{*c} = f(d_*) \quad (1.15)$$

Where d_* is the dimensionless sediment size defined as:

$$d_* = \sqrt[3]{R_{*c}^2/T_{*c}} = \sqrt[3]{g\Delta d_{50}^3/\nu^2} \quad (1.16)$$

The second equation is usually preferred to original one because the critical shear stress appears only in one dimensionless parameter.

1.1.3. Sediment transport mechanism

There are two types of sediment transport mechanisms. Transported sediment material that is maintained in suspension and sediment material transported by rolling, sliding and saltation motion along the bed.

1.1.3.1. Bed-load transport

When the bed shear stress exceeds a critical value, sediments are transported in the form of bed load and suspended load. For bed-load transport, the basic modes of particle motion are rolling motion, sliding motion and saltation motion. (Figure 1.5)

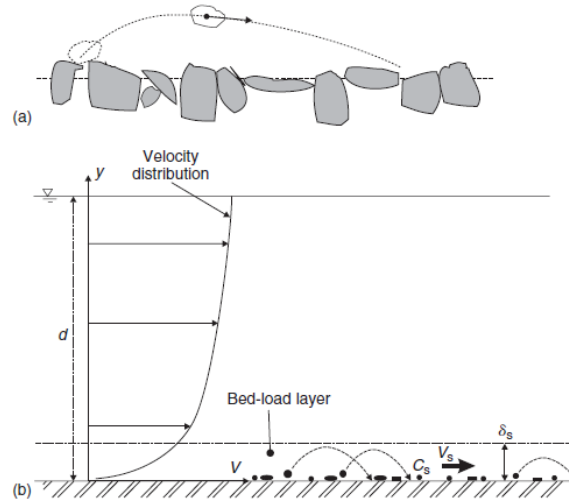


Figure 1.5: Bed-load motion: (a) Sketch of saltation motion (b) definition sketch of bed-load layer

The sediment transport rate may be measured by weight (units: N/s), by mass (units: kg/s) or by volume (units: m^3/s). In practice the sediment transport rate is often expressed by meter width and is measured either by mass or by volume. These are related by:

$$\dot{m}_s = \rho_s q_s \quad (1.17)$$

Where \dot{m}_s is the mass sediment flow rate per unit width, q_s is the volumetric sediment discharge per unit width and ρ_s is the specific mass of sediment.

1.1.3.2. Bed-load transport rate

The bed-load transport rate per unit width may be defined as:

$$q_s = C_s \delta_s V_s \quad (1.18)$$

Where V_s is the average sediment velocity in the bed-load layer (Fig.1.5 (b)). Physically the transport rate is related to the characteristics of the bed-load layer; its mean sediment concentration C_s , its thickness s which is equivalent to the average saltation height measured normal to the bed, and the average speed V_s of sediment moving along the plane bed.

1.1.3.3. Suspended-load transport

The other type of sediment transport mechanism is suspended-load transport. Although this type of sediment transport mechanism is not too relevant with the topic of this study, but it will be briefly discussed in this section for the sake of completeness.

Sediment suspension can be described as the motion of sediment particles during which the particles are surrounded by fluid. The grains are maintained within the mass of fluid by turbulent agitation without (frequent) bed contact. Sediment suspension takes place when the flow turbulence is strong enough to balance the particle weight. The amount of particles transported by suspension is called the suspended load.

The transport of suspended matter occurs by a combination of advective turbulent diffusion and convection. Advective diffusion characterizes the random motion and mixing of particles through the water depth superimposed to the longitudinal flow motion. In a stream with particles heavier than water, the sediment concentration is larger next to the bottom and turbulent diffusion induces an upward migration of the grains to region of lower concentrations. A time-averaged balance between settling and diffusive flux derives from the continuity equation for sediment matter:

$$D_s \frac{dC_s}{dy} = -w_0 C_s \quad (1.19)$$

Where C_s is the local sediment concentration at a distance y measured normal to the channel bed, D_s is the sediment diffusivity and w_0 is the particle settling velocity. Sediment motion by convection occurs when the turbulent mixing length is large compared to the sediment distribution length scale. Convective transport may be described as the entrainment of sediments by very large scale vortices: e.g. at bed drops, in stilling basins and hydraulic jumps (Fig 1.6).

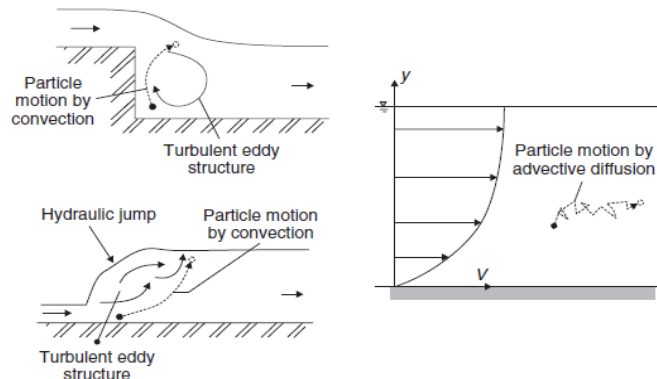


Figure 1.6: Suspended-sediment motion by convection and diffusion processes.

1.1.4. Bed formation

In most practical situations, the sediments behave as a non-cohesive material (e.g. sand and gravel) and the fluid flow can distort the bed into various shapes. The bed form results from the drag force exerted by the bed on the fluid flow as well as the sediment motion induced by the flow onto the sediment grains. This interactive process is complex.

The basic bed forms which may be encountered are the ripples (usually of heights less than 0.1 m), dunes, flat bed, standing waves and antidunes. The typical bed forms are summarized in Fig1.7 and Table 1.1.

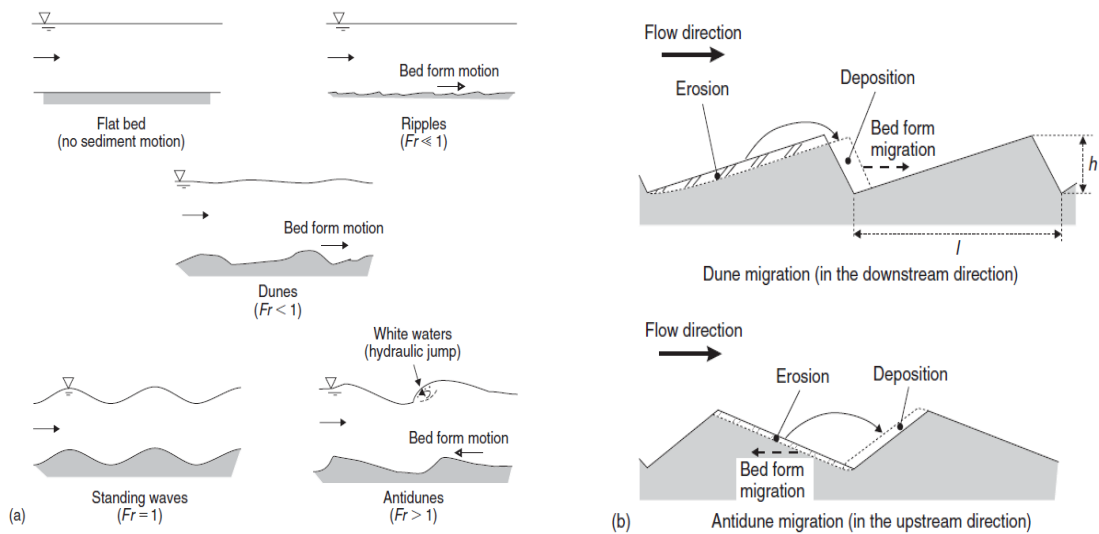


Figure 1.7: Bed form is movable boundary hydraulics: (a) typical bed forms and (b) bed form motion.

Bed form (1)	Flow (2)	Bed form motion (3)	Comments (4)
Flat bed Ripples	No Flow (or $Fr \ll 1$) $Fr \ll 1$	NO D/S	No sediment motion Three-dimensional forms; observed also with air flows (e.g. sand ripples in a beach caused by wind)
Dunes	$Fr < 1$	D/S	Three-dimensional forms; sand dunes can also be caused by wind
Flat bed Standing waves	$Fr \leq 1$ $Fr = 1$	NO NO	Observed also with wind flow Critical flow conditions; bed standing waves in phase with free-surface standing waves
Antidunes	$Fr > 1$	U/S	Supercritical flow with tumbling flow and hydraulic jump upstream of antidune crests
Chute-pools Step-pools	$Fr > 1$ $Fr > 1$	U/S -	Very active antidunes Cascade of steps and pools; steps are often caused by rock bed

References: Henderson (1966) and Graf (1971).

Notes: D/S = in downstream flow direction; Fr = Froude number; U/S = in upstream flow direction.

Table 1.1: Basic bed forms in alluvial channels (classification by increasing flow velocities)

1.2. Scour

1.2.1. An introduction to scour

Scour is the result of the erosive action of flowing water, excavating and carrying away material from the bed and the bank of streams and from around the piers and abutments of bridges. Different materials scour at different rates. Loose soils are tending to scour more rapidly than cohesive or cemented soils which are more scour-resistant. However ultimate scour in both cases can be as deep as each other. Under constant flow condition, scour will increase with respect to time and reach to a nearly constant maximum depth after a period of time. Under flow conditions typical of actual bridge crossings, several floods may be needed to attain maximum scour. Determining the magnitude of scour is complicated by the cyclic nature of some scour processes.

The equations for estimating scour depth time history or equilibrium scour depth are based on laboratory experiments with limited field verification. Uncertainty in predicting scour still remains in all of the equations that were published in literature. But the attempt of decreasing the amount of uncertainty and remaining in the safe side for the estimation of scour depth during all of the researches can be observed.

One of the most important factors for estimation of scour depth is whether it is clear-water or live-bed scour. Clear-water scour occurs where there is no transport of bed material upstream of crossing bridge and live-bed scour occurs where there is transport of bed material from the upstream reach into the crossing. A more detailed discussion is presented in the following sections.

1.2.2. Contribution to total scour

Total scour at a bridge crossing considers three primary components:

- Long-term degradation of the river bed;
- General scour at bridge: a. Contraction scour b. Other general scour,
- Local scour at the piers and abutments.

Total scour and its components are illustrated in figure 1.8.

1.2.2.1. Aggradation and Degradation

Aggradation and degradation are long-term elevation changes due to the natural or man-induced causes which can affect the reach of the river on which the bridge is located. Aggradation involves the deposition of material eroded from the channel or watershed upstream of the bridge; whereas, degradation involves the lowering or scouring of the streambed due to a lack in sediment supply from upstream.

1.2.2.2. General Scour (contraction scour & other general scour)

General scour is a lowering of the streambed across the stream or waterway bed at bridge. This lowering may be uniform across the bed or non-uniform, that is, the depth of scour may be deeper in some part of the cross section. General scour may result from contraction of the flow, which results in removal of material from the bed across all or most of the channel width, or from other general scour conditions such as flow around a bend where the scour may be concentrated near the outside of the bend. General scour is different from long-term degradation in that general scour may be cyclic and/or related to the passing of a flood.

1.2.2.3. Local scour

Local scour, which is the target of this study specifically among other types of scour, involves removal of material from around piers, abutments, spurs, and embankments. It is caused by an acceleration of flow and resulting vortices induced by obstruction to the flow. Local scour can be either clear-water or live-bed scour. Local scour may occur even where general and constriction scour are not present.

1.2.2.4. Lateral stream migration

In addition to the types of scour mentioned above, naturally occurring lateral migration of the main channel of a stream within a floodplain may affect the stability of piers in a floodplain, erode abutments or the approach roadway, or change the total scour by changing the flow angle of attack at piers and abutments. Factors that affect lateral stream movement also affect the stability of a bridge foundation. These factors are the geomorphology of the stream, location of the crossing on the stream, flood characteristics, and the characteristics of the bed and bank materials.

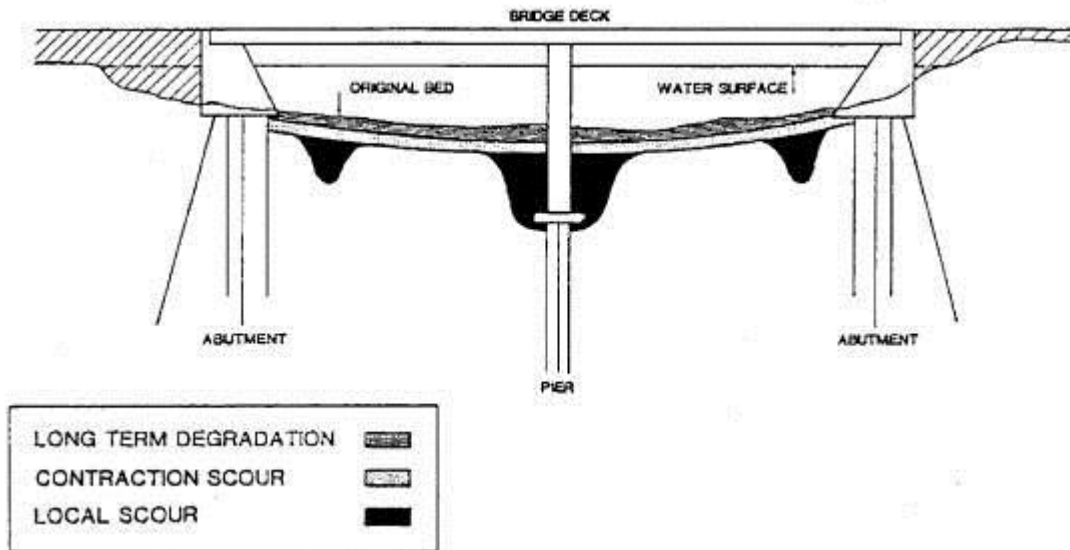


Figure 1.8: Total scour and its components

1.3. Local scour

The following section provides more detailed discussion of the local scour at piers which is the main goal of this research.

1.3.1. Local scour mechanism

The basic mechanism causing local scour at piers or abutments is the formation of vortices (known as the horseshoe vortex) at their base (Figure 1.9). The horseshoe vortex results from the pileup of water on the upstream surface of the obstruction and subsequent acceleration of the flow around the nose of the pier or abutment.

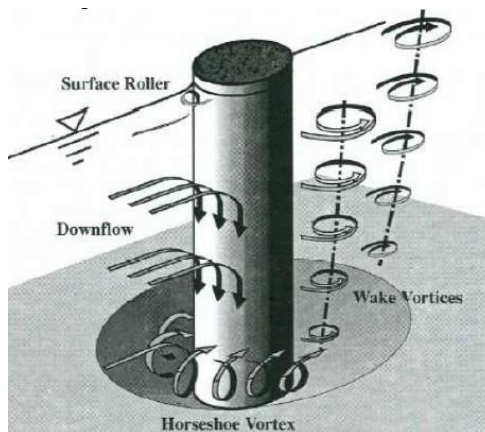


Figure 1.9: Schematic representation of scour at a cylindrical pier

The approach flow velocity goes to zero at the upstream face of the cylinder, in the vertical plane of symmetry, and since the approach flow velocity decreases from the free surface downward to zero at the bed, the stagnation pressure, $\rho u^2/2$, also decreases. This downward pressure gradient drives the downflow (Figure 1.9). The downflow, in the vertical plane of symmetry, has at any elevation a velocity distribution, with zero in contact with the cylinder and again some distance upstream of it. The so-called horseshoe vortex develops as the result of separation of flow at the upstream rim of the scour hole. The horseshoe vortex extends downstream, past of the sides of the pier, for a few pier diameters before losing its identity and becoming part of general turbulence. The horseshoe vortex also pushes the maximum downflow velocity within the scour hole closer to the pier. The action of the vortex removes bed material from around the base of the obstruction. The transport rate of sediment away from the base region is greater than the transport rate into the region, and, consequently, a scour hole develops. As the depth of scour increases, the strength of the horseshoe vortex is reduced, thereby reducing the transport rate from the base region. Eventually, for live-bed local scour, equilibrium is reestablished between bed material inflow and outflow and scouring ceases. For clear-water scour, scouring ceases when the shear stress caused by the horseshoe vortex equals the critical shear stress of the sediment particles at the bottom of the scour hole.

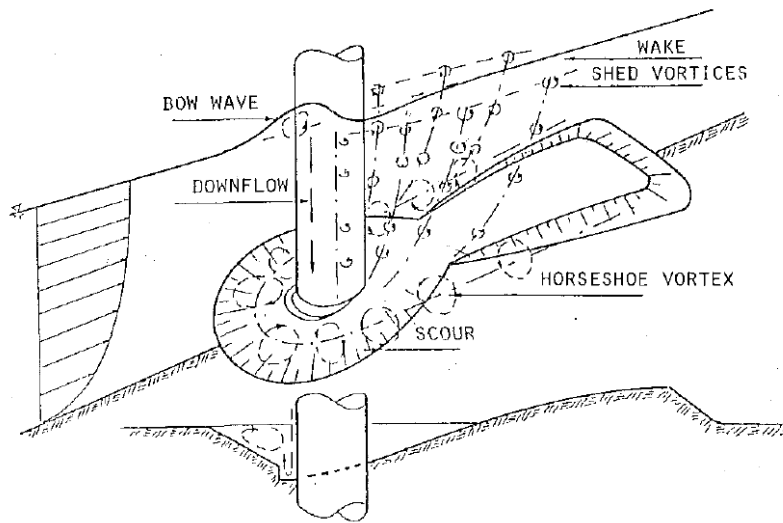


Figure 1.10: Diagrammatic Flow Pattern at Cylindrical Pier

In addition to the horseshoe vortex around the base of a pier, there are vertical vortices downstream of the pier called the wake vortices (Figure 1.10). Both the horseshoe and wake vortices remove material from the pier base region. However, the intensity of wake vortices decrease rapidly as the distance downstream of the pier increases. Therefore, immediately downstream of a long pier there is often deposition of material.

1.3.2. Clear-water and Live-bed scour

Local scour at a pier commences when the shear velocity u^* or velocity u exceeds a fraction of the critical or threshold value for movement of the sediment. There are two conditions for contraction and local scour, clear-water and live-bed scour. Clear-water scour occurs when there is no movement of the bed material in the flow upstream of the crossing or the bed material

being transported in the upstream reach is transported in the suspension through the scour hole at the pier or abutment at less than the capacity of the flow. In clear water condition velocity is below the critical velocity and there is no sediment transport and no sediment supply into the scour hole from upstream. At the pier or abutment the acceleration of the flow vortices created by these obstructions cause the bed material around them to move. Live-bed scour occurs when there is transport of bed material around them to move. Live-bed local scour is cyclic in nature; that is, the scour hole that develops during the rising stage of a flood refills during falling stage.

Typical clear-water scour situation (1) coarse-bed material streams, (2) flat gradient streams during low flow, (3) local deposition of larger bed materials that are larger than the biggest fraction being transported by the flow (rock riprap is a special case of this situation), (4) armored streambeds where the only location that tractive forces are adequate to penetrate the armor layer are at piers and/or abutments, and (5) vegetated channel or overbank areas.

During a flood event, bridge over streams with coarse-bed material are often subjected to clear-water scour at low discharge, live-bed scour at the higher discharges and clear-water scour at low discharges on the falling stages. Clear-water scour reaches its maximum over a longer period of time than live-bed scour (Figure 1.11). In fact, local clear-water scour may not reach a maximum until after several floods and reach to its equilibrium asymptotically over a period of days. Live-bed scour develops rapidly and its depth fluctuates in response to the passage of bed features. (Figure 1.11(a)). This is due to the variability of the bed material sediment transport in the approach flow when the bed configuration of the stream is dunes. Shen et al.(1969) suggested that the mean value of the live-bed scour depth was about 10% less than the maximum clear-water scour depth (Figure 1.11(b)).

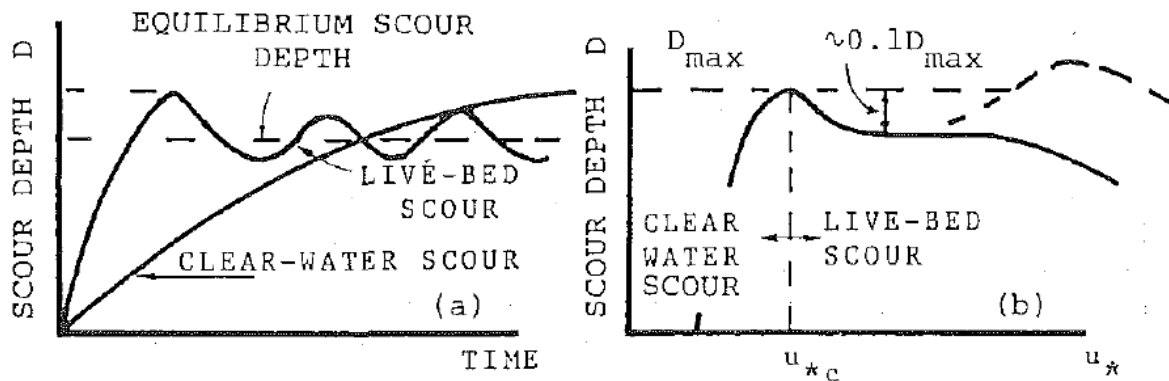


Figure 1.11: (a) Time development of clear-water and live-bed scour (b) scour depth as a function of shear velocity (after Chabert & Engeldinger 1956)

Critical velocity equations with the reference particle size equal to d_{50} can be used to determine the velocity associated with the initiation of motion. They are used as an indicator for clear-water or live-bed scour conditions. If the mean velocity (u) in the upstream reach is equal to or less than the critical velocity (u_c) of the median diameter (d_{50}) of the bed material, then contraction and local scour will be clear-water scour. If the mean velocity is greater than the critical velocity of the median bed material size, live-bed scour will occur.

1.3.3. The parameters of local scour at piers:

Factors which affect the magnitude of local scour depth at piers can be stated as a general function of fluid, flow, pier and sediment properties and time evolution.

- **Fluid:** In mechanics a fluid is defined by its density ρ , kinematic viscosity ν , at temperature T .
- **Flow:** The flow of a fluid is determined by its mean depth h , energy slope s_0 , and the acceleration due to gravity g which generates the flow. The slope s_0 , which produces through the component of gravity the shear stress, τ , to maintain the flow, is more suitably replaced by the shear velocity $u_* = \sqrt{g \cdot h \cdot s_0}$
Flow velocity also affects local scour depth. The greater the velocity, the deeper the scour will be. There is a high probability that scour is affected by whether the flow is subcritical or supercritical. However, most research data are for subcritical flow (i.e., flow with a Froude Number less than 1.0, $Fr < 1$).
- **Pier:** The action of pier is determined by the effective blockage it presents to the flow. A cylindrical pier is defined by its diameter b . Other shaped piers are specified relative to b in terms of shape factors. Consideration also can be made by introducing some factors for the angle of the approach flow to the pier. As pier width increases, there is an increase in scour depth. There is a limit to the increase in scour depth as width increases.
Pier length has no appreciable effect on local scour depth as long as the pier is aligned with the flow. When the pier is skewed to the flow, the pier length has a significant influence on scour depth. For example, doubling the length of the pier increases scour depth from 30 to 60 percent (depending on the angle of attack).
- **Sediment:** A layer of uniform cohesionless bed material of specific thickness is described by the specific gravity and the sieve diameter of its particles. The degree of uniformity of particle size distribution of a sediment is defined by the value of its standard deviation, σ . The most common and convenient measure of standard deviation used in studies of the distribution of particle size of a sediment is the graphic standard deviation, which is derive by reading two values on the cumulative particle size curve,

$$\sigma = \sigma_g = \left(\frac{d_{84.1}}{d_{15.9}}\right)^{0.5} = \frac{d_{84.1}}{d_{50}} = \frac{d_{50}}{d_{15.9}} \quad (1.20)$$

The inclusive graphic standard deviation of Folk (1968) gives a better measure of the uniformity of a sediment as it embraces 90 percent of distribution which is used in some of the studies:

$$\sigma_I = \left(\frac{d_{84.1}}{d_{15.9}}\right)^{0.250} \cdot \left(\frac{d_{95}}{d_5}\right)^{0.152} \quad (1.21)$$

According to Ettema (1980), bed material in the sand-size range has little effect on local scour depth. Likewise, larger size bed material that can be moved by the flow or by the vortices and turbulence created by the pier or abutment will not affect the maximum scour, but only the time it takes to attain it. Very large particles in the bed material, such as coarse gravels, cobbles or boulders, may armor the scour hole. Fine bed material (silts and clays) will have scour depths

as deep as sand-bed streams. This is true even if bonded together by cohesion. The effect of cohesion is to influence the time it takes to reach maximum scour. With sand-bed material the time to reach maximum depth of scour is measured in hours and can result from a single flood event. With cohesive bed materials it may take much longer to reach the maximum scour depth, the result of many flood events.

Bed configuration of sand-bed channels affects the magnitude of local scour. In streams with sand-bed material, the shape of the bed (bed configuration) may be ripples, dunes, plane bed and etc. The bed configuration depends on the size distribution of the sand-bed material, hydraulic characteristics, and fluid viscosity. The bed configuration may change from dunes to plane bed during an increase in flow for a single flood event. It may change back with a decrease in flow. The bed configuration may also change with a change in water temperature or suspended sediment concentration of silts and clays. The type of bed configuration and change in bed configuration will affect flow velocity, sediment transport, and scour.

- **Time:** Scour is a dynamic process which seeks to establish a new equilibrium, between the flow of the fluid and the resistance to motion of the bed particles, by the erosion of the flow boundary; the local scour deepens progressively with time.

In summary, the down-flow impingement on the bed, along with the wide range of turbulence structures present in the flow field, entrain and transport material from the scour hole. The details and interaction of the flow field vary with pier characteristics such as shape, angle of attack, and the stage of scour development between initiation and equilibrium, but the essential consideration is that these flow features are responsible for scour.

1.3.4. Dimensionless analysis of local Scour depth

The large number of interacting parameters makes the analysis of local scour at bed sediment around a bridge pier very difficult. This has forced the researchers to use of dimensional analysis. However the dimensional analysis is only a technique for grouping of variables, and yields in itself no information. The relation between the depth of local scour at a bridge pier d_s , and its dependent parameters can be written:

$$d_s = f_1(\text{Flood Flow}(\rho, \mu, h, g, u, l_c), \text{Bed Sediment}(d_{50}, \sigma, \rho_s), \text{Bridge Pier Geometry}(b), \text{Time}(t)) \quad (1.22)$$

Where,

ρ = fluid density;

μ = fluid dynamic viscosity;

h = mean approach flow depth;

g = acceleration of gravity;

u = mean approach flow velocity;

d_{50} = median size;

σ = geometric standard deviation of the sediment particle size distribution ;

ρ_s = sediment density;

b = pier width;

l_c = width of the flow; and

t = time.

An expression for the depth of local scour at a cylindrical pier of diameter b can be written as a combination of dimensionless parameters:

$$\frac{d_s}{b} = f_2\left(\frac{\rho u h}{\mu}, \frac{u}{\sqrt{gh}}, \frac{l_c}{h}, \frac{h}{b}, \frac{b}{d_{50}}, \sigma, \frac{\rho_s - \rho}{\rho}, \frac{tu}{b}\right) \quad (1.23)$$

Where we can substitute these terms by consider the following definitions:

$$\Delta = \frac{\rho_s - \rho}{\rho} = \text{relative submerged weigh of sediments}$$

Considering Reynolds number (Re) that is being used as a criterion to distinguish between laminar and turbulent flow and is a measure of the ratio of the inertia force on an element of fluid to the viscous force on an element and is equal to:

$$Re = \frac{\rho u l}{\mu} \quad (1.24)$$

Where l is a characteristic length. Thus, particle Reynolds number can be written as:

$$Re_p = \frac{d_{50} \sqrt{\frac{\rho_s - \rho}{\rho} \cdot g d_{50}}}{\nu} \quad (1.25)$$

Froude number (Fr) is also defining as a measure of the ratio of the inertia force on an element of fluid to the weight of the element and it is equal to:

$$Fr = \frac{V}{\sqrt{gh}} \quad (1.26)$$

As mentioned before, the Shield diagram defines a u_c^* for a given d_{50} . A corresponding u_c can be found for the given flow depth, and thus the Froude number can be written, using the given data as u/u_c .

Thus the equation (1.23) can be rewritten as:

$$\frac{d_s}{b} = f_3\left(Re, \frac{l_c}{h}, \frac{h}{b}, \frac{u}{u_c}, \frac{b}{d_{50}}, \sigma, \Delta, \frac{tu}{b}\right) \quad (1.27)$$

The density ratio is assumed constant, and the Reynolds number influences are assumed negligible for the highly turbulent flows envisaged. On the other hand, the effect of width of the

flow, l_c in wide flows can be neglected and also by considering uniform sediment it is possible to disregard the dependency to σ . Therefore, the other form which can represent the scour depth as the function of dimensionless parameters is:

$$D_s = f(U, H, D_{50}, T) \quad (1.28)$$

$$\text{Where: } U = \frac{u}{u_c}, H = \frac{h}{b}, D_{50} = \frac{b}{d_{50}} \text{ and } T = \frac{tu}{b}$$

The functional relationships between dimensionless variables have to be obtained from experiments, but when the number of dimensionless numbers is large severe experimental problems occur. In this way the relationship between the four parameters mentioned above can be obtained by less effort and in a more economical manner.

1.3.5. Some existing formula for evaluation of local scour

In literature, it is possible to find several empirical or semi-empirical formulas for the determination of the scour depth at equilibrium condition (final stage) or with respect to time evolution. The differences in these formulas are mostly due to their various experimental conditions. Moreover, the validity range of existing formulas in literature is not similar for all of them. This is the consequence of the difference in selection of the under consideration range for dependent parameters of these studies. In addition, it is necessary to have constant values of different effective parameters when the dependency of two parameters on each other is under study. In some cases the mentioned required stability condition is failed and put a negative effect on the accuracy of the final proposed formula. This dispersion in resulting formula by different authors shows that scour depth determination is not clearly defined yet.

Each formula is only valid for the limited range of the author's studies and cannot be extended to other conditions such as different pier size, river width and flow velocity outside of the mentioned range by the author.

In literature there are many authors who have expressed the dimensionless Scour depth D_s as a function of multiplication of different factor in which each of them take into account the dependency of specific parameter. One of the most relevant combinations is as below:

$$D_s = K_1(T) \cdot K_2(U) \cdot K_3(H) \cdot K_4(D_{50}) \quad (1.29)$$

Where K_1, K_2, K_3 and K_4 define empirically through interpolation of the results usually independently. It should be noted that, other factors rather than those mentioned here also can be considered.

Below, they are few definitions of the mentioned factors define by various authors:

- **Franzetti et al (1994)**

$$K_T = 1 - e^{(-0.028T^{\frac{1}{3}})}$$

$$K_U = 1 - 10(1 - U)^3 \quad 0.67 \leq U \leq 1$$

$$K_H = 1 - e^{(1.3.H)} \quad H \geq 2$$

$$K_{D_{50}} = 3.868 \cdot D_{50}^{1.572} \cdot e^{[-2.64(D_{50})^{0.234}]}$$

- **Chiew (1995)**

$$K_U = 3.77 U^{-1.13} \quad 0.3 \leq U \leq 1$$

$$K_{D_{50}} = 0.398 \ln(D_{50}) - 0.034[\ln(D_{50})]^2 \quad 1 \leq D_{50} \leq 50$$

$$K_{D_{50}} = 1 \quad D_{50} \geq 50$$

$$K_H = 0.783[(D_0)]^{0.322} - 0.106 \quad 0 < H < 3$$

$$K_H = 1 \quad H \geq 3$$

- **Dey et al. (1999)**

$$K_U = [21.28 U^{3.508} - 1]^{0.5} \quad 0.42 \leq U \leq 1$$

$$K_H = (H)^{0.15}$$

- **Melville and Chiew (1999)**

$$K_U = U \quad U < 1$$

$$K_U = 1 \quad U > 1$$

$$K_H = 2.4 H \quad H < 0.7$$

$$K_H = 2 \cdot H^{0.5} \quad 0.7 < H < 5$$

$$K_H = 4.5 H \quad H > 5$$

$$K_{D_{50}} = 0.57 \log(2.24 \cdot H) \quad D_{50} < 25$$

$$K_{D_{50}} = 1 \quad D_{50} > 25$$

$$\frac{d_s}{d_{se}} = \exp \left[-0.03 \left| \frac{u_c}{u} \ln \left(\frac{t}{t_e} \right) \right|^{1.6} \right]$$

$$t_e(\text{days}) = 48.26 \frac{b}{u} (U - 0.4) \quad H > 6$$

$$t_e(\text{days}) = 30.89 \frac{b}{u} (U - 0.4) H^{0.25} \quad H \leq 6$$

- **Oliveto and Hager (2002)**

$$K_U = c_0 U^{1.5}$$

- **Sheppard (2002)**

$$K_U = 1 - 3.31 (U - 1)^2$$

$$K_H = \tanh[(H)^{0.4}]$$

$$K_{D_{50}} = \frac{3.03}{2.6 e^{0.43 \log(D_{50}) - 0.707} + 0.43 e^{-2.6 \log(D_{50}) + 4.27}}$$

- **Chang et al (2004)**

$$K_U = U - 0.4$$

$$0.4 \leq U \leq 1$$

$$K_{D_{50}} = 0.398 \ln(D_{50}) - 0.034 [\ln(D_{50})]^2$$

$$1 \leq D_{50} < 50$$

$$K_{D_{50}} = 1$$

$$D_{50} \geq 50$$

$$K_H = 0.783 [(H)]^{0.322} - 0.106$$

$$0 < H < 3$$

$$K_H = 1$$

$$H > 3$$

K_σ = Obtain by a graph

- **Sheppard et al (2004)**

$$K_U = 1 - 1.75 [\ln(U)]^2$$

$$K_H = \tanh[(H)^{0.4}]$$

$$K_{D_{50}} = \frac{D_{50}}{0.4 D_{50}^{1.2} + 10.6 D_{50}^{-0.13}}$$

- **Raikar and Dey (2005)**

$$K_{D_{50}} = 0.26 \ln(3.88 \cdot D_{50})$$

$$D_{50} \leq 9$$

$$K_{D_{50}} = 0.08 \ln(14070 \cdot D_{50})$$

$$9 < D_{50} \leq 25$$

$$K_{D_{50}} = 1$$

$$D_{50} > 25$$

K_{σ} = Obtain from graph

- **Lanca et al. (2013)**

$$K_T = \frac{d_s}{d_{se}} = 1 - e^{-a_1 T^{a_2}}$$

Where:

$$a_1 = 1.22(D_{50})^{-0.764}$$

$$a_2 = 0.09(D_{50})^{0.244}$$

$$K_{H-D_{50}} = 7.3(D_{50})^{-0.29}H^{0.12} \quad 60 \leq D_{50} \leq 500, H \geq 0.5$$

$$K_H = 1.2H^{0.12} \quad D_{50} > 500, H \geq 0.5$$

1.4. Objectives

The objectives of this research work can be summarized as below:

- ✓ Collection of clear-water scour data for cylindrical piers from reliable sources in literature;
- ✓ Selection of long-duration, suitable and reliable data from previous research and experiments by imposing appropriate selection criteria;
- ✓ Homogenization of the available data, particularly by an analysis of threshold conditions to choose a suitable criterion to be applied to all the experiments for defining the threshold for inception of bed material motion;
- ✓ Investigation of the effect of nondimensional time, T (t.u/b), sediment coarseness, D_{50} (b/d₅₀), and upstream flow intensity, U (u/u_c), on the scour depth;
- ✓ Regression-based calibration of a predictive formula;
- ✓ Comparison of the final proposed equation with several previous ones available in the literature.

Chapter 2

AVAILABLE DATA AND LITERATURE REVIEW

2.1. Introduction

Relatively large quantities of local scour data have been used for the purpose of the analysis. The sources and quantities of these data are listed in table 2.1 and 2.2. Laboratory data are derived from experiments that were carefully performed and all the dependent parameters are given by the author.

A total number of 516 experiments was used in this study. The data that have been employed can be divided into two general categories:

1. *Full trend scour depth data (324 experiments)*; which are the experiments where the full scour depths evolution from the beginning of the experiments until the experiments stops, with respect to time, were reported by authors. (Table 2.1)

2. *Isolated scour depth points (97 experiments)*; which are the data where only final or maximum scour depth is provided by the authors and the time history of the scour holes evolution were not reported or measured. (Table 2.2)

Main characteristics of data sources are given in the following section.

Full trend scour depth data	
sources	Number of data
Alabi (2006)	3
Ettema (1980)	96
Yanmaz-Altinbilek (1991)	18
Chang et al (2004)	10
Raikar-Dey (2005)	16
Franzetti et al (1989)	1
Azzaroli (1983?)	1
Oliveto-Hager (2002)	88
Lanca et al (2013)	46
Chabert-Engeldinger (1956)	12
Mignosa (1980)	19
Sheppard et al (2002)	14
Total Number of series	324

Table 2.1: Full trend data sources and number for each source.

Isolated scour depth points	
sources	Number of data
Yanmaz, Altinbilek (1991)	15
Sheppard and Miller 2006	24
Ettema et al 2006	6
Lee and Sturm (2009)	4
Raikar and Dey (2005)	4
Dey et al (1995)	18
Chiew and Melville 1987	26
Total Number of points	97

Table 2.2: Isolated points sources and number for each source.

2.2. Data Characteristics

In this section a brief summary about the experiments done by the various authors and the aim and an achievement of their study is provided to have a better understanding about the data that are going to be used in this study. For employing different experiment results from various sources it is necessary to understand the assumptions which have been made. In this way, it is possible to use these experiments as a unique database and attempt to make all of them homogenous via analysis. It should be remembered that, all the collected experiments are in *clear-water condition* according to authors report.

2.2.1. Full trend scour depth data

2.2.1.1. Ettema (1980)

- **Introduction and objectives**

The aim of this project was to investigate experimentally the development of local scour in uniform and non-uniform sediments as well as in beds formed of layers of uniform sediments. It was hoped that each set of experiments would lead to recommendation for design of bridge piers. Three main series of experiments were augmented.

In all the experiments cylindrical piers were used. The approach flow was steady for all experiments.

For the purpose of this study the experiments related to local scour of uniform sediment around a pier were used. The stage of particle motion, expressed in terms of shear velocity parameter u^*/u_c^* , was set on that all the experiments were performed at clear water local scour.

The experimental study was conducted in two parts:

The first part investigated the temporal development of local scour for a range of bed particle sizes and cylindrical pier diameter, at similar values of the shear velocity parameter u^*/u_c^* with different value of 0.95, 0.9, 0.75 or 0.5 at the center line of the approach flow. Two different

flumes were used in this study. The greater part of the study was performed in a 1.52 m wide re-circulating flume for which the approach flow depth was kept constant at 0.6 m. Additional experiments were conducted in a 0.46 m wide flume with flow provided by an outlet pipe from the ring-main system of the laboratory with constant approach flow equal to 0.2 m for these experiments.

The second parts was concerned with the influence of the approach flow depth, h (y_0 by Ettema notation), on the development of local scour at a cylindrical pier found in uniform sediment. Shear velocity parameter was held constant at $u^*/u_c^* = 0.9$, at the center line of the approach flow to the pier. The experiments were carried out in the 1.52 m wide flume. Three piers sizes and three uniform bed sediments were used to investigate the influences of flow depth, as well as that of pier and particle sizes, on the development of local scour.

- **Hydraulic Models**

Most of the experiments on the temporal development of local scour were carried out in a 1.52 m wide, 1.22 m deep, glass-sided flume of approximately 45 m length (Figure 2.1). The flow through the flume was re-circulated by two variable speed axial flow pumps driven by thyristor controlled electric motors. In all experiments the flume slope was adjusted to ensure that the depth of the flow was constant over the full length of the working section.

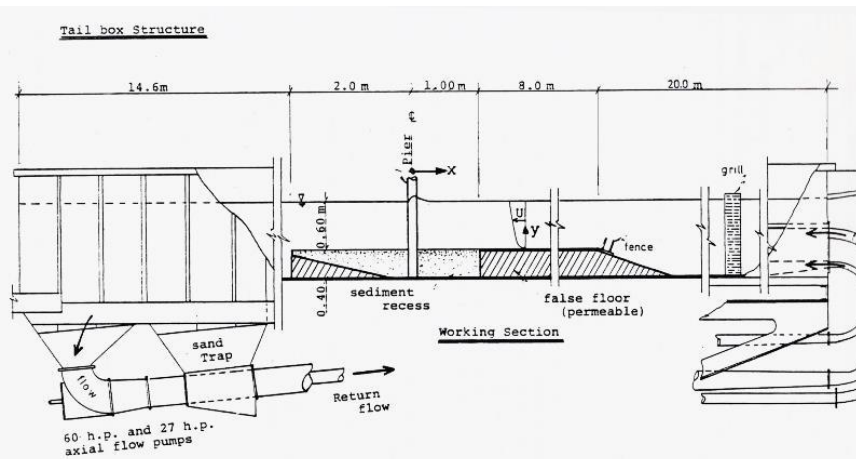


Figure 2.1: Cross-section of the working section of 1.52 m wide, flow recirculating, flume by Ettema (1980)

The working section of the flume commenced at 20 m from the upstream end of the flume. It consisted of an 8 m length false floor, upstream of 1.5 m wide and 3 m long sediment recess, in which the pier was placed.

The approach bed roughness was simulated with the use of roughened sheet metal covers which were fixed to the false floor. A selection of roughened sheets was made to cover the range of sediment sizes used in the study.

An additional series of experiments was performed in a smaller glass-sided flume 0.456 m wide, 0.44 m deep and approximately 19 m in length, served with water circulation system of the

laboratory. The water level in the flume was controlled by a tail gate. The roughness of the approach bed was simulated in a similar manner to that described for the approach bed in 1.52 m wide flume (Figure 2.2).

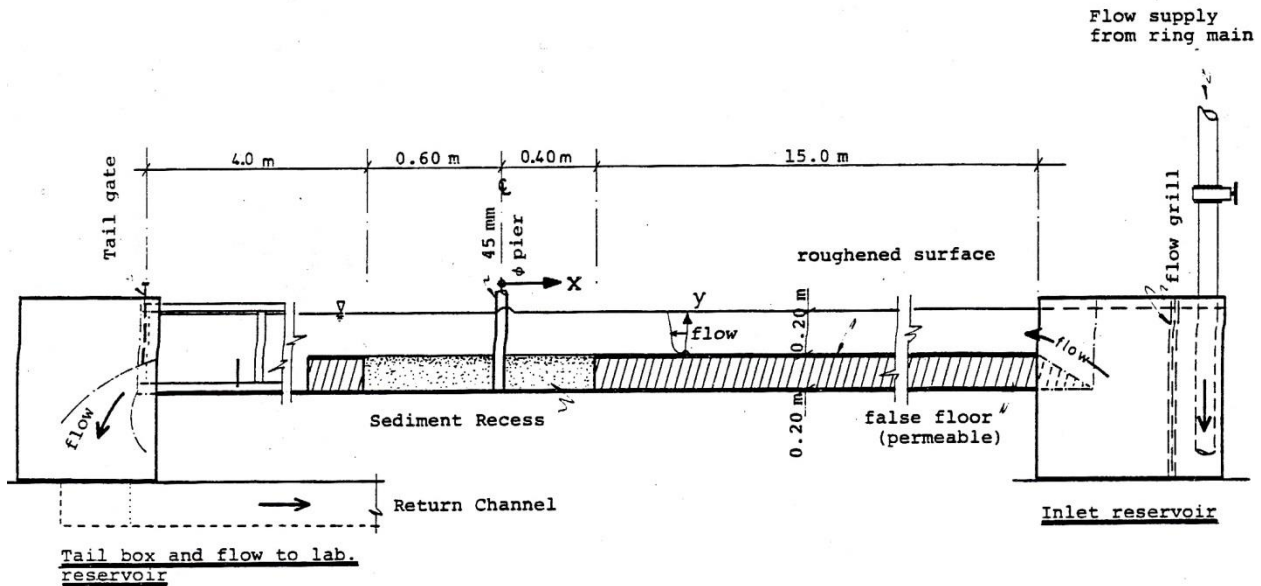


Figure 2.2: Cross-section of the working section of the 0.46 m wide flume by Ettema (1980)

- **The bed sediments**

Sediment properties used in this experiment are listed in Table (2.3) where d_{50} is mean particle size of uniform sediments, σ_g and σ_l are two measurements of standard deviation of particle size distribution of each bed sediments ($\sigma_g < 1.5$ may be considered as being virtually of a uniform particle size. All of the eight bed sediment that used in this experiments fulfill this limit so they can be considered as uniform sediments.), S_s is specific gravity, u_c^* is critical shear velocity and computed by using shields function. S.F is particle shape factor which has a negligible influence of u_c^* , W_{50} is fall velocity of the mean particle size determined by Rouse (1937) and α is the angle of static particle response.

	Bed Sediment Number							
	1	2	3	4	5	6	7	8
d_{50} (mm), d	0.24	0.38	0.80	0.84	1.90	3.80	5.37	7.80
σ_g	1.18	1.29	1.33	1.17	1.34	1.07	1.24	1.10
σ_I	1.20	1.30	1.39	1.19	1.33	1.08	1.24	1.12
S_B	2.65	2.65	2.65	2.65	2.65	2.65	2.65	2.65
u_{*c} ($\times 10^2 \text{ ms}^{-1}$)	1.30	1.52	2.13	2.18	3.41	5.87	6.93	8.41
S.F.	1.0	1.0	1.0	1.0	1.0	0.82	0.76	0.70
w_{50} (ms^{-1})	0.03	0.06	0.14	0.15	0.27	0.32	0.45	0.49
α	29°	31°	34°	36°	37°	38°	38°	38°

Table 2.3: Sediment properties used in Ettema experiment

- **Piers and scour depth**

The sizes of the cylindrical piers used in the experiments are given in table (2.4) below:

Flume Width B (mm)	Pier Diameter D (mm)	$\frac{B}{D}$
1524.0	28.5	53.5
	50.8	30.0
	101.6	15.0
	150.0	10.2
	240.0	6.4
457.2	45.0	10.16

Table 2.4: Pier size used in Ettema experiment

Several techniques were adopted to measure the depth of the local scour. Scour depths could be read to within ± 1 mm. It is worthy to mention that the value of B/D is provided as 10.6 instead of 10.16 for the last row of table (2.4) in the authors report.

- **Approach flows and flow measurement**

The approach flow for each experiment was initially set so that the experiments were run for similar values of the shear velocity ratio, u^*/u_c^* , for all the sediment sizes. For each flow and sediment size, the channel slope, S_0 , was adjusted so that the flow had a uniform depth over the working section. Required value of the slope, S_0 were estimated from:

$$S_0 = \frac{u_*^2}{gh} \quad (2.1)$$

The magnitudes of d_{65} and u_c^* for corresponding value of d_{50} is provided by author in table (2.5).

d65(mm)	corresponding d50(mm)	Shields u_c^*
0.225	0.24	0.013
0.432	0.38	0.0152
1.054	0.8	0.0213
0.862	0.84	0.0218
1.935	1.9	0.0341
3.829	3.8	0.0587
5.497	5.37	0.0693
1.013	7.8	0.0841

Table 2.5: Ettema (1980) critical shear velocity definition

The mean approach flow velocity, u , of the center line velocity profile was determined from equation:

$$u = u^* [5.75 \log \left(\frac{h}{d_{65}} \right) + 6] \quad (2.2)$$

Similarly for critical approach flow velocity:

$$u_c = u_c^* \left[5.75 \log \left(\frac{h}{d_{65}} \right) + 6 \right] \quad (2.3)$$

It can be concluded from equation (2.2) and (2.3):

$$\frac{u}{u^*} = \frac{u_c}{u_c^*} \rightarrow \frac{u}{u_c} = \frac{u^*}{u_c^*} \rightarrow u = \frac{u^*}{u_c^*} \cdot u_c \quad (2.4)$$

The approach flow velocity profiles were measured with two mini-propeller flow meters.

• Results and procedure

Following observations were made for each experiment:

- *The temporal development of the scour hole.* The frequency of scour depth measurement decreased as the rate scouring decrease. The experiment was stopped when no change occurred to the maximum depth of scour hole over a minimum period of four hours.
- *The mechanisms of local scour.* A visual record of the important feature distinguishing the development of local scour around a cylindrical pier kept with aid of photographs.
- Water temperature.
- *Scour hole profile.* At the completion of each experiment the profile of the scour hole, in the plane of symmetry of the pier and parallel to the flow direction was recorded with 3 mm diameter pointer gauge.

It is assumed that the following relationship can be stated for the depth of local scour at a pier:

$$\frac{d_s}{b} = f\left(\frac{h}{b}, \frac{b}{d_{50}}, \frac{t}{t_0}, \frac{u^*}{u_c^*}\right) \quad (2.5)$$

The curve formed by the collapse of the data is defined by four straight-line segments which approximate the different local scour development. The principal erosion phase is approximated by two straight-line segments. Each segment is of the form:

$$\frac{d_s}{b} = k_1 \ln\left(\frac{d_{50}}{b} \cdot \frac{u^* t}{b} \cdot \frac{v}{u^* \cdot b}\right) + \ln k_2 \quad (2.6)$$

Where k_1 and k_2 are constants defined for each phase segments.

2.2.1.2. Sheppard, et al. (2002)

- **Introduction and objectives**

This bridge scour research program at the University of Florida was directed at increasing the understanding of scour processes and improving the accuracy of design scour depth prediction through large-scale experiments.

All of the experiments were conducted in large, flow-through type flume. Three circular cylinder diameters (0.915 m, 0.305 m and 0.114 m), three different sediment grain sizes (d_{50} equal to 0.22 mm, 0.80 mm and 2.9 mm) and a range of water depths were investigated. This study covers the clear-water scour range of velocities (i.e., $0.45 \leq u/u_c \leq 1$).

Normalized equilibrium local scour depths was described in terms of three dimensionless parameters, h/b , u/u_c , and b/d_{50} where according to the author notation are:

h = water depth,

b = structure diameter/width,

u = the depth averaged Velocity,

u_c = the depth averaged Critical Velocity,

d_{50} = the median sediment grain diameter.

In this experiments indicated a trend in the data with increasing values of b/d_{50} . Thus, one of the objectives of his research was to obtain local scour data for larger values of b/d_{50} .

The rate at which local scour occurs and the dependence of this rate on the sediment, flow and structure parameters is another object of this experiment.

- **Hydraulic models**

All of the tests were conducted in a large 6.1 m wide, 6.4 m deep, and 38.4 m long flow through type flume. Schematic drawings of the flumes used in this research are shown in figure 2.4 and 2.5.

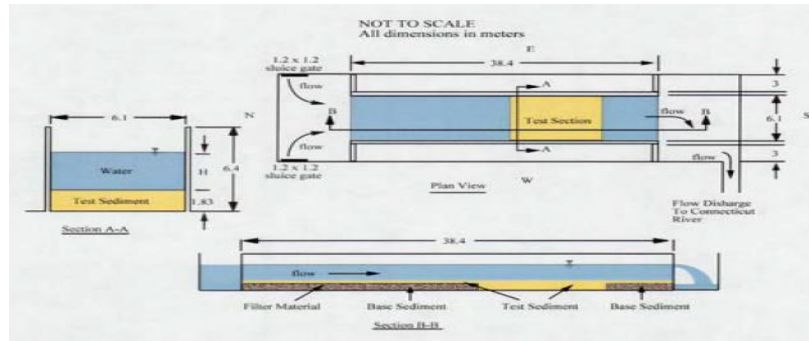


Figure 2.3: Schematic drawing of flume used for Sheppard et al.'s (2002) research

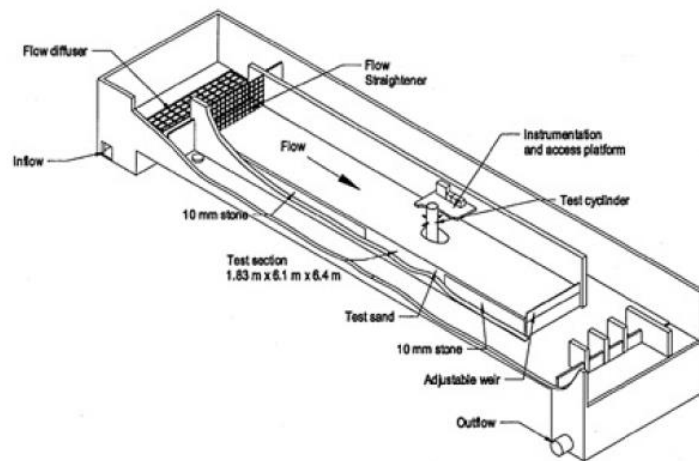


Figure 2.4: Isometric drawing of the flume

The test section was the width of the flume, 9.8 m long and started 24.4 m downstream of the entrance. The sediment in the test area was 1.83 m deep. Water for the flume was supplied from hydroelectric power plant reservoir adjacent to building housing the flume. Water flowed from the reservoir, through the flume, and discharged into river downstream of control structure. The flow discharge and depth-averaged velocity was controlled with a weir located at the downstream end of the flume.

The instrumentation used in this research can be divided into two categories: 1) That which measures the flow parameters, and 2) That which measures scour depth. The flow parameters monitored were flow discharge, velocity at specific locations, water depth, and temperature. The scour hole depth was monitored with internal and (on some occasions) external video cameras and with arrays of acoustic transponders.

- **Bed sediment**

Three different sediment grain sizes with $d_{50}=0.22$ mm, 0.80 mm and 2.9 mm where used in this experiment and the value of their standard deviation, σ , are 1.51, 1.29 and 1.21 respectively. In table 2.6 the value of d_{50} and σ correspond to each test are listed.

- **Pier and scour depth**

Three circular cylinder piers with 0.915 m, 0.305 m and 0.114 m diameter were used. Quantitative scour depth measurements were obtained by video cameras mounted on a platform that traversed vertically and the length scales were attached to the inside of the cylinders in view of the cameras. Miniature video cameras were also mounted in streamline waterproof housing for viewing scour hole from outside the structure.

Three arrays of acoustic transponders were attached to the cylinder just below the water surface. This system provided scour hole depth measurement at the 12 locations along three radial lines throughout the experiments.

Pier and scour depth measurement summary of all tests are provided in table 2.6.

- **Approach flows and flow measurement**

Flow velocities were measured at two locations, 2 m upstream and 1 m to the side of the center of the test structure with electromagnetic flow meters. The vertical position of the meters was set at 40 % of the water depth from the bed. The velocity at this location was considered approximately equal to the depth-averaged velocity for the fully developed logarithmic velocity profile.

A commercial water level instrument, which used a near bottom mounted pressure transducer measured water depth at a location between the test structure and the weir. The water temperature was measured just downstream of the structure. The value of flow depth and velocity for each test is provided in table 2.6.

Test	Flow		Sediment		Structure
	Depth (m)	Velocity (m/s)	D ₅₀ (mm)	σ	Diameter (m)
1	1.19	0.29	0.22	1.51	0.114
2	1.19	0.31	0.22	1.51	0.305
3	1.27	0.40	0.80	1.29	0.915
4	0.87	0.39	0.80	1.29	0.915
5	1.27	0.39	0.80	1.29	0.305
6	1.27	0.41	0.80	1.29	0.114
7	1.22	0.76	2.90	1.21	0.915
8	0.56	0.65	2.90	1.21	0.915
9	0.29	0.57	2.90	1.21	0.915
10	0.17	0.50	2.90	1.21	0.915
11	1.90	0.70	2.90	1.21	0.915
12	1.22	0.40	0.22	1.51	0.305
13	0.18	0.30	0.22	1.51	0.305
14	1.81	0.30	0.22	1.51	0.915

Table 2.6: Flow, sediment and structure parameters summary

- **Procedure and results**

The procedure used in performing the local sediment scour experiments is outlined below.

➤ **Pre-experiment**

1. Compact and level the bed in the flume.
2. Fill the flume slowly and allow standing for approximately 12 hours or until all the air trapped in the sediment has escaped. Drain the flume and re-compact the bed.
3. Take pre-experiment photographs.
4. Fill the flume slowly and allow trapped air to escape (approximately six hours).
5. Start and check all instrumentation

➤ **During experiment**

1. Measure the scour depth as a function of time with acoustic transponders and video cameras.
2. Measure the velocity, water depth, and temperature. Observe water clarity as an indicator of suspended sediment.

➤ **Post-experiment**

1. Take post-experiment photographs.
2. Observe and note bed condition throughout the flume (presence of bed forms, etc.)
3. Survey the scour hole with a point gauge.
4. Reduce and analyze the data.

A significant amount of local sediment scour data and information were gathered during this research program. A brief summary of the results is given in tables 2.7. Two different scour depths are given in this table, the measured values at the end of the experiment and the estimated equilibrium depth. Most of the experiments conducted as part of this work were long in duration and thus the scour depths were near equilibrium at the end of the test. During some of the test there was an increase in suspended sediment in the water from the reservoir and this proved to impact the equilibrium scour depth.

Test	Test Duration (hr)	Time to 90% d_{se} (equil.) (hr)	Max. Measured Scour Depth (m)	Estimated Equilibrium Scour Depth (m)
1	89	111	0.133	0.17
2	163	408	0.257	0.41
3	360	322	1.112	1.10
4	143	905	0.638	0.99
5	88	128	0.416	0.51
6	41	29	0.185	0.23
7	188	151	1.270	1.41
8	330	186	1.058	1.14
9	448	347	0.896	0.96
10	616	831	0.659	0.72
11	350	720	1.004	1.24
12	256	71	0.377	0.39
13	216	66	0.296	0.31
14	580	913	0.787	0.97

Table 2.7: The local Scour results summery

Equilibrium depths were estimated by extrapolating a curve fit to the data. The function used to fit the data was first used by J. Sterling Jones and is:

$$d_s = a \left(1 - \frac{l}{1+abr} \right) + c \left(1 - \frac{l}{1+cdt} \right) \quad (2.7)$$

The resulting Sheppard's equation is:

$$\frac{d_s}{b} = K_s K_{cp} f_1 \left(\frac{h}{b} \right) f_2 \left(\frac{u}{u_c} \right) f_3 \left(\frac{b}{d_{50}} \right) \quad (2.8)$$

K_s = shape factor (1 for circular piles)

K_{cp} = Peak values of normalized Clearwater scour depth= 2.5 in these equations.

For $K_{cp}=2.5$ we are going to have:

$$\frac{d_s}{b} = k_s 2.5 \left\{ \tanh \left[\left(\frac{h}{b} \right)^{0.4} \right] \right\} \left\{ \left[1 - 3.31 \left(\frac{u}{u_c} - 1 \right)^2 \right] \right\} \quad (2.9)$$

$$\left\{ \frac{3.03}{2.6 \exp \left[0.43 \log_{10} \left(\frac{b}{d_{50}} \right) - 0.707 \right] + 0.43 \exp \left[-2.6 \log_{10} \left(\frac{b}{d_{50}} \right) + 4.27 \right]} \right\}$$

2.2.1.3. Oliveto and Hager (2002)

- **Introduction**

This work presents new research on bridge pier and abutment scour based on a large data set collected at ETH Zurich, Switzerland. In total six different sediments were tested, of which three were uniform. Also a large variety of scour elements were considered, from 1 to 60% of the channel width, and flow depths ranging from 1 to about 40% of the channel width.

- **Hydraulic models**

The experiments were conducted in two rectangular channels, one having a width $l_c=1.00$ m, the other $l_c=0.50$ m. The 1 m channel had a total length of 11 m, with a working section of about 5 m, a glass wall on the left side, and a smooth steel wall on the right side. The sediment was placed horizontally, and the free surface measured along the flow. The determining approach flow depth h was taken at $(l_c-b)/2$ upstream from the scour element face, with b as the pier diameter. All experiments were run essentially under plane bed conditions. The sediment surface was measured with a so-called shoe gauge having a 4 mm by 2 mm wide horizontal plate at its base, whereas the water surface was read with a conventional point gauge, typically to ± 0.5 –1 mm, depending on the local surface turbulence.

- **The bed sediment**

Six different sediments were used, three of which were uniform with grain sizes 0.55, 3.3, and 4.8 mm, and three mixtures, with $d_{50}=5.3, 1.2,$ and 3.1 mm, and $\sigma=(d_{84}/d_{16})^{1/2}=1.43, 1.80,$ and $2.15,$ respectively. The uniform sediment with $d_{50}=3.3$ mm had a density of $\rho_s=1.42$ t/m³, whereas the remainder had $\rho_s=2.65$ t/m³. The plastic sediment originated from a circular extruder, the rest was from Swiss rivers with a typical ellipsoidal shape.

- **Pier and scour depth**

The circular cylinders had diameters $b=0.011, 0.022, 0.050, 0.064, 0.110, 0.257, 0.400,$ and 0.500 m. All elements were fabricated in transparent plexi-glass to allow for visual determination of scour depths to 1 mm during the progress of an experiment.

The temporal start of an experiment ($t=0$) was set at scour inception. Subsequent measurements were taken at times $t=1, 3, 6, 10, (15),$ and 20 min up to several days and even several weeks in selected runs.

The scour surface was measured at the maximum scour depth z along the element side, the maximum lateral and upstream scour extensions, and the aggradation maximum downstream of the element. Figure 2.6 shows a definition sketch with typical points of interest measured for all experiments.

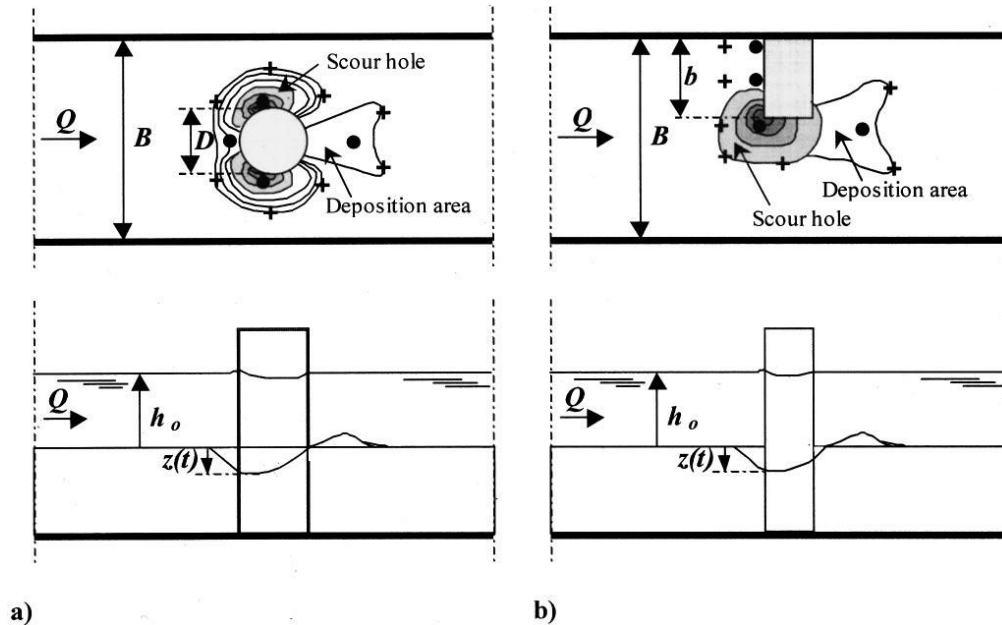


Figure 2.5: Definition sketch and measurement points for: (a) pier and (b) abutment. Points defining (•) scour or aggradation depths; (+) scour or aggradation area

- **Approach flow and flow measurement**

The channel had a closed-loop water system, with a pump at the upstream channel side, of maximum discharge $Q = 0.130 \text{ m}^3/\text{s}$ with an accuracy of about 1%. A submerged sill at the end of the working section inhibited sediment movement out of the working section.

The flow depths measured at a certain time t always included the section 1 m downstream from the flow straightener, the section upstream from the pier and at a downstream section located between 3.3 and 3.8 m. Flow depths ranging from 1 to about 40% of the channel width.

In table 2.8, densimetric particle Froude number $F_d = u/(g'd_{50})^{1/2}$ with $g' = \{(\rho_s - \rho)/\rho\}g$, threshold Froude number F_t , and approach Reynolds number $R_0 = 4hu/\nu$, with u =upstream velocity and ν =kinematic viscosity is provided. The value for approach flow velocity is given as cross-sectional velocity (average bulk velocity) and in terms of Froude and Reynolds numbers in the table.

- **Results:**

In total 200 scour experiments were conducted over almost 2 years. Summary of test condition is provided in the table 2.9 and include the mean grain size d_{50} , its standard deviations, and relative density $\rho' = (\rho_s - \rho)/\rho$, test duration in days, pier width b, the ranges of average approach flow depth h.

Series	F_d	F_t	$R_0 \cdot 10^3$
(-)	(-)	(-)	(-)
24	1.48–3.34	0.71–1.30	19–290
10	1.38–2.79	0.54–0.99	82–506
13	2.00–3.52	0.55–0.96	38–298
19	1.47–3.68	0.55–1.31	75–536
11	1.71–2.39	0.44–0.69	50–257
4	2.24–3.86	0.59–1.14	108–393

Table 2.8: VAW Pier Data- Test Conditions

Series	d_{50} (mm)	σ	ρ'	t experiment (days)	b (m)	h (m)
24	3.3	1	0.42	0.11–46.88	0.02–0.26	0.02–0.30
10	4.8	1.25	2.65	0.46–1.87	0.06–0.50	0.05–0.20
13	0.55	1.37	2.65	0.14–21.06	0.06–0.26	0.05- 0.30
19	5.3	1.43	2.65	0.02–4.74	0.06–0.26	0.05–0.20
11	1.2	1.8	2.65	0.88–2.95	0.06–0.40	0.05–0.20
4	3.1	2.15	2.65	0.13–14.30	0.11–0.50	0.05–0.20

Table 2.9: VAW Pier Data- Summary of Test Conditions

2.2.1.4. Lanca, et al. (2013)

- **Introduction**

long-duration clear-water scour data were collected at single cylindrical piers with the objective of investigating the effect of sediment coarseness, b/d_{50} (b = pier diameter; d_{50} = median grain size) on the equilibrium scour depth and improving the scour depth time evolution modeling by making use of the exponential function suggested in the literature. Experiments were carried out for the flow intensity close to the threshold condition of initiation of sediment motion, imposing wide changes of sediment coarseness and flow shallowness, h/b (h = approach flow depth).

- **Hydraulic models**

Two flumes were used in the experimental study. One, located at the University of Beira Interior, is 28.00 m long, 2.00 m wide and 1.00 m deep. Discharge was measured by an electromagnetic flow meter with an accuracy of 0.5% of full scale. The central reach of the flume, starting at 14.00 m from the entrance, includes a 3.00-m-long, 2.00-m-wide, and 0.60-m-deep recess box in the channel bed.

The second flume, located at the University of Porto, is 33.15 m long, 1.00 m wide, and 1.0 m deep; its central reach starts at 16.00 m from the entrance. The recess box is 3.20 m long, 1.0 m wide and 0.35 m deep. The area located around the pier was covered with a thin metallic plate to avoid uncontrolled scour at the beginning of each experiment. The flumes were filled gradually, imposing a high water depth and low flow velocity. The discharge corresponding to the chosen approach flow velocity was then adjusted to pass through the flumes. The flow depth was regulated by adjusting the downstream tailgates. Once the discharge and flow depth were established, the metallic plates were removed and the experiments started. The characteristic of each experiment is provided in table 2.9.

- **The bed sediment:**

A uniform quartz sand ($\rho_s=2650 \frac{kg}{m^3}$; $d_{50}=0.86$ mm; $\sigma_D=1.36$) was used to fill each of the recess boxes of the two channels.

- **Pier and scour depth:**

Single vertical cylindrical piers were simulated by PVC pipes with $b=50, 75, 110, 160, 200, 250, 315, 350, 400$ mm, placed at ~ 1.0 m from the upstream boundary of the bed recess box. The maximum pier diameter was 200 mm, so as to minimize contraction effects.

The depth of scour hole was measured, to an accuracy of ± 1 mm, with adapted point gauges, approximately every 5 minutes during the first hour. Afterwards, the interval between measurements increased and, after the first day, only a few measurements were carried out each day. When the scour rate was less than approximately 2 mm ($\approx 2d_{50}$) in 24 hours and at least 7 days had passed, the experiments were stopped. The sand bed approach reach located upstream of the piers stayed undisturbed through the entire duration of the experiments; this long-term stability ensured that the scour depth was not supplemented by upstream bed degradation.

- **Approach flow and flow measurement**

A reasonably high relative flow depth ($0.050 \text{ m} \leq h \leq 0.400 \text{ m}$; $58 < h/d_{50} < 465$) was always guaranteed. The average flow intensity, u/u_c , varied in the range $0.93 \leq u/u_c \leq 1.04$, with u_c being calculated using the predictor of Neil (1967). The aspect ratio l_c/h was guaranteed to be greater than 5.0, to avoid significant wall effects on the flow field. All of the velocities are given in terms of average bulk velocity. The corresponding velocity for each test is represented in table 2.10.

Test	l_c	h	b	u	td	d_{se}
	(m)	(mm)	(mm)	(m/s)	Hour	mm
1	2	55	110	0.28	170	180.1
2	2	80	160	0.29	168	226.2
3	2	100	200	0.29	170	263.1
4	2	125	250	0.3	168	282.1
5	2	158	315	0.29	223	348.1
6	2	175	350	0.33	306	337.3
7	2	200	400	0.31	288	409.2
8	2	50	50	0.27	168	115.6
9	2	75	75	0.28	168	163.9
10	2	110	110	0.29	168	198.9
11	1	160	160	0.3	285	231.1
12	1	200	200	0.31	261	296.5
13	2	250	250	0.32	263	365
14	2	315	315	0.33	186	388.3
15	2	350	350	0.33	291	408.7
16	2	400	400	0.33	224	448.4
17	2	75	50	0.28	168	118.9
18	2	113	75	0.3	168	175.8
19	1	165	110	0.3	241	224.6
20	2	225	160	0.33	267	305.7
21	2	300	200	0.33	262	360.6
22	2	375	250	0.33	221	373.8
23	2	100	50	0.29	170	127.1
24	2	150	75	0.3	169	162.7
25	2	220	110	0.33	216	208.9
26	2	300	160	0.33	330	267.1
27	2	400	200	0.33	219	329.4
28	2	125	50	0.3	168	111
29	1	188	75	0.31	191	146.7
30	2	275	110	0.33	184	234.3
31	2	375	160	0.33	313	278.8
32	1	150	50	0.3	173	109.7
33	2	225	75	0.33	197	170.6
34	2	330	110	0.33	169	222.6
35	2	200	50	0.31	170	133.7
36	2	300	75	0.33	314	197.6
37	2	250	50	0.33	237	116.6
38	2	375	75	0.33	315	184.3

Table 2.10: Characteristic controlling variable of Lanca et al.'s (2013) experiment

- **Results**

It was postulated here that finite equilibrium scour depth must exist (Table 2.10). It was recognized that the probability of occurrence of a sufficiently strong turbulent event capable of entraining sediment grains from the scour hole will never be null though this probability decreases as scour develops, tending asymptotically to zero. Also it was assumed that the time needed to achieve finite equilibrium scour may be rather large, conceptually infinite. For this reason, scour depth records were fitted by using regression as follow:

$$d_s = p_1 \left(1 - \frac{1}{1 + p_1 p_2 t} \right) + p_3 \left(1 - \frac{1}{1 + p_3 p_4 t} \right) + p_5 \left(1 - \frac{1}{1 + p_5 p_6 t} \right) \quad (2.10)$$

Where p_1 to p_6 are constants. For $t \rightarrow \infty$ it is assumed that $d_s = d_{se} = p_1 + p_3 + p_5$. For practical applications, the following upper-bound predictor was suggested:

$$\frac{d_{se}}{b} = K_h K_{d_{50}} \quad (2.11)$$

K_h and $K_{d_{50}}$ are defined as below:

$$K_h = \begin{cases} 2.3 \left(\frac{h}{b} \right)^{1/3} & 0.5 \leq \frac{h}{b} \leq 1.45 \\ 2.6 & \frac{h}{b} > 1.45 \end{cases} \quad (2.12)$$

$$K_{d_{50}} = \begin{cases} 1, & 60 < \frac{b}{d_{50}} \leq 100 \\ 5.8 \left(\frac{b}{d_{50}} \right)^{-0.38}, & 100 < \frac{b}{d_{50}} \leq 500 \\ 0.55, & 500 < \frac{b}{d_{50}} \end{cases} \quad (2.13)$$

Where b is pier diameter, h is approach flow average depth, d_{se} is equilibrium scour depth, K_h is flow shallowness factor and $K_{d_{50}}$ is sediment coarseness factor. Total numbers of 38 series were obtained from this experiment. The full scour depth is represented for these series by the author.

Simarro, G. et al. (2011) have published five long-duration experiments on scouring at cylindrical piers. The data from these experiments were used for validation of the suggested scour time evolution model. Three experiments from Grimaldi, C. (2005) were also included in the analysis (Table 2.11).

AUTOR	t real time	d _s (measure d scour)	σ	h (flow depth)	b (pier width)	d ₅₀	u (data)	ρ	l _c channel Width
	[hr]	[m]	[-]	[m]	[m]	[m]	[m/s]	[kg/m ³]	[m]
GRIMALDI 1 14,0 days	96.00	0.121	1.46	0.15	0.0750	0.00128	0.400	2550	0.80
GRIMALDI 2 6,2 days	147.94	0.179	1.46	0.25	0.0900	0.00086	0.340	2550	2
GRIMALDI 3 6,2 days	146.08	0.225	1.46	0.25	0.1200	0.00086	0.340	2550	2
SIMARRO 1 34,9 days	837.55	0.167	1.40	0.16	0.0750	0.00086	0.270	2650	0.82
SIMARRO 2 45,6 days	1094.50	0.196	1.40	0.16	0.0800	0.00086	0.300	2650	0.82
SIMARRO 3 29,7 days	713.57	0.130	1.46	0.16	0.0800	0.00128	0.340	2650	0.82
SIMARRO 4 24,9 days	596.48	0.135	1.46	0.15	0.0750	0.00128	0.340	2650	0.82
SIMARRO 5 29,0 days	695.67	0.127	1.46	0.13	0.0630	0.00128	0.340	2650	0.82

Table 2.11: Summary of Girmaldi (2005) and Simarro et al (2011) experiment used for validation

2.2.1.5. Change et al. (2004)

- **Introduction**

The main objective of this study was to investigate and analyze the experimental data on the scour-depth evolution at circular piers. A method was proposed based on the mixing layer concept for calculation of equilibrium scour depth in nonuniform sediment. Based on analysis of scour-rate data obtained in experiments, a model for simulating the scour-depth evolution under steady flow in nonuniform sediment is presented herein. In addition, a scheme for computing the scour-depth evolution under unsteady flow is also proposed.

- **Hydraulic models**

The experiments were conducted in a 36m long, 1 m wide, and 1.1 m deep flume with glass sidewalls at the Hydrotech Research Institute of National Taiwan University, Taipei, Taiwan. A false floor was set in the flume with a recess of 2.8 m long and 0.3 m deep where sediment was placed.

- **The bed sediment**

Uniform sediments having sizes of 1.0 and 0.71 mm, and nonuniform sediments having the same median sizes with σ of 2.0 and 3.0, respectively, were used for experiments. All of these sediments had a specific gravity of 2.65. The sediment size distribution curves were designed to be log-normal for nonuniform sediment (Table 2.12).

test	σ	d ₅₀ (mm)
S1	1.20	1.00
S2	1.20	1.00
S3	2.00	1.00
S4	3.00	1.00
S5	1.20	0.71
S6	1.20	0.71
S7	2.00	0.71
S8	2.00	0.71
S9	3.00	0.71
S10	3.00	0.71

Table 2.12: Sediments characteristics

- **Pier and scour depth**

A hollow cylindrical pier made of transparent plexiglass with a diameter of 0.1 m was located at the center of the recess. The temporal variation of the bed surface profile around the pier was recorded using two 3 cm long charge coupled device cameras with 2 mm diameter lenses, placed in the hollow Plexiglas pier.

- **Approach flow and flow measurement**

The velocity for each test was given in terms of average depth velocity. Clear-water scour conditions were imposed in the experiments, in which no sediment was picked up upstream of the scour hole. The summary of approach flow velocities and flow depths are presented in table 2.13.

test	u(m/s)	h(m)
S1	0.390	0.2
S2	0.280	0.2
S3	0.280	0.2
S4	0.280	0.2
S5	0.355	0.3
S6	0.227	0.15
S7	0.355	0.3
S8	0.227	0.15
S9	0.355	0.3
S10	0.227	0.15

Table 2.13: Approach flow Characteristics

- **Results**

Since the maximum scour depth mostly occurred at the pier nose from observations, experiments in the present study were focused at the pier nose. The measured scour depths at the pier nose plotted against time are presented in figure 2.7:

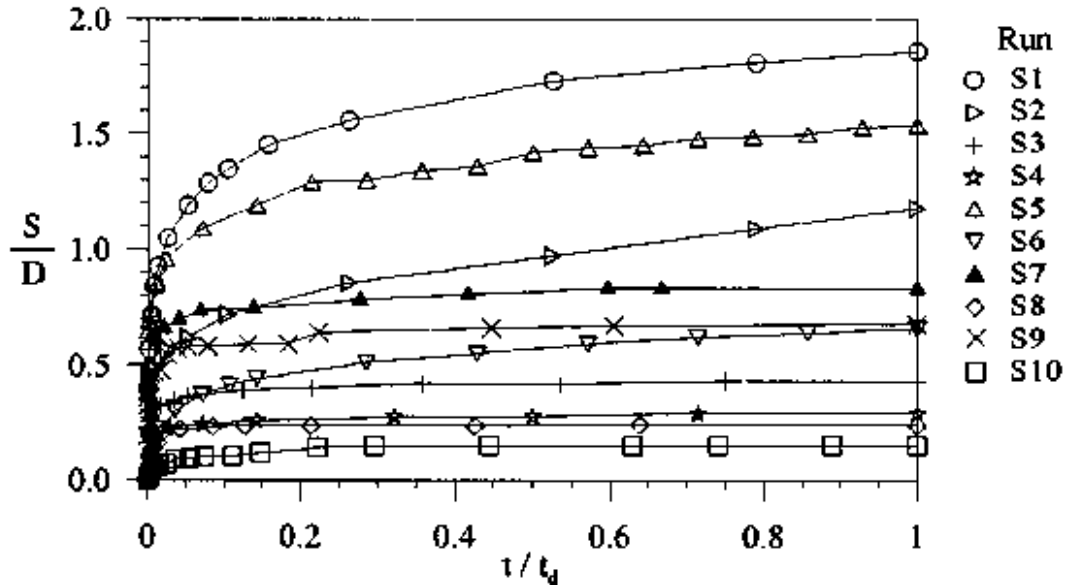


Figure 2.6: Evolution of dimensionless scour depth at pier nose under steady flow (Chang et al. (2005))

2.2.1.6. Yanmaz and Altinbilek (1991)

- **Introduction**

The objective of this study is to develop a semi empirical method to determine the time variation of clear water local scour depth around single cylindrical and square bridge piers. The method to be presented is based on the application of the sediment continuity equation to the scour hole around bridge piers.

- **Hydraulic models**

Experiments to study the development of scour hole around bridge pier models were conducted in a glass flume at the Hydromechanics Laboratory of Middle East Technical University, Ankara, Turkey. The glass flume is an L-shaped horizontal rectangular open channel 90 cm deep, 67 cm wide with a concrete bottom. Side walls (except the test section for visual observations) of the flume are made of steel (Figure 2.8).

- **The bed sediment**

Two different uniform bed materials (quartz sand) were used with the specific weights of 26.4 kN/m^3 and 26.3 kN/m^3 , the mean particle sizes of 1.07 mm and 0.84 mm with $\sigma= 1.13$ and 1.28, respectively. Bed materials were placed as a 15-cm thick layer in the flume bed with a bed slope of 0.001.

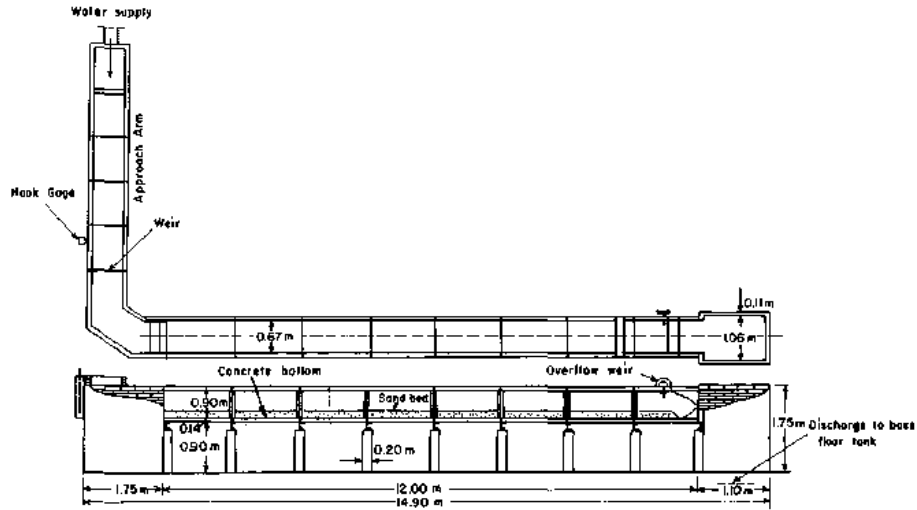


Figure 2.7: Test flume, plan and profile

- **Pier and scour depth**

Cylindrical piers with diameters of 6.7 cm, 5.7 cm, and 4.7 cm were tested. In the experiments, the maximum scour depths around the bridge piers d_s , were measured against time t , relative to the initial bed level using a vertical scale attached to the interior wall of hollow Plexiglas pier with a stick having a small inclined mirror at its end.

- **Approach flow and flow measurement**

The flow rate in the flume is adjusted by a valve on the pipe. Then the corresponding head on the sharp-crested weir is measured. The upstream flow depth was varied between 4.5 cm to 16.5 cm.

During the experiments, the upstream valve was slowly adjusted without causing any disturbance to the bed material until the desired discharge was given to the flume and the velocities are stated as average bulk velocity. Only clear water conditions with a flatbed were studied. No sediment inflow was allowed into the scour hole from upstream.

- **Results**

The time variation of local scour depth around bridge piers is investigated. Total of 38 cylindrical pier tests were done in this study. The maximum duration of an experiment, was about six hours during which the final equilibrium scour depths were not achieved although the rate of scour did decelerate to smaller values for all experiments. It was observed that the maximum scour depths occurred at the midpoint of the upstream face of cylindrical and square piers.

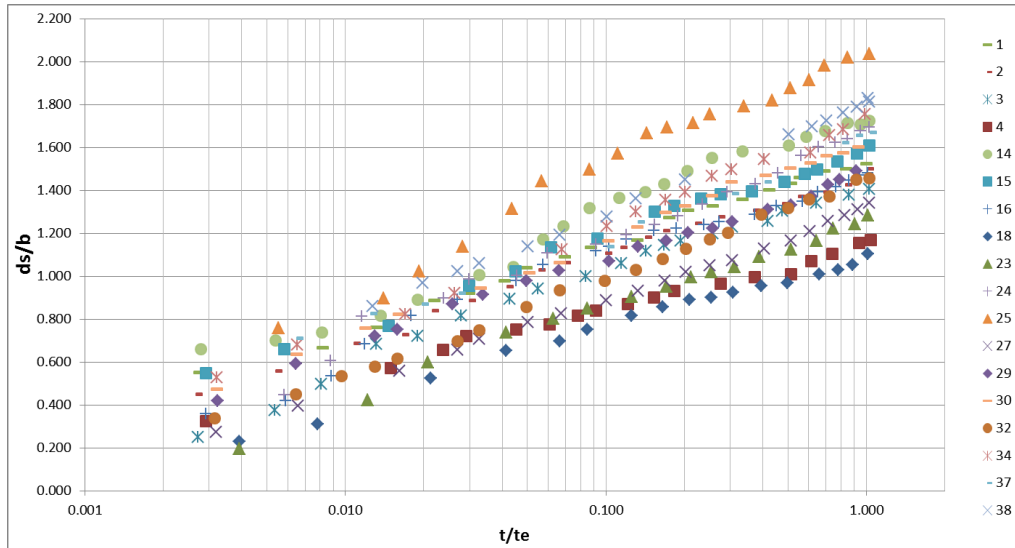


Figure 2.8: Scour data for cylindrical pier

2.2.1.7. Raikar and Dey (2005)

- **Introduction**

This study aims to investigate scour depth at circular and square piers in uniform and non-uniform gravels (fine and medium sizes, $4.10 \leq d_{50} \leq 14.25$ mm) under clear-water scour at limiting stability of gravels. The findings of the experiments were used to describe the effects of gravel size and gradation on scour depth, including time variation of scour depth.

- **Hydraulic models**

Experiments were conducted in a flume that has length, width, and depth of 12, 0.6, and 0.7 m, respectively. Two types of pier models were used, namely circular and square, having different widths b , where only circular pier were taken into consideration for the purpose of the analysis.

- **The bed sediment**

The sizes and gradations of uniform gravels (fine and medium, $4.10 \text{ mm} \leq d_{50} \leq 14.25 \text{ mm}$) used in the experiments are furnished in the Table (2.10). The particle size distribution is less than 1.4 for uniform gravels.

d50(mm)	σ
4.10	1.13
5.53	1.10
7.15	1.08
10.25	1.16
14.25	1.09

Figure 2.9: Uniform sediments size and gradations

- **Pier and scour depth**

Circular pier size with 32, 38, 60 and 77 cm were used in this experiment. The instantaneous scour depth at a pier was measured observing the position of the base of the scour hole by sliding a periscope up and down the pier. After the run was stopped, the maximum equilibrium scour depth d_s was then carefully measured by a vernier point gage.

- **Approach flow and flow measurement**

All experiments were run at constant upstream flow depth of 0.25 m, maintaining a clear-water scour condition by adjusting the upstream flow condition for a period of 18–36 h until the scour equilibrium was reached. The method for measuring the upstream flow measurement is not reported by the author.

- **Results**

16 series of time variation of local scour depth around cylindrical piers were provided by the author for the purpose of this study analysis and the remaining four test results were used as isolated data (Total of 20 tests).

2.2.1.8. Chabert and Engeldinger (1956)

- **Introduction**

In this study, additional experimental result of Chabert, J. and Engeldinger, P. (1956) was used that relate to circular piers in a sandy bed.

- **Hydraulic models**

A rectangular channel with variable inclination was used in this study. The total length was equal to 21 m and the width of the channel remains constant in all of the tests and it was equal to 0.8 m. The slope of the channel was able to change between 0 to 10%. The schematic view of the channel is illustrated in figure 2.11.

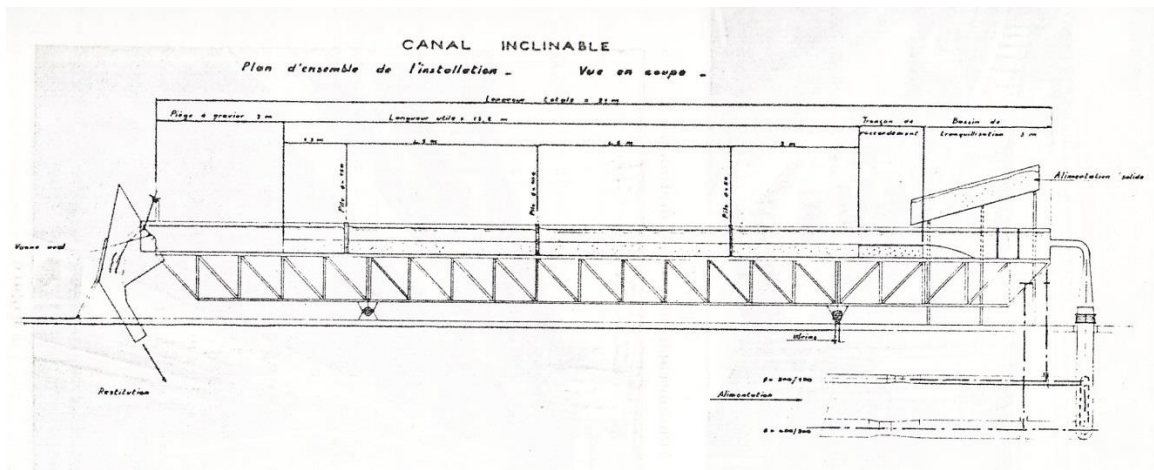


Figure 2.10: Test flume from Chabert and Engeldinger (1956)

- **The bed sediment**

Two different sediments were used with median size d_{50} equal to 1.5 and 0.52 mm with constant sediment standard deviation equal to 1.39 and with density equal to 2680 kg/m^3 .

- **Pier and scour depth**

In these tests, three different circular piers with diameter equal to 0.05, 0.075, 0.1 m were used. The scour depth evolution was measured by point gauge around circular piers.

- **Approach flow and flow measurement**

Flow depth varies between 0.1 m to 0.35 m. The approach flow velocity was reported in terms of average bulk velocity for all the experiments.

- **Results**

Total number of 12 series was obtained from Chabert, J. and Engeldinger, P. (1956). Table 2.14 gives the values of the fundamental physical, geometrical and kinematic quantities of these tests.

	t test duration	ds measured scour	σ	h flow depth	b pier width	d50	u Velocity	ρ	lc channel Width
	[hr]	[m]	[-]	[m]	[m]	[m]	[m/s]	[kg/m ³]	[m]
1	233.83	0.114	1.39	0.35	0.05	0.0015	0.325	2680	0.8
2	139.13	0.112	1.39	0.1	0.05	0.0015	0.375	2680	0.8
3	210.75	0.124	1.39	0.2	0.05	0.0015	0.350	2680	0.8
4	227.25	0.191	1.39	0.2	0.1	0.0015	0.350	2680	0.8
5	116.13	0.114	1.39	0.35	0.05	0.0015	0.375	2680	0.8
6	113.81	0.194	1.39	0.35	0.1	0.0015	0.375	2680	0.8
7	156.28	0.080	1.39	0.2	0.05	0.00052	0.245	2680	0.8
8	156.28	0.113	1.39	0.2	0.075	0.00052	0.245	2680	0.8
9	72.73	0.110	1.39	0.2	0.05	0.00052	0.325	2680	0.8
10	119.25	0.103	1.39	0.35	0.05	0.00052	0.305	2680	0.8
11	73.85	0.136	1.39	0.2	0.1	0.00052	0.325	2680	0.8
12	143.11	0.103	1.39	0.2	0.05	0.00052	0.325	2680	0.8

Table 2.14: Chabert, J. and Engeldinger, P. (1956) test characteristic Summary

2.2.1.9. Mignosa (1980)

- **Introduction**

In addition to data mentioned above, 13 series were employed from experiment done by Mignosa, P (1980).

- **Hydraulic models**

A rectangular channel was used in this experiment. The channel length and width were equal to 5 m and 0.495 m respectively and the slope of the channel was zero.

- **The bed sediment**

In this study, synthetic sediment with only one size is used with d_{50} equal to 2.5 mm, σ equal to 1.39 and density equal to 1180 kg/m^3 .

- **Pier and scour depth**

Two pier sizes equal to 0.0267 m and 0.048 m were used. The scour depth around piers was measured by point gauge.

- **Approach flow and flow measurement**

In this study, a recirculating system with the capability of flow discharge up to 30 lit/s was used. Approach flow depth varies between 0.125 to 0.127 meter and all of the velocity quantities are given as average bulk velocity by the author.

- **Results**

The final results and the duration of each experiment are summarized in table 2.15.

#	t test duration	ds measured scour	σ	h flow depth	b pier width	d50	u Velocity
	[hr]	[m]	[-]	[m]	[m]	[m]	[m/s]
1	216.00	0.0555	1.39	0.126	0.0267	0.0025	0.136
2	216.00	0.0795	1.39	0.126	0.0480	0.0025	0.136
3	213.50	0.0545	1.39	0.125	0.0267	0.0025	0.141
4	71.00	0.0525	1.39	0.126	0.0267	0.0025	0.139
5	71.00	0.0720	1.39	0.126	0.0480	0.0025	0.139
6	190.50	0.0642	1.39	0.125	0.0267	0.0025	0.150
7	190.50	0.0855	1.39	0.125	0.0480	0.0025	0.150
8	166.50	0.0940	1.39	0.127	0.0480	0.0025	0.161
9	213.50	0.0638	1.39	0.125	0.0480	0.0025	0.141
10	95.50	0.0458	1.39	0.127	0.0480	0.0025	0.170
11	95.50	0.0980	1.39	0.127	0.0480	0.0025	0.170
12	237.50	0.0422	1.39	0.127	0.0480	0.0025	0.183
13	237.50	0.0960	1.39	0.126	0.0480	0.0025	0.185

Table 2.15: Mignosa, P. (1980) test characteristic Summary

2.2.1.10. Franzetti et al (1989)

One series from Franzetti et al (1989) was obtained for using in analyses.

- **Hydraulic models**

A rectangular channel with 7 m length and 0.495 m width was used in this study.

- **The bed sediment**

The bed sediment was made by synthetic material with specific weight equal to 11571 N/m³ and d₅₀= 2.5 mm.

- **Pier and scour depth**

A smooth metallic circular pier was used with b=4.8 cm. The reading of the maximum scour depth at upstream of the pier and also the scour evolution was carried out by using a hydrometer.

- **Approach flow and flow measurement**

A recirculating system was used in this study. The upstream fellow velocity was measured in terms of average bulk velocity.

- **Results**

The final result of this experiment is shown in figure 2.12.

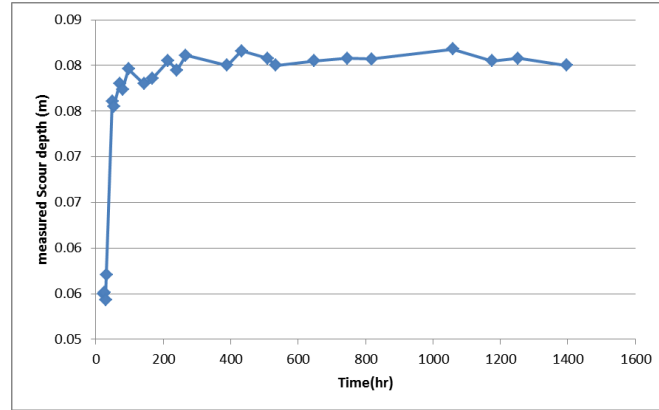


Figure 2.11: Scour depth with respect to time trend taken from Franzetti et al.'s (1981) experiment

2.2.1.11. Azzaroli (1983)

Moreover one more series from Azzaroli, D. (1983) is used in this study; characteristics of the work were obtained through personal communication. In table 2.16 the parameters of this test are provided. The velocity is given in terms of average bulk velocity. The scour depth time evolution is indicated in figure 2.13.

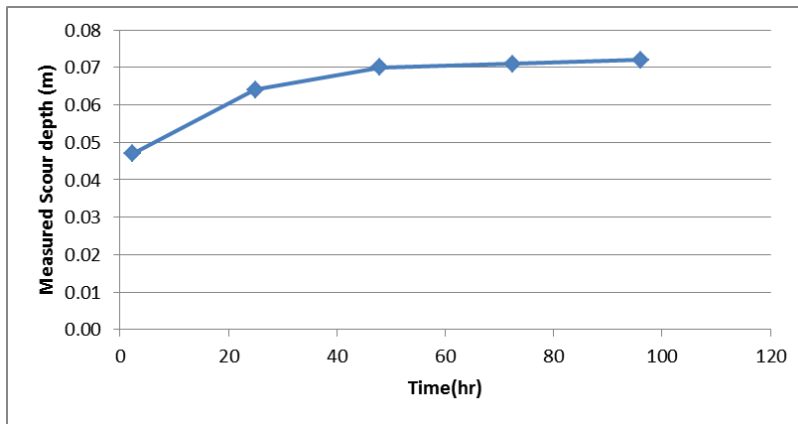


Figure 2.12: Scour depth with respect to time graph taken from Azzaroli, D.'s (1983) experiment

code	t real time	ds measured scour	σ	h flow depth	b pier width	d50	u velocity	ρ	lc channel Width
	[hr]	[m]	[-]	[m]	[m]	mm	[m/s]	[kg/m ³]	[m]
Azzaroli, D. (1983)	96.17	0.0720	1.32	0.098	0.0300	0.98000	0.285	2635	0.500

Table 2.16: Franzetti et al (1989) and Azzaroli, D. (1983) tests characteristic Summary

2.2.2. Isolated scour depth points

In this study use has been made also of 97 isolated points that was previously collected by Paleari (2014). These data refer to different experiments by various authors. The Table 2.2 provides a brief summary of the available isolated points. A precise check has been made to verify the validity of collected data.

CHAPTER 3

DATA ANALYSIS

3.1. Introduction

This chapter is devoted to three main parts, first, the selection of appropriate tests according to the test selection criteria, second, analysis of the of the selected tests and finally, comparison of the obtained model with previous studies.

The data which are presented in the previous chapter are not unified due to the fact that these data are collected from different experiments done by different authors. Therefore, unification process is the objective of the analysis.

One of the most important parameter that characterizes the evolution of scour depth is flow velocity, as it appears in two out of four effective dimensionless parameters (T and U). Velocity is typically made dimensionless by the critical velocity for inception of sediment motion.

In order to choose an appropriate criterion to estimate the value of u_c^* , which is the threshold shear velocity for initiation of sediment motion the criteria presented in the previous study on this topic which is done by Seyed Kamran Jalali under supervision of Dr. Alessio Radice and Prof. Silvio Franzetti has been used.

According to the mentioned study, there are several methods for expressing the upstream flow velocity. It can be measured in terms of cross-sectional bulk average or as a depth-averaged velocity according to the researcher's choice. Thus, a formula tuned by Paleari (2014) was used for converting average bulk velocity to central velocity for data analysis. This formula was used to unify the method of velocity measurement among all the collected data, according to the idea that, the pier is located at the center of the flume in all of the experiments, the central depth-averaged velocity is a better indicator of velocity in this region compared to average bulk one.

A dimensionless framework is performed to analyze the unified data base. Thanks to this dimensionless framework and calibration of data, a scour function is derived.

Finally, the performance of the derived scour function is illustrated and it is also compared with some of the available predictive equations in the literature.

3.2. Selected threshold conditions

Particle at the riverbed would start to move when the destabilizing forcing moment become larger than the stabilizing moment of the weight force. Shields (1936) by introducing stability parameter τ_* show that, if its value reaches to a specific value τ_c^* the initiation of bed load transport occurs. It is also worthy to note that, for sediment particles in water, the Shields

diagram exhibits different trends corresponding to different turbulent flow regimes. Shields diagram is represented as a series of dispersed experimental point for defining τ_c^* with respect to Re^* and τ^* . Thus there is no function for finding the value of u_c^* for a given sediment median size, specific water and sediment density. This problem lead to the fact that there is no possibility to find unique value of u_c^* .

Various authors define different criteria for computing u_c , u_c^* and τ_c^* . The selected criteria here are the one presented by the previous study in which the proposed formula of several authors has been compared and a suitable final formula for computing stability parameters is given.

According to the before mentioned study, the most suitable criteria for finding the value of sediment incipient motion is *Melville & Coleman (2000)*. Therefore, in order to make all the experiments which are going to be used in the analysis uniform, *Melville & Coleman (2000)* criterion was used for computing the threshold of sediment motion for all the tests. As a result, new value of flow intensity is calculated for each experiment based on this criterion and U (u/u_c) value provided by the author is discarded.

Some of the experiments are presented by the velocity which is provided in terms of central velocity (average depth velocity) and on the other hand, some of them are provide the average bulk velocity. The following formula which is presented by Paleari (2014) is able to convert the average bulk velocity to central velocity with an acceptable approximation:

$$\frac{u_c}{u_m} = -16.48 \log\left(\frac{l_c}{D}\right) + (a \cdot \frac{\varepsilon}{D} + b) / (c \cdot \frac{\varepsilon}{D} + d) \quad (3.1)$$

Where u_c is the central velocity, u_m is the average bulk velocity, l_c is the width of the channel, ε is the bed roughness that assumed to be equal to d_{50} , D is hydraulic diameter and is equal to $4R$ where R is hydraulic radius of channel. Constant values of a , b , c and d are obtained by interpolation:

$$a= 0.582423, b= 0.001007, c= 0.019616, d= 5.07218E-05$$

For taking advantage of this formula, it is necessary to have a fully turbulent flow according to author, unless the formula results are not reliable. In the section 3.3.3, the choices made to select the data with fully turbulent flow are described.

As mentioned before, due to the fact that the pier is located at the center of the flume in all of the experiments, the central average depth velocity is a better indicator of velocity in this region compare to average bulk velocity.

3.3. Data selection

3.3.1. Introduction

For the purpose of selecting suitable experiments among the existing database various criteria were taken into consideration. The general goal for imposing these conditions is to disregard the experiments which were taken in special conditions that can affect the final interpolation for having a scour depth time evolution model.

As previously discussed, it is necessary to have constant values of different effective parameters when the dependency of two parameters on each other is under study. In database there would be some experiments that their results are not reliable because of failure in satisfying this stability condition during the experiments. Therefore, these experiments should be neglected to increase the quality of the analyses.

3.3.2. Selection Criteria

The same criteria as the previous study are taken for the selection of the series and isolated tests which are going to be considered in the data analysis. According to what is presented in the mentioned study, the following restrictions are applied:

- $H=(h/b) \geq 2$

As mentioned before, in this analysis the dependency on flow shallowness (H) is disregarded. In order to satisfy the need to simulate a condition in which the estimation of scour depth only depend on the pier size (b) rather than the flow depth (h), this limitation was imposed. In this way the condition would be restricted to narrow piers case as shown in figure 3.1.

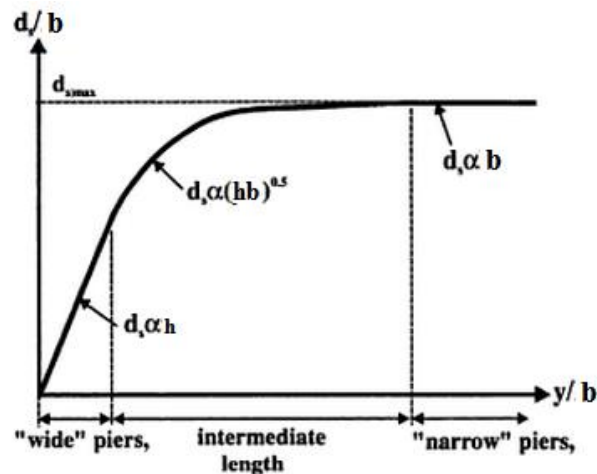


Figure 3.1: Local scour depth variations with respect to flow shallowness

- $L_c = (l_c/h) \geq 2$

In order to avoid the wall effect the ratio of width of the flow with respect to flow depth is considered to be greater than 2. Lateral walls may increase the complexity of flow movements around the piers and change the trend of scour depth evolution.

Thus together with choice of $L_c > 2$ and $H > 2$ it can be concluded that the ratio between pier width and width of flow (b/l_c) would be restricted to be greater than 0.25. In this case the contraction effects for narrow flows will be controlled. From the continuity principle, a decrease in flow area results in an increase in average velocity and bed shear stress and as a consequence, more bed material is going to remove from riverbed. Thus in narrow channel the local scour will increase compared to wide channel due to contraction effect and this condition should be avoided.

- $\sigma \leq 1.4$

Standard deviation of sediment particle size distribution is considered to be less than 1.4 to have an approximately uniform sediment distribution. For non-uniform sediments, armoring occurs on the channel bed. Armor layer formation within the scour hole reduces the local scour depth.

- $d_{50} \geq 0.5 \text{ mm}$

For clear water scour, the sediment median size of the acceptable experiments is considered to be greater than 0.5 mm to avoid the effects of ripples. The formation of ripples with fine sands limits the scour depth observed in laboratory experiments under clear-water conditions, because ripples can form sub-threshold condition.

- $T = \frac{t.u}{b\sqrt{\Delta}} \geq 10^6$

Time plays an important role in scour and under clear-water conditions scour evolves very slowly and scour depth tend to reach its equilibrium condition after long duration.

Measurements of scour depth at initial phases due to high rate of evolution of scour holes may have high level of uncertainty and by increasing time duration these errors will become less and it is possible to do the interpolation process with more reliability. In this regard, the test with dimensionless time (T) more than 10^6 has been selected.

3.3.3. Flow regime verification

In order to have an integrated database, it is necessary to compute central velocity (average depth velocity) for tests that the value of velocity is given in term of average bulk velocity. As mentioned in section 3.2, for this conversion and using the existing formula, it is mandatory to have a fully turbulent regime.

Friction factor was estimated for each of the tests by Colebrook-White formula (Colebrook 1939) as follow:

$$\frac{1}{\sqrt{f}} = -2.0 \log_{10} \left(\frac{k_s}{3.71D_H} + \frac{2.51}{Re\sqrt{f}} \right) \quad (3.2)$$

Where k_s is the equivalent sand roughness height that can be assumed equal to d_{50} and D_H is the hydraulic diameter. Equation (3.23) is a non-linear equation and it is necessary to do a nonlinear analysis for solving it. This task was carried out by Excel solver and the value of friction factor for each test was computed.

For distinguishing whether the test are in fully turbulent condition or is in transitional condition, the Reynolds values were compared to Reynolds value of case $Re^*=70$.

First, only the series experiments are considered to be inserted into the Moody diagram. There are totally 324 initial valid series tests which are shown in Figure 3.2. As it can be seen, a few portions of valid tests are in fully turbulent condition (109 tests) and most of the tests are in turbulent transitional conditions. As mentioned before, for the tests with fully turbulent condition, in case the corresponding velocity is in bulk velocity, it can be converted to the central velocity through the equation found by Paleari (2014).

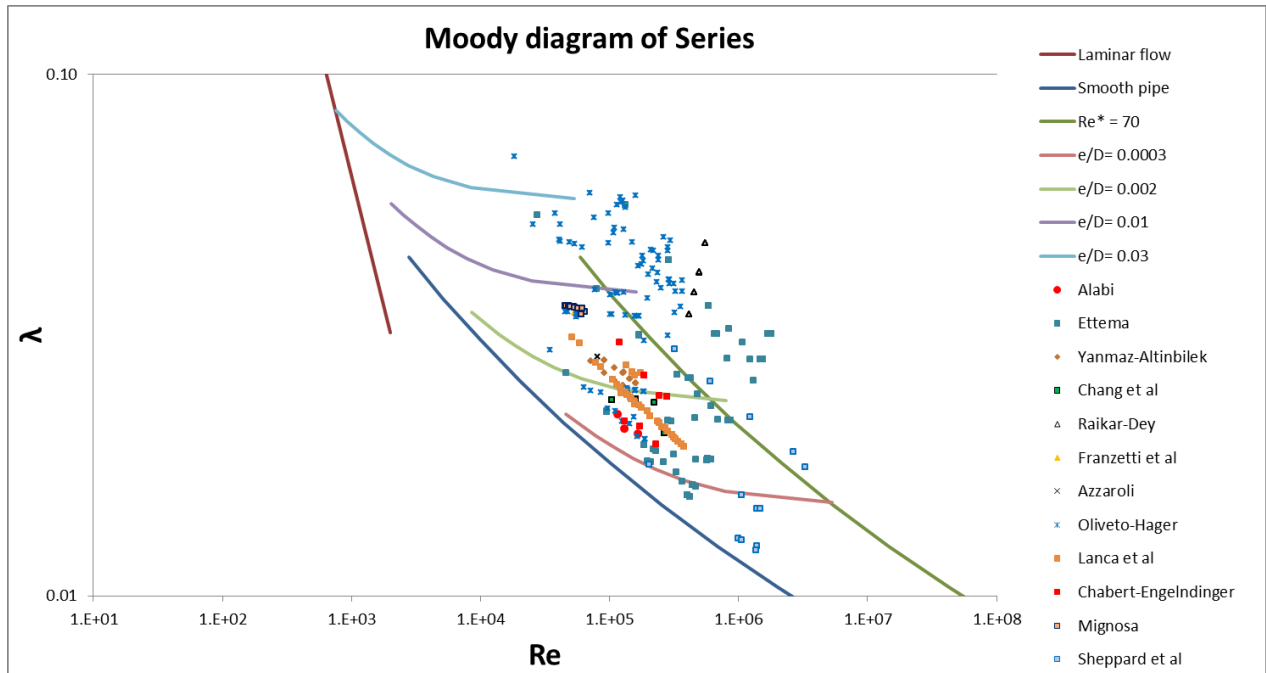


Figure 3.2: Position of all the experiments (series) on the Moody diagram

The distance of any hydrodynamic condition from the fully turbulent state can be quantified with the ratio λ/λ_{inf} that is the ratio of the resistance coefficient to the value of the latter in fully turbulent flow. Where λ_{inf} can be computed from the equation 3.3:

$$\lambda_{inf} = \left(-2 \times \log \left(\frac{\frac{d_{50}}{4RH}}{3.71} \right) \right)^{-2} \quad (3.3)$$

In principle, if the mentioned ratio is relatively small, a test may be considered as slightly transitional (almost fully turbulent). The table 3.2 shows the number of remaining test for considering different values of λ/λ_{inf} ratio.

λ/λ_{inf} Ratio	Fully Turbulent flow	$\lambda/\lambda_{inf} < 1.02$	$\lambda/\lambda_{inf} < 1.03$	$\lambda/\lambda_{inf} < 1.04$	$\lambda/\lambda_{inf} < 1.05$	$\lambda/\lambda_{inf} < 1.1$
Number of remaining test	109	134	146	166	208	282

Table 3.1: Remaining tests (series) for different values of λ/λ_{inf}

As the tests with the ratio $\lambda/\lambda_{inf} < 1.05$ are almost in fully turbulent flow, it is decided to consider these tests as fully turbulent flow so in case the corresponding velocity is presented in bulk velocity by the author it can be converted to the central velocity through the equation found by Paleari (2014).

Therefore, the entire tests within this range will be considered for the further analysis. The final selected tests are depicted in the figure 3.3 with red circles.

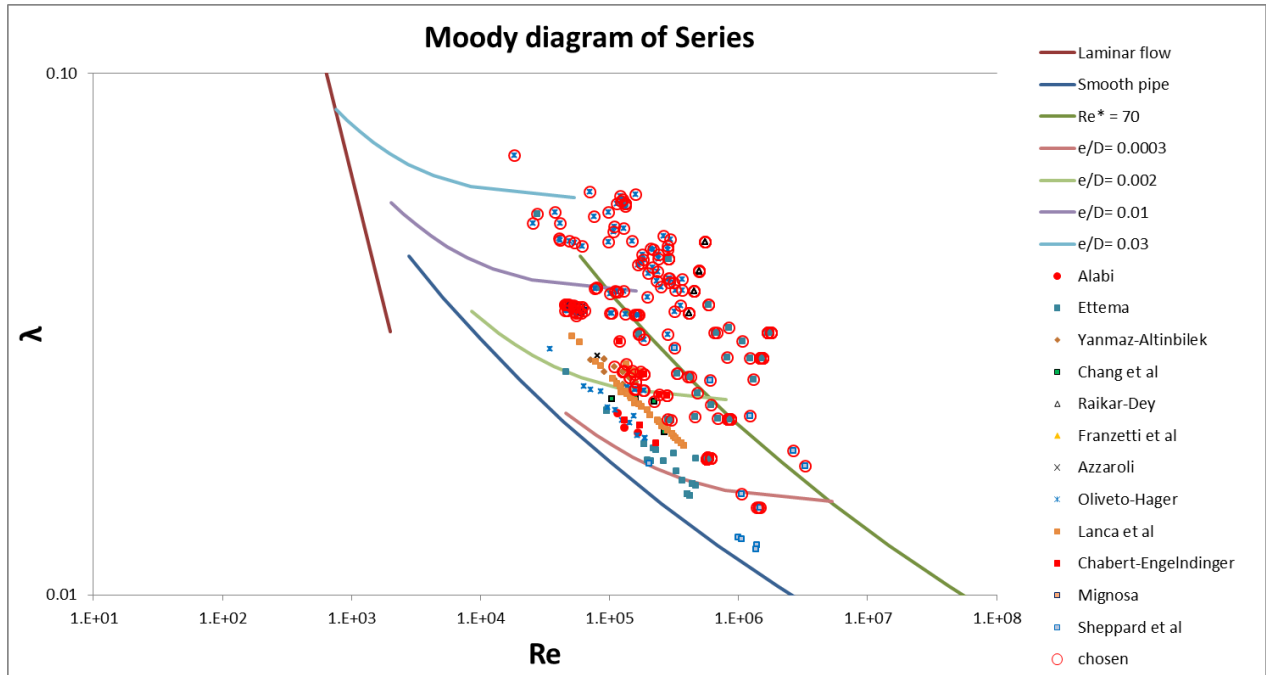


Figure 3.3: Chosen experiments (series) on the Moody diagram

Second, the isolated points and series are added to the Moody diagram at the same time. The same procedure is taken to choose the tests. Hence, there are 324 initial valid series tests and 97 isolated points which are 421 tests in total that has been considered in this configuration. The entire 421 tests are inserted to the Moody diagram as it is depicted in figure 3.4.

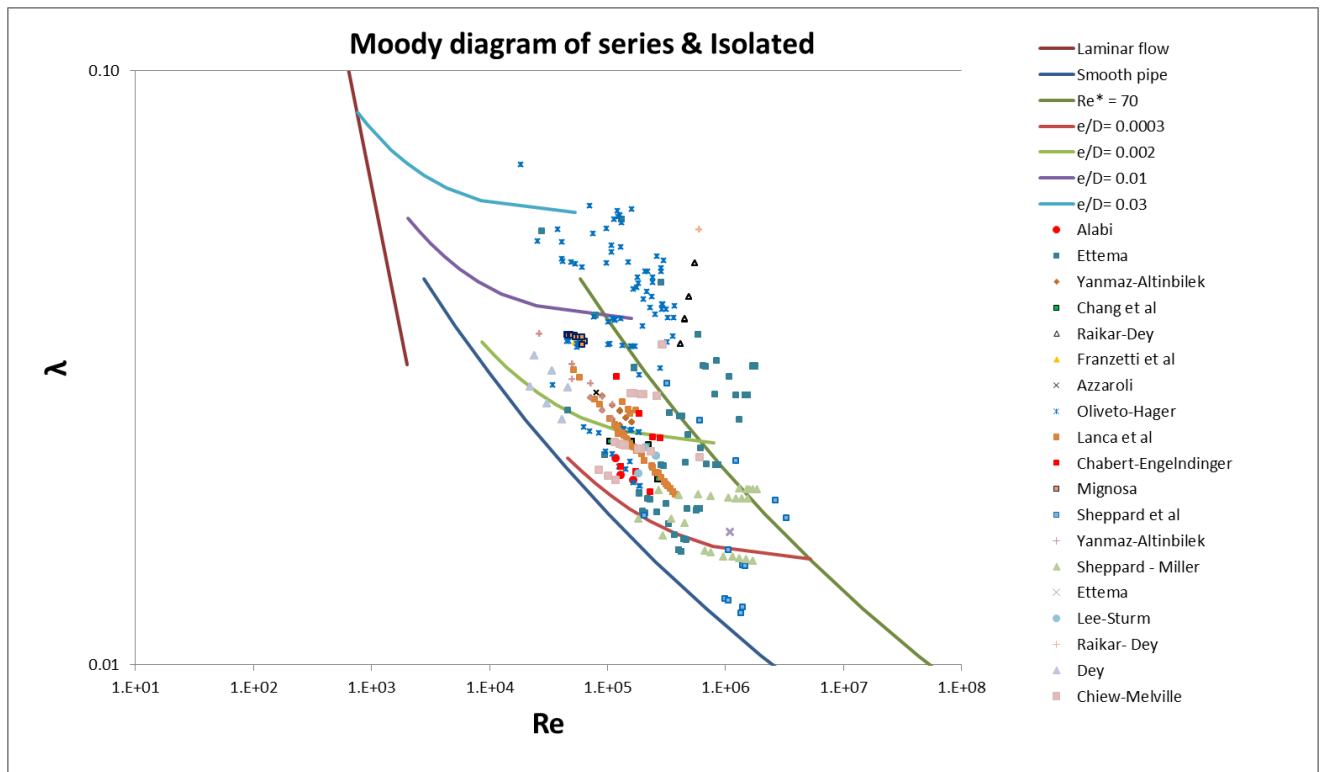


Figure 3.4: Position of all the experiments (series & Isolated) on the Moody diagram

The test with $\lambda/\lambda_{inf} < 1.05$ are depicted in Figure 3.5 with red circles. Table 3.2 shows the number of remaining test by considering different values of λ/λ_{inf} ratio. As can be seen there are 119 tests in fully turbulent condition and by considering the ratio $\lambda/\lambda_{inf} < 1.05$, 250 tests will remain.

λ/λ_{inf} Ratio	Fully Turbulent flow	$\lambda/\lambda_{inf} < 1.02$	$\lambda/\lambda_{inf} < 1.03$	$\lambda/\lambda_{inf} < 1.04$	$\lambda/\lambda_{inf} < 1.05$	$\lambda/\lambda_{inf} < 1.1$
Number of remaining test	119	152	170	201	250	359

Table 3.2: Remaining tests (series and Isolated) for different values of λ/λ_{inf}

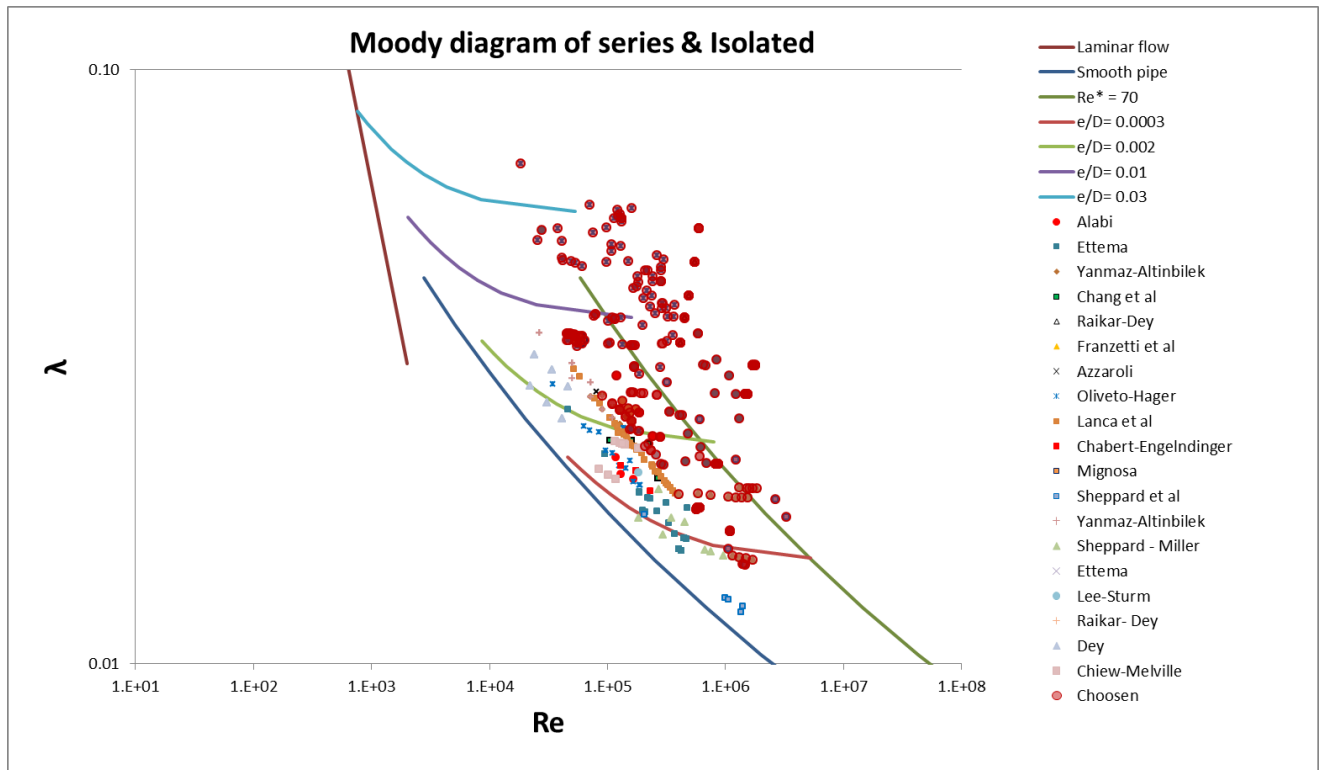


Figure 3.5: Chosen experiments (series & Isolated) on the Moody diagram

3.4. Scour trend

3.4.1. Dimensional scour trend

For final analysis which is mostly based on the series experiments, it is decided to use only data that satisfy the regime verification $\lambda/\lambda_{inf} < 1.05$. Therefore, Totally 208 tests test are considered in the following analysis.

The temporal trend of scour depth of the remained tests is depicted in figure 3.6. As can be seen, most of the tests have final scour time greater than 10^6 .

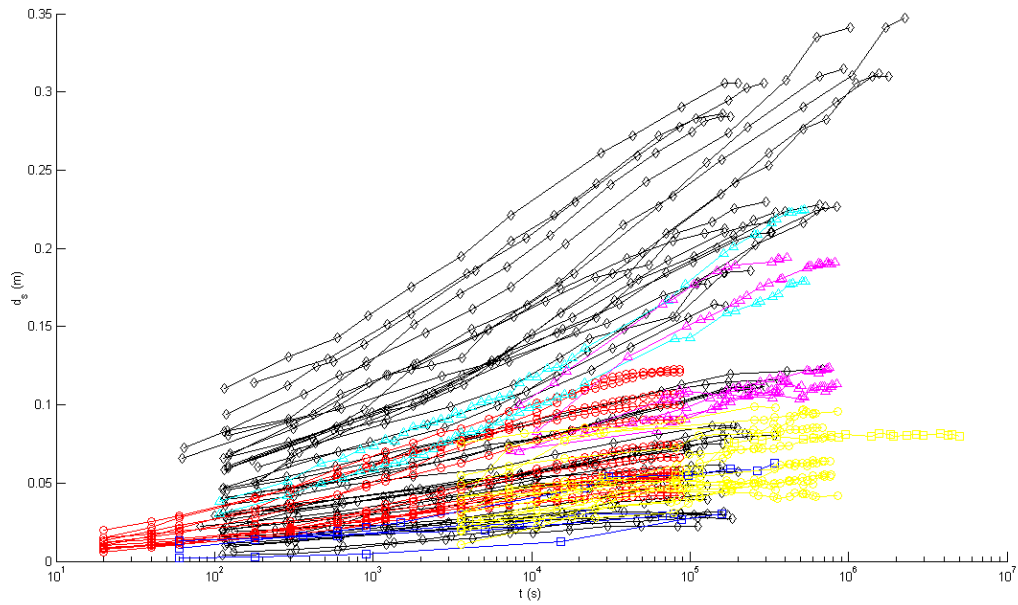


Figure 3.6: Temporal trend of scour depth (Dimensional)

3.4.2. Dimensionless scour trend

A basic normalization is performed to the dimensional temporal trend of scour depth of the valid data to have the data in a dimensionless form.

The experiments are presented in Ds-T plot. Where, Ds is dimensionless scour depth (ds/b) and T as mentioned before is dimensionless scour time ($\frac{t \cdot u}{b \cdot \sqrt{\Delta}}$).

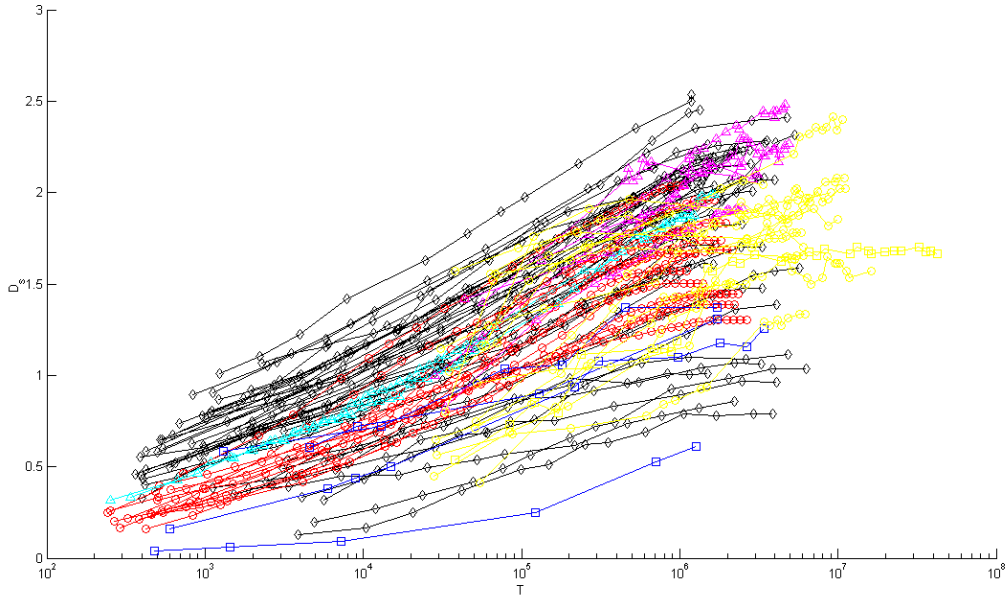


Figure 3.7: Temporal trend of scour depth (Dimensionless)

As can be seen, the dimensionless temporal trend of the scour depth is more concentrated than the dimensional one.

3.5. Strategy for data analysis

According to section 1.3.4 the form which can represent the scour depth as the function of dimensionless parameters is:

$$D_s = f(T, D_{50}, U, H) \quad (3.4)$$

$$\text{Where: } U = \frac{u}{u_c}, D_{50} = \frac{b}{d_{50}} \text{ and } T = \frac{tu}{b\sqrt{\Delta}}$$

Thus, the dimensionless Scour depth D_s , may be defined as a function of multiplication of control parameters:

$$D_s = f_1(T) \cdot f_2(D_{50}) \cdot f_3(U) \cdot f_4(H) \quad (3.5)$$

The functional relationships between dimensionless variables have to be obtained from experimental results and by means of interpolation. In this section, the effort has been made to verify the existence of possible dependency between dimensionless parameter. The procedure of finding a suitable equation for each of the dimensionless variables will be discussed in detail in the next section on the basis of the initial idea which is obtained in this section.

Thanks to the choices made in section 3.4.2 for selection of valid data, by considering $H \geq 2$ there is no need to take into account the effect of $f_4(H)$ and it is possible to neglect this function from the scour depth predictive formula. Therefore equation of dimensionless scour depth 3.5 can be presented as follow:

$$D_s = f_1(T) \cdot f_2(D_{50}) \cdot f_3(U) \quad (3.6)$$

3.5.1. Calibration of $f_2(D_{50})$, $f_3(U)$

In order to calibrate function $f_2(D_{50})$ and $f_3(U)$ two different dimensionless time $T=10^5$ and $T=10^6$ are selected. As mentioned before, when the dependency of two parameters on each other is under study it is necessary to have constant values of different effective parameters. In this regard, the flow intensity (U) of the tests is considered to be in the range $0.8 \leq U \leq 1.2$ as most of the tests are in this range. Then it is possible to calibrate $D_s = f_2(D_{50})$ and after that all the possible tests can be used to calibrate $D_s/f_2 = f_3(U)$. As a result, f_2 will have equation of type 3.7, while f_3 will have the equation of type 3.8.

$$f_2(D_{50}) = A D_{50}^B \exp(C D_{50}^D) \quad (3.7)$$

$$f_3(U) = E - F(G - U)^4 \quad (3.8)$$

The parameter A shall depend on the dimensionless time, while all the others shall be constants.

In order to find these unknown parameters, firstly, $f_2(D_{50})$ is calibrated for at dimensionless time $T = 10^5$ and $T=10^6$ by considering $0.8 \leq U \leq 1.2$ as follow:

The first step is to plot, D_{50} vs. D_s at dimensionless time $T = 10^5$ and $T=10^6$. Only those tests which have T larger than 10^5 and 10^6 are used respectively to create the plot at mentioned dimensionless times.

Due to the fact that the presented points by different authors are varying and they are not exactly at $T = 10^5$ and $T=10^6$, then an interpolation is needed to find the exact value of the scour depth at the mentioned dimensionless times. To this aim, interpolation of the scour depth values is developed with a Matlab code. Having inserted the points into the plot, the equation 3.7 is fitted in order to find the unknown parameters. The results are shown in the plots of figure 3.8 for series.

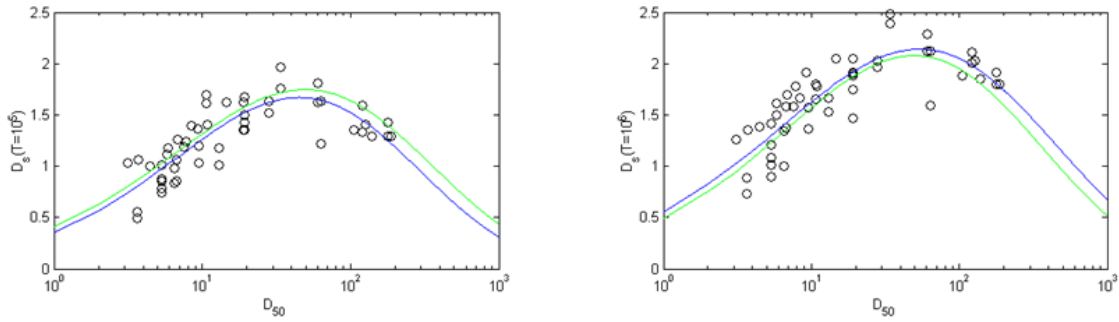


Figure 3.8: Calibration of $f_2(D_{50})$ for 10^5 and 10^6 (Series)

The same procedure is done to by considering the isolated and series at the same time. In the following graphs the isolated points are added to the graphs of figure 3.8. The same as the case that only series were taken to the consideration, to plot, D_{50} vs. D_s at dimensionless time $T=10^5$ and $T=10^6$ only those tests which have T larger than 10^5 and 10^6 are used respectively to create the plot at mentioned dimensionless times.

Since the isolated points are not presented at the mentioned dimensionless times, it is needed to use only the tests in a range. Therefore, the scour depth values with dimensionless time T in the range $10^5/K \leq T \leq 10^5 \times K$ and $10^6/K \leq T \leq 10^6 \times K$ are used. Where, K is considered to be equal to 3.

Plots of figure 3.9 and 3.10 show the calibration of $f_2(D_{50})$ for dimensionless times 10^5 and 10^6 respectively for the case that both series and isolated points are considered. Although the isolated points which are added are few, but they show the same trend as the series except for some of the presented tests by chiew and Melville which seem to be out of bound.

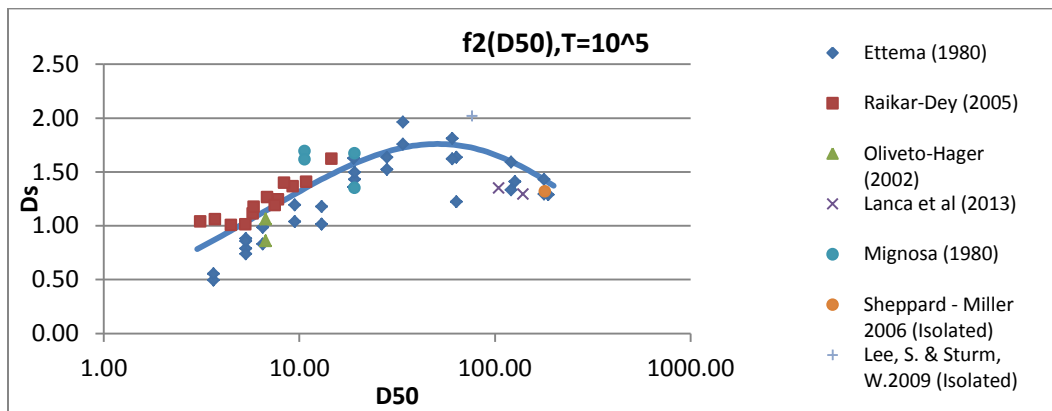


Figure 3.9: Calibration of $f_2(D_{50})$ for 10^5 (Series and Isolated)

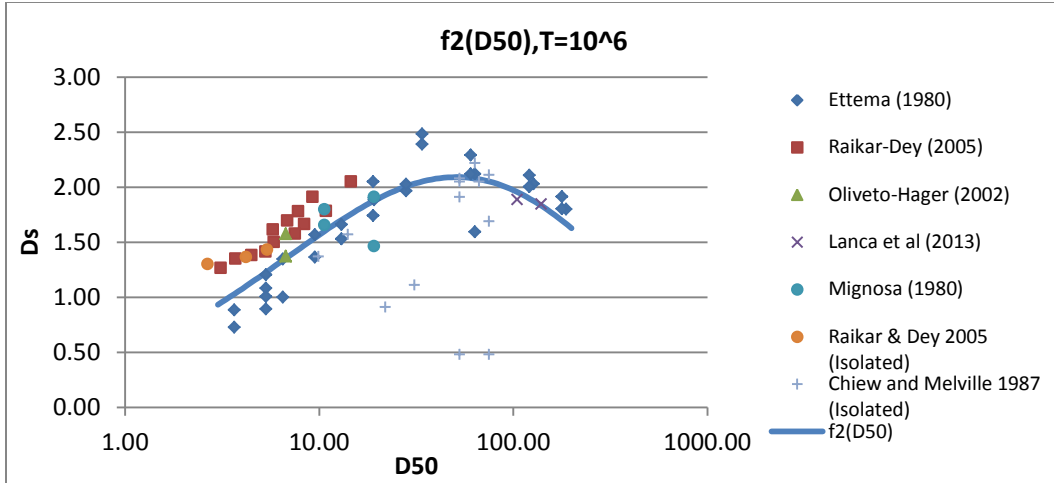


Figure 3.10: Calibration of $f_2(D_{50})$ for 10^6 (Series and Isolated)

The second step is to plot D_s vs. U . In order to calibrate $f_3(U)$ all the possible tests can be used to calibrate $D_s/f_2 = f_3(U)$.

The same as the previous case, the scour depth from the valid tests with dimensionless time T larger than 10^6 are considered to be inserted into D_s vs. U plot. Then the scour values are interpolated by Matlab code for the dimensionless time 10^5 and 10^6 .

Having inserted the points into the plot, equation 3.8 is fitted to find the unknown parameters. The plots of figure 3.11 depicts the points from series experiments and the fitted equation for dimensionless time 10^5 and 10^6 .

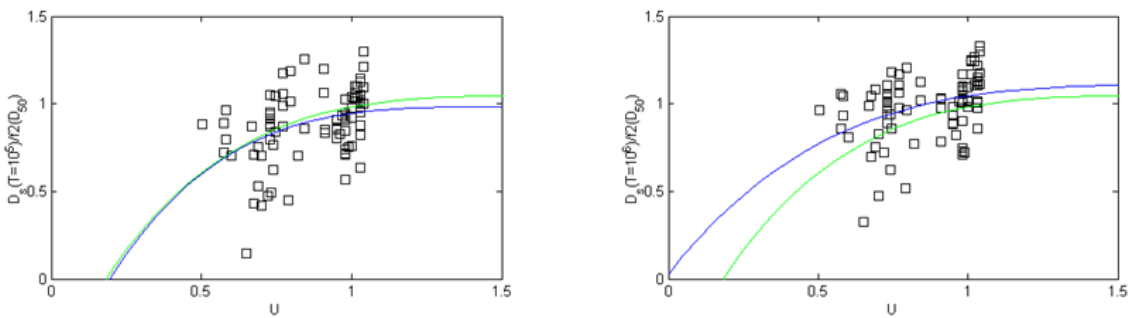


Figure 3.11: Calibration of $f_3(U)$ for 10^5 and 10^6 (Series)

In order to see the position of isolated points, they are added into the plots of figure 3.11. Similarly, the isolated points with dimensionless time greater than 10^6 are selected. Then, in order to plot the test at 10^5 and 10^6 , the test with dimensionless time in the range $10^5/K \leq \tau \leq 10^5 \times$

κ and $10^6/\kappa \leq T \leq 10^6 \times \kappa$ are used to create the corresponding plots. κ is considered to be equal to 3. In the following graphs both isolated points and series are depicted. As can be seen, the isolated points have the same trend as the series for most of the tests. Whereas, some of the tests of Chiew and Melville at $T=10^6$ are out of bound. The graphs of figure 3.12 and 3.13 show the isolated points and series for the dimensionless time 10^5 and 10^6 respectively.

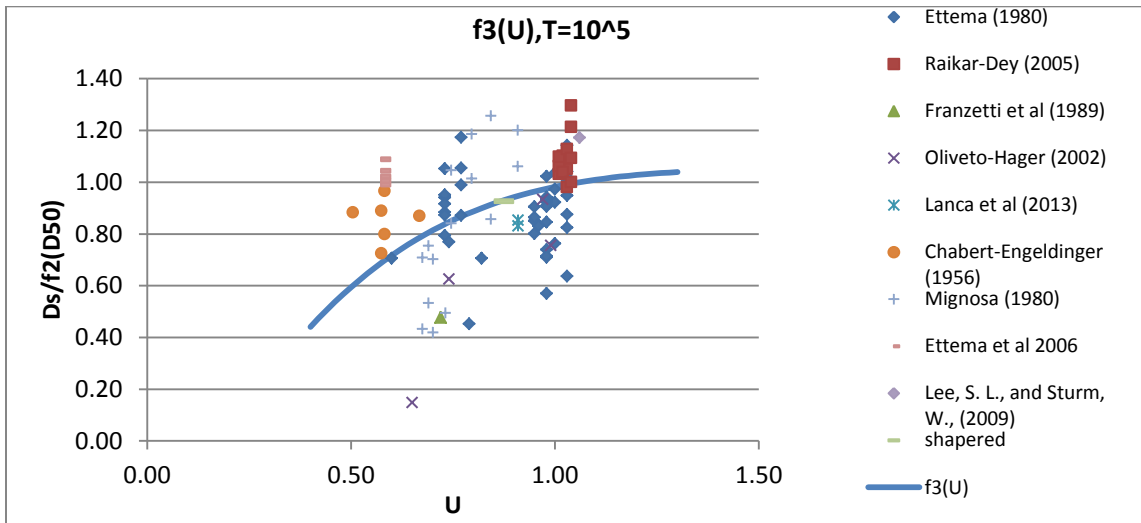


Figure 3.12: Calibration of $f_3(U)$ for 10^5 (Series and Isolated)

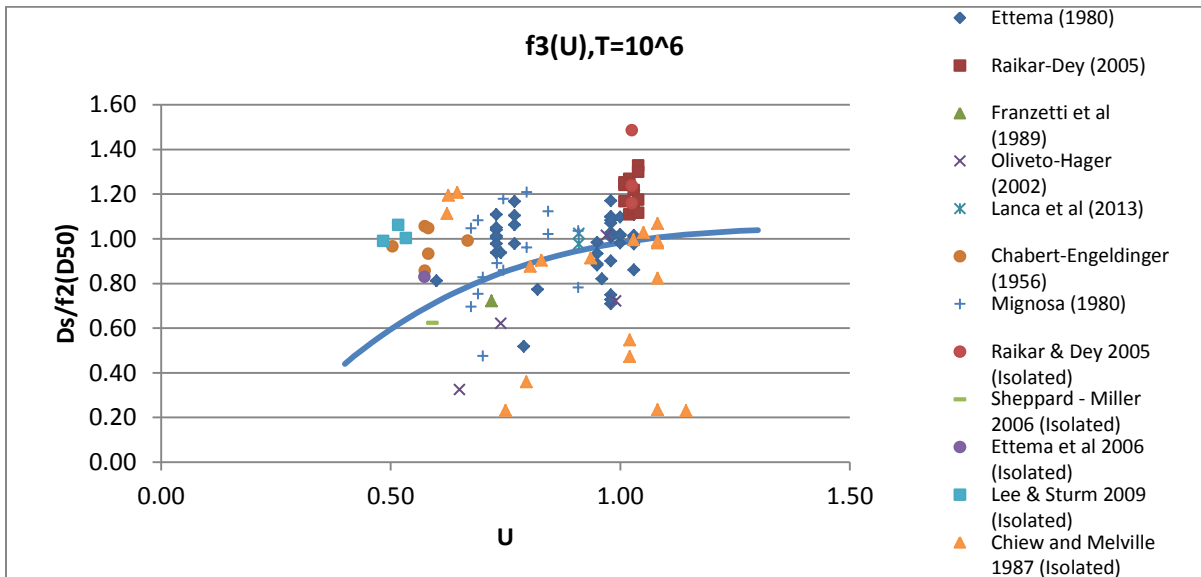


Figure 3.13: Calibration of $f_3(U)$ for 10^6 (Series and Isolated)

It is decided not to use the isolated points in the calibration of $f_2(D_{50})$ and $f_3(U)$ due to several reasons: first of all these points are proved to have the same trend as the series so they would not affect the fitted equation so much. Secondly, there are a few isolated points in the data base that can be used. Therefore, the equation will not be affected by them. Finally, some of the

isolated points seem to be out of bound so taking into account of these points will create a huge error in the computation of the unknown parameters of the equation 3.7 and 3.8.

According to what is mentioned above, the unknown parameters of equations 3.7 and 3.8 are computed by calibration of $f_2 (D_{50})$ and $f_3 (U)$ for $T=10^5$ and $T=10^6$ which is reported in the table 3.3.

	A	B	C	D	E	F	G
$T = 10^5$	4.6161	1.2656	-2.5563	0.2168	0.9838	0.2230	1.6462
$T = 10^6$	5.4920	1.0607	-2.2831	0.2051	1.1111	0.0684	1.9946
Average	4.6161 / 5.4920	1.1631	-2.4197	0.2109	1.0457	0.1457	1.8204

Table 3.3: Calibrated parameters at $T = 10^5$ and $T=10^6$

Substituting the calibrated parameters into equation 3.7 and 3.8 the following equations are produced:

$$f_2(D_{50}) = \left(\frac{4.62}{5.49} \right) D_{50}^{1.16} \exp(-2.42 D_{50}^{0.21}) \quad (3.9)$$

$$f_3(U) = 1.05 - 0.15(1.82 - U)^4 \quad (3.10)$$

According to the equation 3.10, the scour would be maximum for $U = 1.82$, that is not what one would expect from typical descriptions of the process where the maximum is around $U = 1$. However, considering that firstly, u_c has somehow lost the meaning of a threshold velocity and is just a scaling parameter in this analysis secondly, f_3 is however quite flat for $U > 1$. Finally, it is notable that the value of f_3 is zero for U around 0.2 since U is considered to be in the range $0.8 \leq U \leq 1.2$.

3.6. Effectiveness of $f_2 (D_{50})$ and $f_3 (U)$

Having calibrated the two functions, they can be included in the dimensionless scour trend. The plot created by taking into consideration these two functions will show the temporal development of $D_s/f_2/f_3$, but f_2 is not unique so the expression for $T=10^6$ is used to create the plot of figure 3.14 which depicts the dimensionless scour trend accounting for f_2 and f_3 .

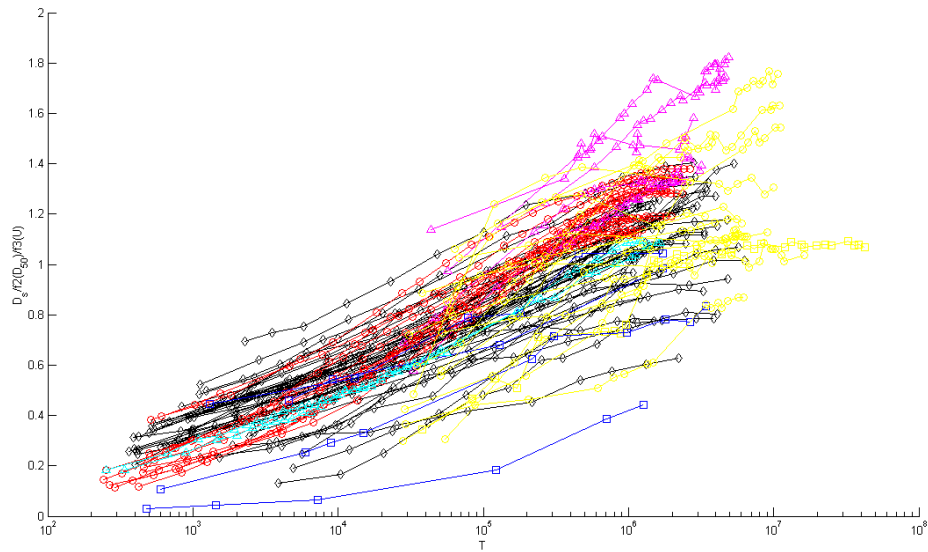


Figure 3.14: Dimensionless trend of scour trend considering f_2 and f_3 (Series)

3.7. Comparison of the point scatter

The point scatter in Figures 3.14, 3.6 and 3.7 are compared to check if considering calibration with f_2 (D_{50}) and f_3 (U) is beneficial or not. In this regard, dimensional times 10^3 , 3×10^3 , 10^4 , 3×10^4 and 10^5 and also dimensionless times 10^4 , 3×10^4 , 10^5 , 3×10^5 and 10^6 are considered. Then, for each chosen time and for each experiment a representative scour value is computed. Finally by interpolating over an interval from $t_0/3$ to $3t_0$, where t_0 is the time (dimensional or dimensionless) which is chosen as reference, samples of scour values are obtained.

Basic statistics such as mean, standard deviation, coefficient of variation, pdf of scour/mean are computed at the mentioned dimensionless times to depict the efficiency of f_2 and f_3 . Plots of figure 3.15 shows how these statistics would change by considering d_s , D_s and $D_s/f_2/f_3$.

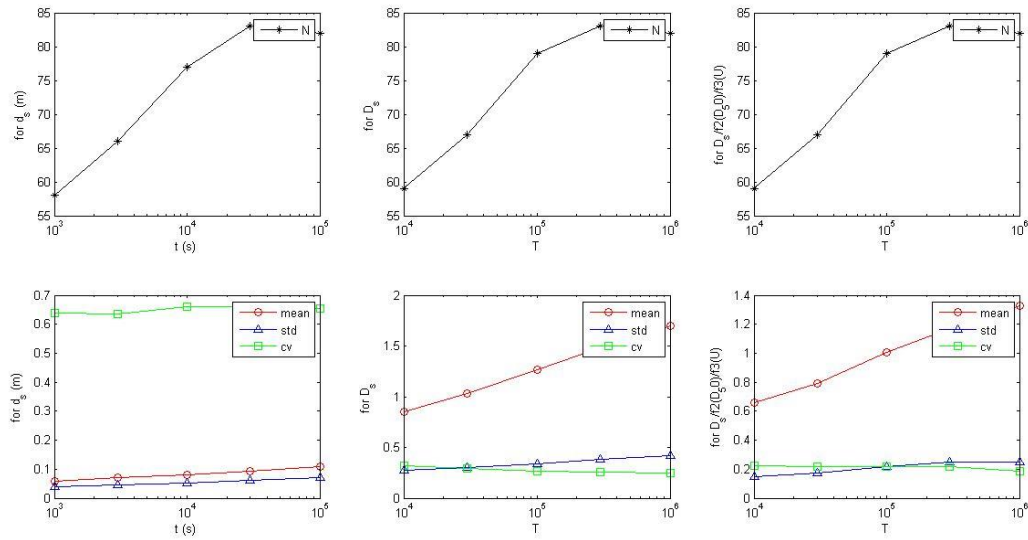


Figure 3.15: Comparison of sample statistics

Another way to compare the simple dimensionless scour trend (by considering D_s) with the one which is done by considering $D_s/f_2/f_3$ is to compare the coefficient of variation.

Table 3.4 contains the values of coefficient of variation for dimensionless time 10^4 , 3×10^4 , 10^5 , 3×10^5 and 10^6 .

	$T = 10^4$	$T = 3 \times 10^4$	$T = 10^5$	$T = 3 \times 10^5$	$T = 10^6$
CV(1) for D_s	0.3209	0.2973	0.2670	0.2572	0.2458
CV(2) for $D_s/f_2/f_3$	0.2259	0.2174	0.1993	0.2052	0.1879
Ratio CV(2)/CV(1)	0.7038	0.7312	0.7456	0.7980	0.7643

Table 3.4: Coefficient of variation

Figure 3.16 presents a graphical comparison of coefficients of variation for basic dimensionless trend and for the dimensionless trend accounting for f_2 and f_3 .

As can be seen, the difference of the coefficient of variation in these two cases is significant at $T = 10^4$ being 0.22 while presenting the basic dimensionless and 0.32 while considering f_2 and f_3 .

The difference between coefficient of variation for these two cases decreases as moving to the dimensionless times 10^5 and 10^6 .

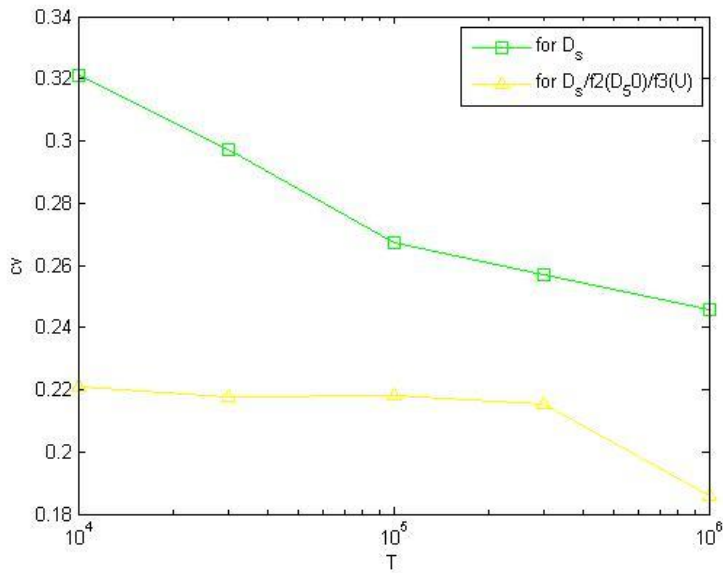


Figure 3.16: Comparison of coefficient of variation

Figures 3.17, 3.18 and 3.19 presents the pdf of scour/mean for the dimensional, dimensionless and dimensionless according to f_2 and f_3 which are referring to the plot of figure 3.14, 3.6 and 3.7 respectively.

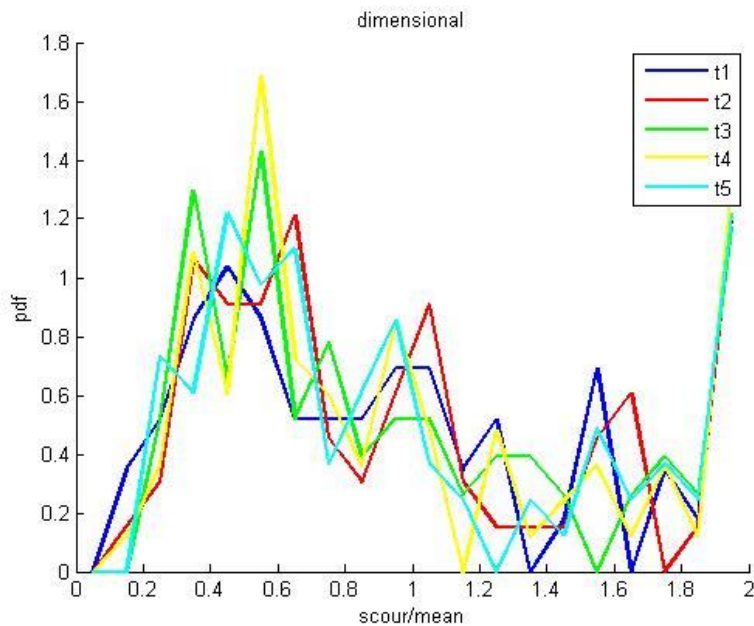


Figure 3.17: pdf of dimensional scour trend

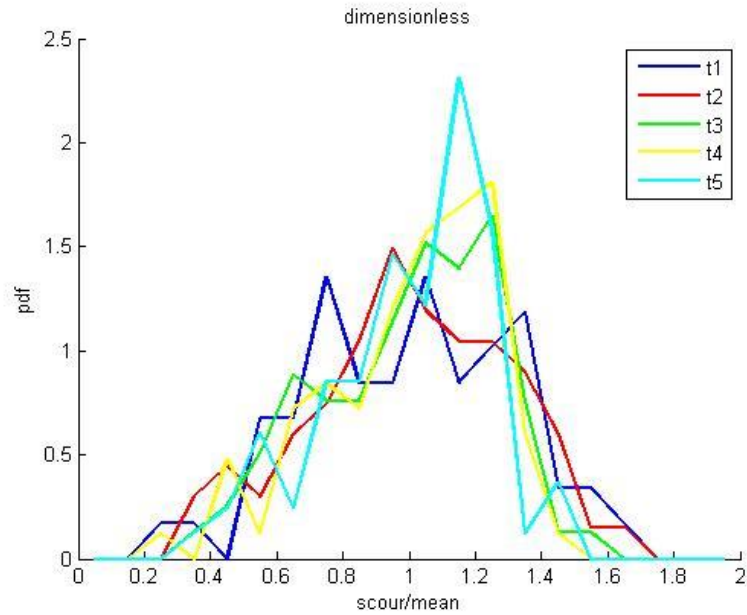


Figure 3.18: pdf of dimensionless scour trend

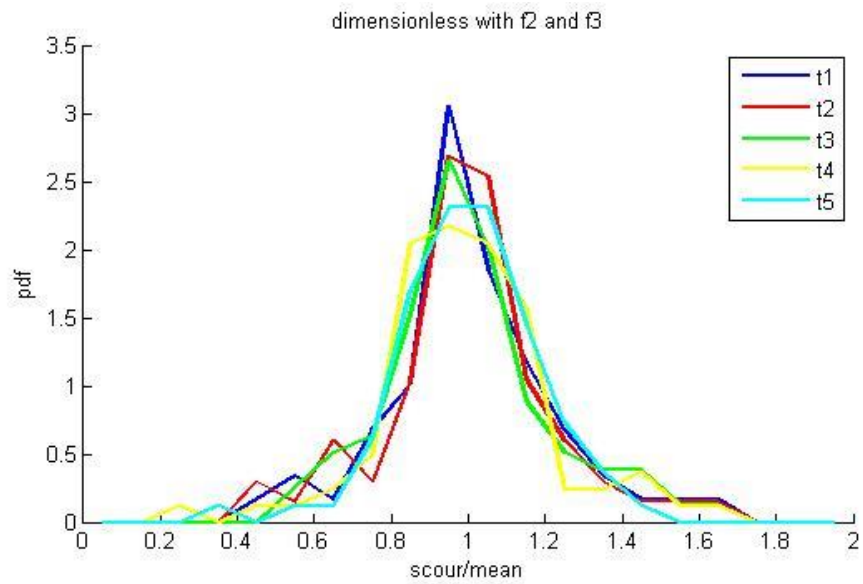


Figure 3.19: pdf of dimensionless scour trend according to f_2 and f_3

As can be seen, the pdf of scour trend has shown a significant improvement by normalization with f_2 and f_3 . It can be concluded that normalization with f_2 and f_3 is indeed beneficial and effective.

3.8. Estimation of temporal scour function

3.8.1. Series

The exponential temporal function which is introduced by Franzetti et al (equation 3.11) is considered to estimate the temporal scour depth. The values of M, P and R are suggested by the author to be 1, 0.028 and 0.33 respectively.

$$f_1(T) = M(1 - \exp(-PT^R)) \quad (3.11)$$

In order to estimate temporal scour function according to the equation 3.10, first, the temporal scour function for each series is computed by taking into account only the points with dimensionless time more than a limit (e.g. 10^5). Then a synthetic curve for each test is developed and used to create a point cloud for a global fit.

As a final step, considering the created curves for all the valid tests, a global temporal function is developed. Figure 3.20 shows the point cloud used for the global regression.

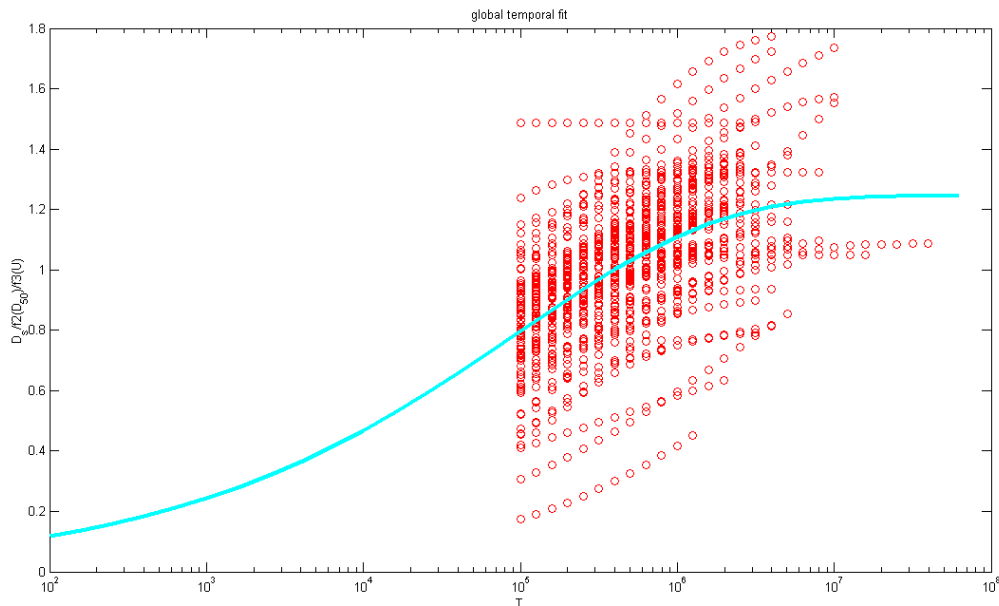


Figure 3.20: Global temporal regression

Due to the fact that, each researcher measured scour depth with different frequency, then, for some experiments scour depth is reported very frequently while for the rest of them it is reported only few times per experiment. Therefore, the values of the dimensionless scour depth is

interpolated for each test to have homogeneous tests in terms of spacing of the presented points in order to prevent overestimation of the global temporal regression.

After interpolation of the tests and obtaining homogeneous tests, the equation of 3.11 is fitted and the unknown parameters are obtained as follow: $M = 1.2464$; $P = 0.021$; $R = 0.336$. The plot of figure 3.21 depicts the fit of the obtained temporal function to the measured points.

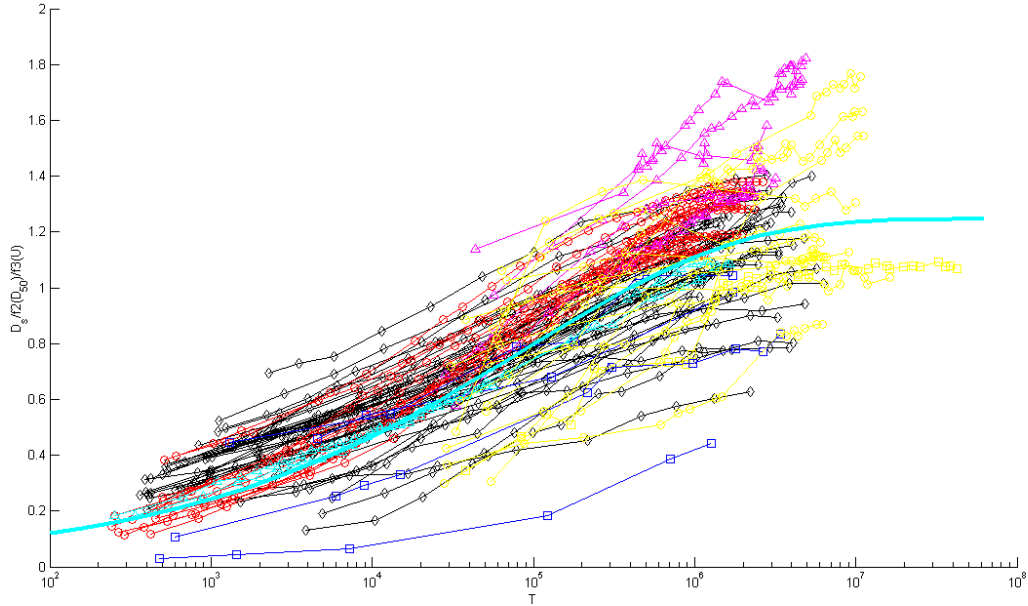


Figure 3.21: global temporal function (Series)

Table 3.5 shows the parameters of equation 3.11 both from the presented dimensionless process in this study by considering f2 and f3 and the original one which is suggested by Franzetti et al. As can be seen, the parameter M has increased significantly as the obtained value is 25% higher than the previous one. On the other hand, there is 25% decrease in the value of P in the obtained results. The parameter R has shown a minor change of about 2% increase in the obtained results.

Parameters	M	P	R
Franzetti et al	1	0.028	0.33
Obtained values	1.2464	0.021	0.336

Table 3.5: Comparison of the obtained and the original values of M, P and R

3.8.1.1. Dispersion of points

In order to characterize the performance of the final scour function, the measured dimensionless scour depth is compared with the one which is computed by the final scour function by taking into account the calibrated coefficients for all the valid tests.

Three reference times; 10^4 , 10^5 and 10^6 are chosen to investigate how the performance of the developed function would change over different dimensionless time.

For each of the mentioned dimensionless time, measured and computed values of dimensionless scour depth D_s are compared.

Figure 3.22 shows the measure vs. computed dimensionless scour depth for the mentioned dimensionless times within a $\pm 25\%$ deviation.

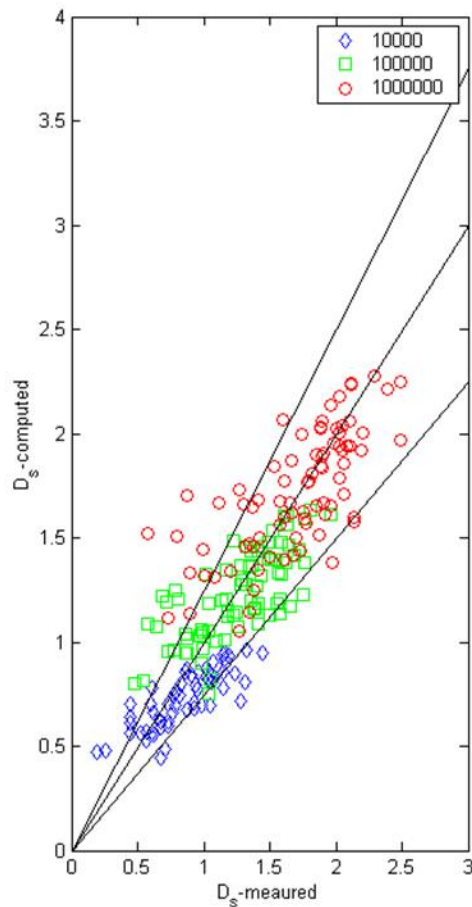


Figure 3.22: comparison of measured and computed D_s (series)

Moreover, PDF and CFD of the ratio D_s measured/ D_s computed are provided in figure 3.23 and 3.24. As can be seen, the performance of the function is increasing by considering higher values of T. Although the function does not show a good performance for $T=10_4$, which is reasonable as this time was excluded by fitting, but it works indeed better for the two other times since for 10^5 and 10^6 , about 80% of points fall within a $\pm 25\%$ deviation.

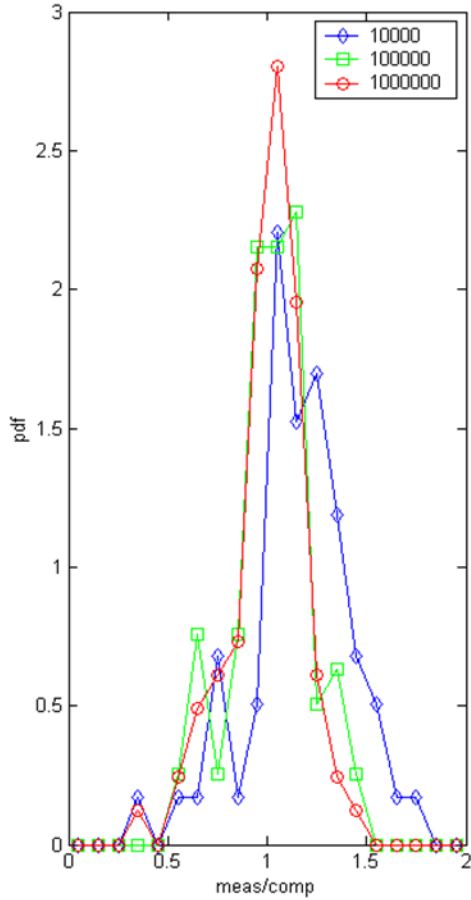


Figure 3.23: PDF of measured and computed D_s (series)

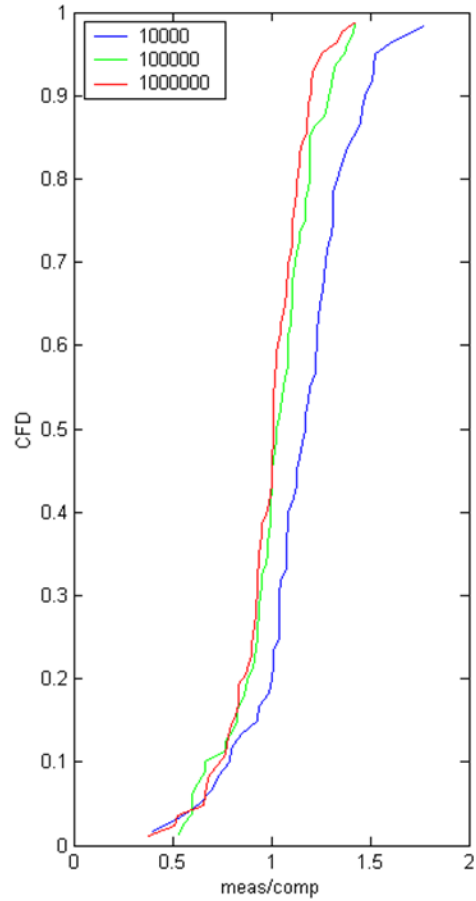


Figure 3.24: CDF of measured and computed D_s (series)

3.8.2. Series and Isolated points

The same procedure has performed by considering both series and isolated points. In this case all the valid isolated points are added to the plot of figure to investigate the effect of this point on the scour trend and to validate the equation.

Therefore, the valid isolated points are inserted to the plot of figure 3.21 as shown in the figure 3.25. Since the temporal function is developed, all the isolated points (with dimensionless time) can be considered.

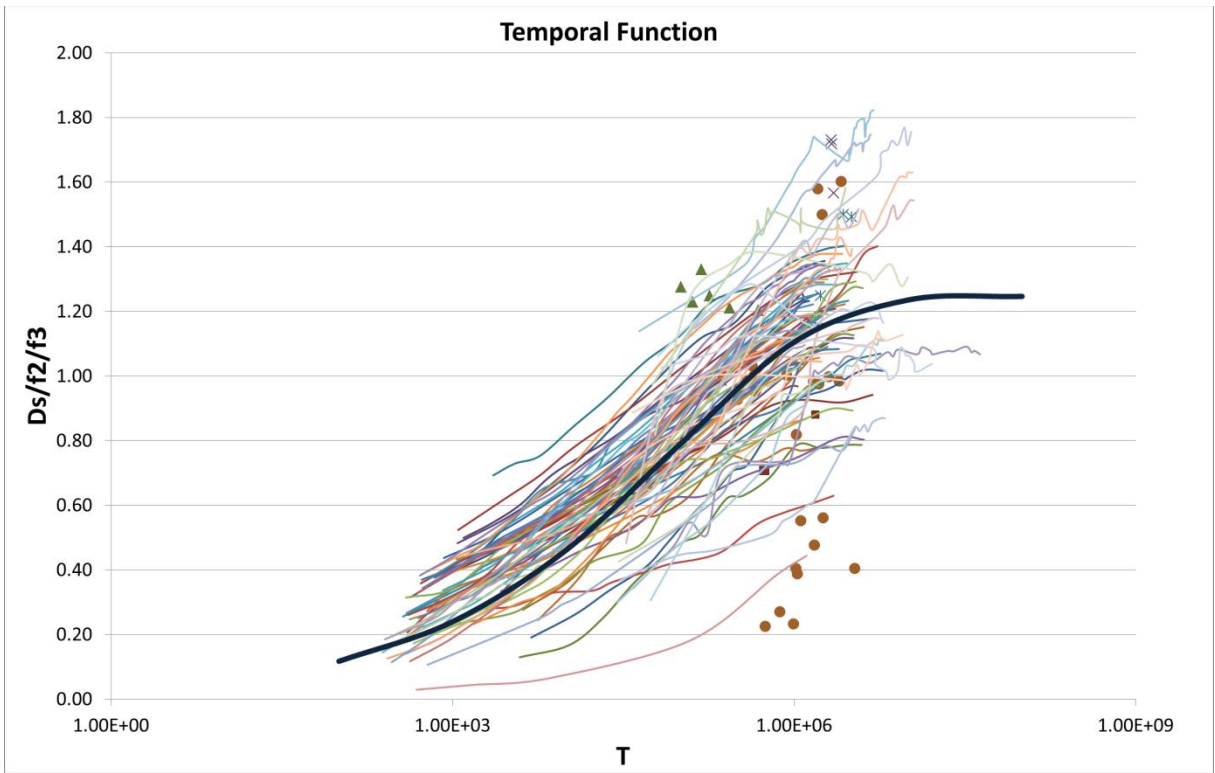


Figure 3.25: global temporal function (Series & Isolated points)

Similar to the previous case, by taking only the isolated points into the consideration, the isolated experiments are inserted into D_s measured vs. D_s computed plot (figure 3.26). The figure 3.27 and 3.28 show the PDF and CFD of the ratio D_s measured/ D_s computed of the isolated points.

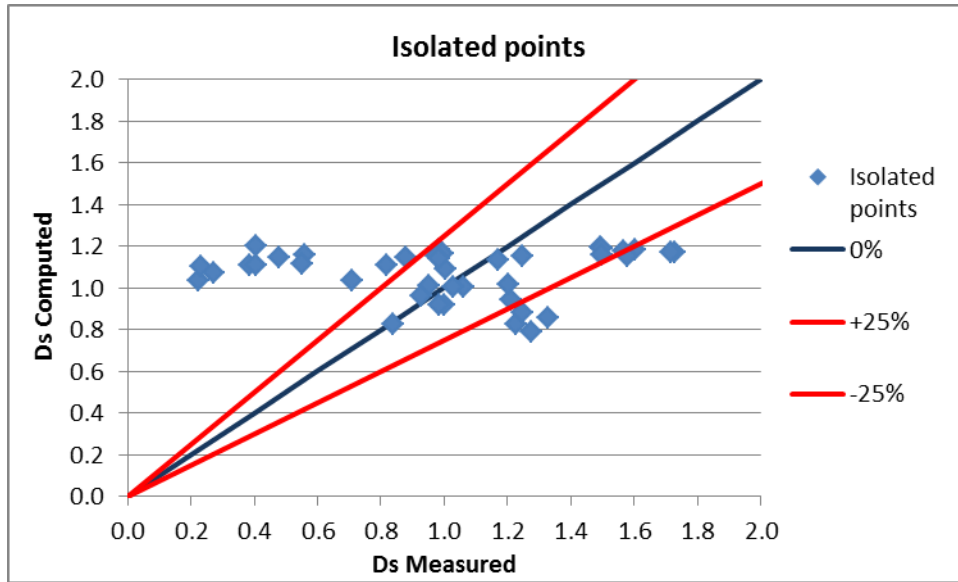


Figure 3.26: comparison of measured and computed D_s (Isolated points)

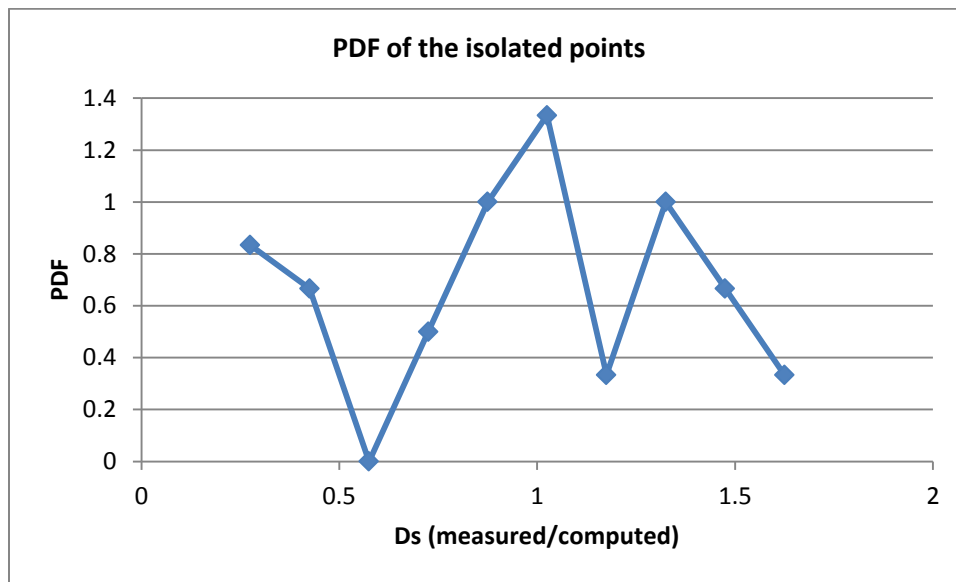


Figure 3.27: PDF of measured and computed D_s (Isolated points)

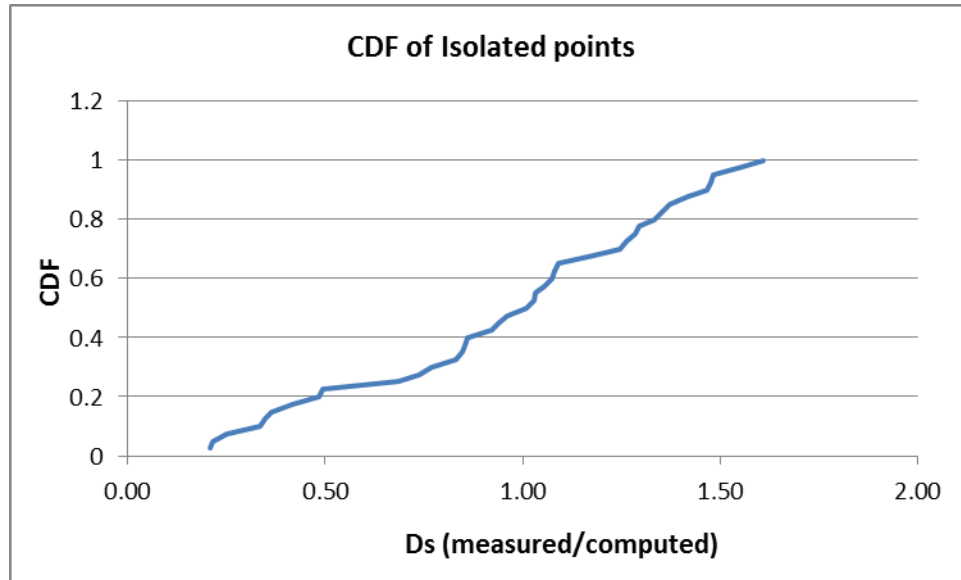


Figure 3.28: CDF of measured and computed D_s (Isolated points)

In conclusion, the control on the validity of the isolated points is much less than series experiments for example some of the isolated points from Chiew and Melville experiments are out of range in the plot of figure 3.25. On the other hand, there are a few isolated points which can be used to fit in the plots.

As a result, due to the mentioned reasons, it is decided not to consider the isolated points in the estimation of temporal scour function.

3.9. Model comparison with previous studies

According to section 1.3.5 there are several formulas for computing equilibrium local scour depth or its time evolution in literature. In this section the values of dimensionless scour depth, D_s , for valid data were computed by means of models provided by Melville & Chiew (1999) and Oliveto & Hager (2002). Thus it is possible to find out the ability of the proposed formula for computing D_s with acceptable precision in compare to previous models.

3.9.1. Melville & Chiew (1999)

In this part the formula presented by Melville and Chiew will be introduced and the efficiency of this formula will be evaluated.

In this model different factors are provided for each of the dependent parameters for estimation of scour depth as below:

Flow Intensity:

$$K_U = U \text{ for } U < 1 \text{ and } K_U = 1 \text{ for } U > 1 \quad (3.12)$$

Flow Depth-Pier Width:

$$K_H = 2.4 \cdot b \quad \text{for } \frac{b}{h} < 0.7 \quad (3.13)$$

$$K_H = 2 \cdot (h \times b)^{0.5} \quad \text{for } 0.7 < \frac{b}{h} < 5 \quad (3.14)$$

$$K_H = 4.5 h \quad \text{for } \frac{b}{h} > 5 \quad (3.15)$$

Particle Size:

$$K_{D_{50}} = 0.57 \log(2.24 \cdot D_{50}) \quad \text{for } D_{50} < 25 \quad (3.16)$$

$$K_{D_{50}} = 1 \quad \text{for } D_{50} > 25 \quad (3.17)$$

Time Factor:

The value of scour depth can be computed by the equation 3.18 as follow:

$$d_s = K_H \cdot K_U \cdot K_{D_{50}} \cdot K_t \quad (3.18)$$

For computing time factor K_t , it is necessary to compute the value of t_e which is the time to develop equilibrium scour depth. According to the author, t_e can be calculated by means of following relation:

$$K_t = \frac{d_s}{d_{se}} = \exp \left[-0.03 \left| \frac{u_c}{u} \ln \left(\frac{t}{t_e} \right) \right|^{1.6} \right] \quad (3.19)$$

$$t_e(\text{days}) = 48.26 \frac{b}{u} (U - 0.4) \quad H > 6 \quad (3.20)$$

$$t_e(\text{days}) = 30.89 \frac{b}{u} (U - 0.4) H^{0.25} \quad H \leq 6 \quad (3.21)$$

In order to compare the Melville and Chiew formula with the one which is developed in this study, first of all, the criteria of selection of the suitable isolated points and series which is mentioned before (section 3.3.2) are applied to all the valid data. Moreover, only the tests which are rigorously in fully turbulent condition are selected. Then, the selected data are inserted into the plot of figure 3.29 in which the axis are the one proposed by Melville and Chiew.

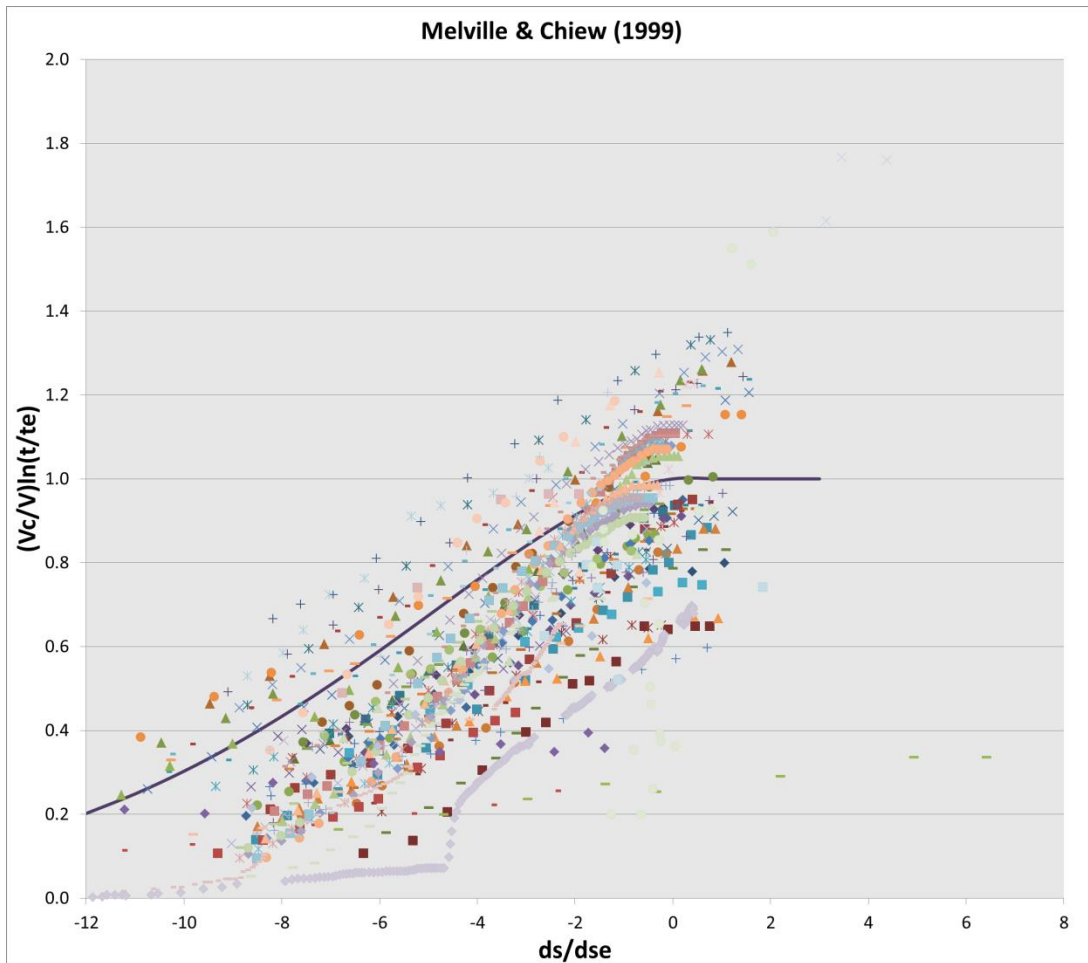


Figure 3.29: Melville & Chiew formula

3.9.1.1. Comparison at the dimensionless times 10^5 and 10^6

In the previous sections (section 3.8) the efficiency of the developed formula has been evaluated at two dimensionless times (T) 10^5 and 10^6 . Therefore the efficiency of the formula presented by Melville and Chiew will be checked at the same dimensionless times in order to be able to compare these two formulas.

To this aim, the tests with dimensionless times 10^5 and 10^6 are selected to be compared. Therefore, the efficiency of Melville and Chiew formula at dimensionless time 10^5 and 10^6 will be investigated in the following.

- **T=10⁵**

After selection of the tests which are fitting the test selection criteria, due to plot the measured dimensionless scour depth D_s vs. the computed one at $T=10^5$, firstly, the tests within the range $10^5/K \leq T \leq 10^5 \times K$ (K assumed to be equal to 3) are chosen. Then the value of D_s is computed for each of these dimensionless times according to Melville's formula. Finally, the measured and computed values are plotted as shown in figure 3.30.

In case there is more than one dimensionless time in the mentioned range, the one which has the lowest relative error to 10^5 is selected.

The PDF and CDF of the ratio measured/calculated D_s are also plotted in figure 3.31 and 3.32.

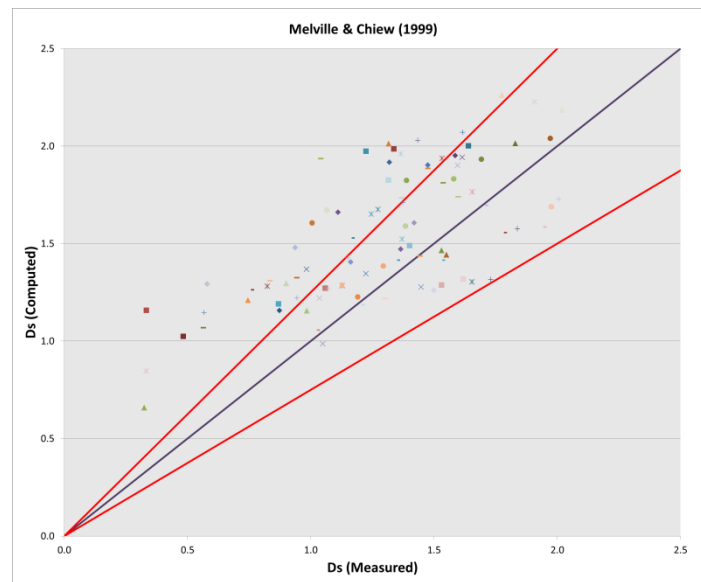


Figure 3.30: Measured vs. Computed value of D_s using Melville & Chiew formula at $T=10^5$

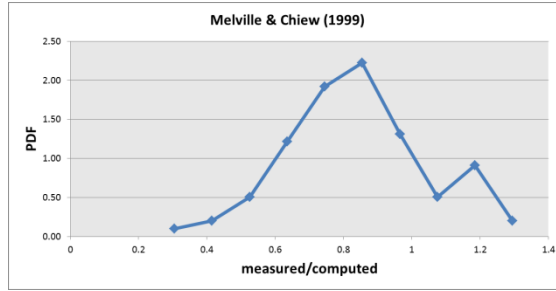


Figure 3.31: PDF of Melville & Chiew formula at T=10⁵

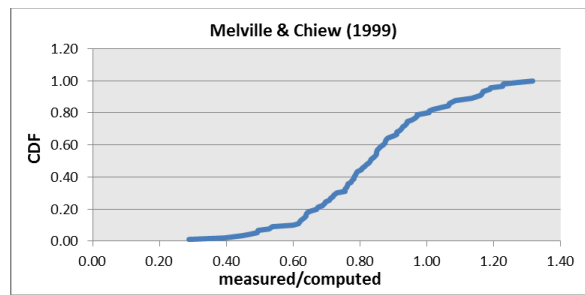


Figure 3.32: CDF of Melville & Chiew formula at T=10⁵

- **T=10⁶**

The same as previous case the tests are selected and among the selected tests the dimensionless times within the range $10^6/K \leq T \leq 10^6 \times K$ (K assumed to be equal to 3) are plotted in figure 3.33.

In case there is more than one dimensionless time in the mentioned range, the one which has the lowest relative error to 10⁶ is selected.

Moreover the Pdf and CDF at T=10⁶ is computed as presented in figure 3.34 and 3.35.

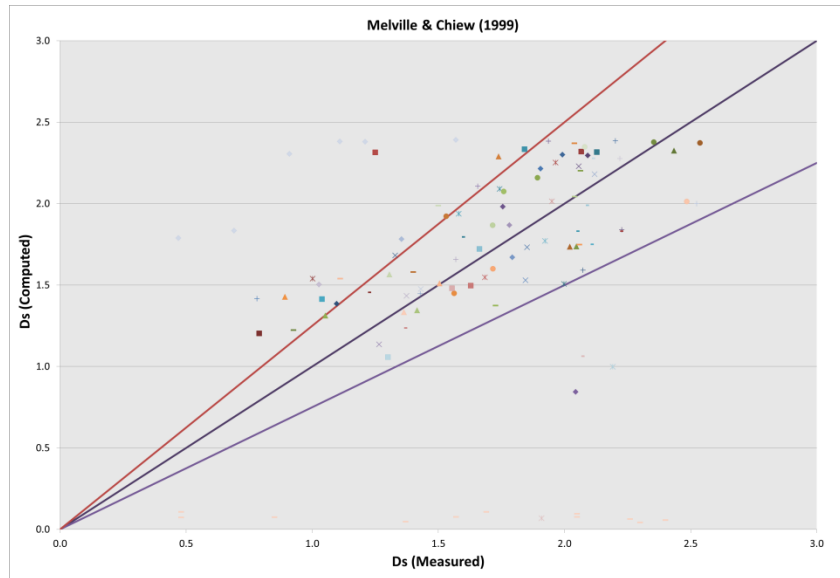


Figure 3.33: Measured vs. Computed value of D_s using Melville & Chiew formula at $T=10^6$

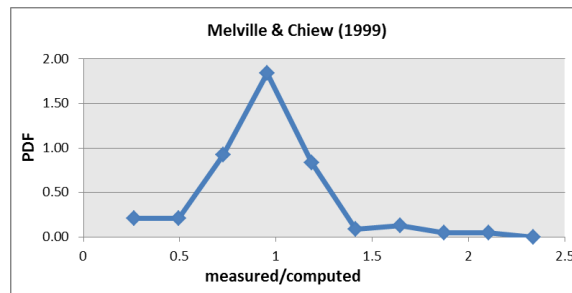


Figure 3.34: PDF of Melville & Chiew formula at $T=10^6$

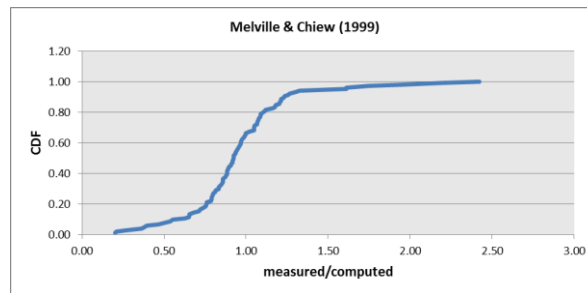


Figure 3.35: CDF of Melville & Chiew formula at $T=10^6$

3.9.1.2. Comparison at the dimensionless scour depth -4 and -1

As can be seen in figure 3.29 according to the formula presented by Melville and Chiew the horizontal axis contains the ratio between the scour depth and the equilibrium scour

depth. The values presented by this formula are in a range of -12 to 8. On the other hand, in the previous sections (section 3.8) the efficiency of the developed formula has been evaluated at two dimensionless times 10^5 and 10^6 . Therefore the efficiency of the formula presented by Melville and Chiew will be checked at the same dimensionless times.

Having compared the plot of figure 3.29 and 3.21, it is realized that the dimensionless time 10^5 in the figure 3.21 is more or less equivalent to -4 in the figure 3.29. Similarly, the dimensionless time 10^6 in the figure 3.21 is more or less equivalent to -1 in figure 3.29. Therefore, the efficiency of Melville and Chiew formula at -4 and -1 will be investigated in the following.

- **ds/dse= -4**

The same as previous case the tests are selected and among them the tests within the range $(-4 - a) < \left(\frac{u_c}{u} \ln\left(\frac{t}{t_c}\right)\right) < (-4 + a)$ are plotted in figure 3.36 (a assumed to be equal to 0.5). Moreover the Pdf and CDF at ds/dse = -4 are computed as presented in figure 3.37 and 3.38.

In case there is more than one point in the mentioned range, the one which has the lowest relative error with respect to -4 is selected.

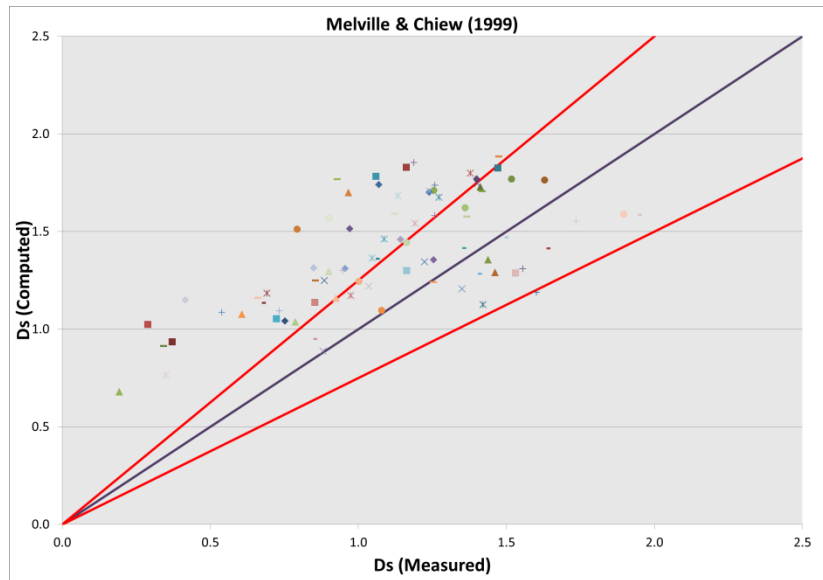


Figure 3.36: Measured vs. Computed value of Ds using Melville & Chiew formula at ds/dse= -4

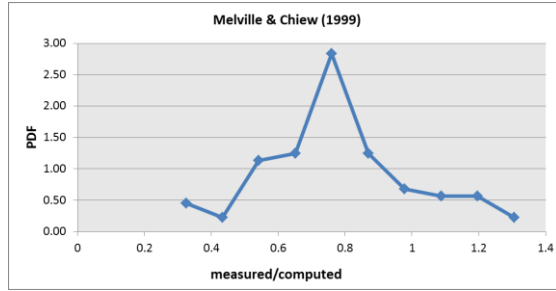


Figure 3.37: PDF of Melville & Chiew formula at ds/dse= -4

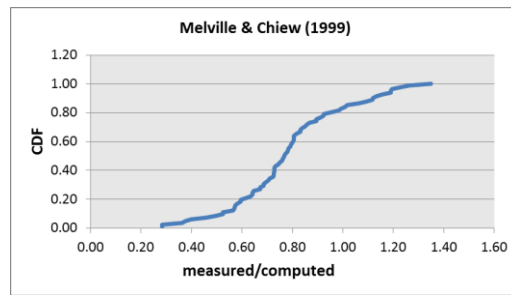


Figure 3.38: CDF of Melville & Chiew formula at ds/dse= -4

- **ds/dse= -1**

The same as previous case the tests are selected and among the selected tests the dimensionless times within the range $(-1 - a) < \left(\frac{u_c}{u} \ln\left(\frac{t}{t_0}\right)\right) < (-1 + a)$ are plotted in figure 3.39 (a assumed to be equal to 0.5).

In case there is more than one point in the mentioned range, the one which has the lowest relative error with respect to -1 is selected.

Moreover the Pdf and CDF at ds/dse = -1 are computed as presented in figure 3.40 and 3.41.

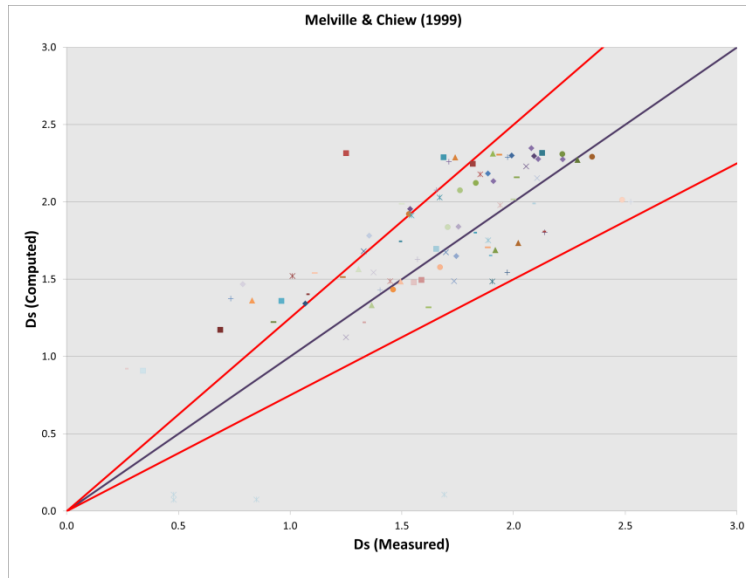


Figure 3.39: Measured vs. Computed value of D_s using Melville & Chiew formula at $ds/dse = -1$

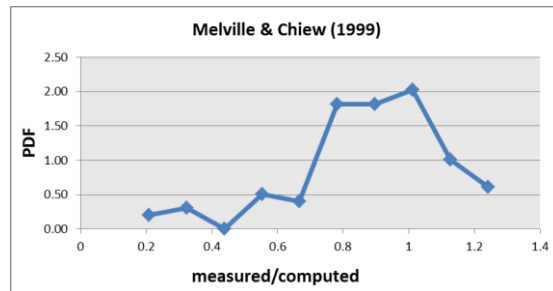


Figure 3.40: PDF of Melville & Chiew formula at $ds/dse = -1$

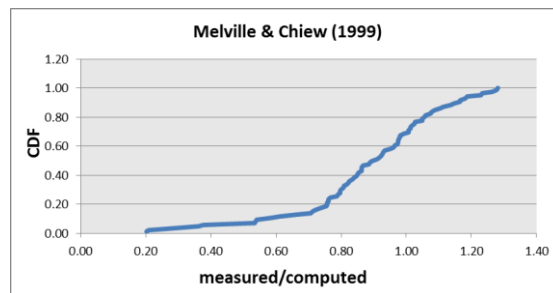


Figure 3.41: CDF of Melville & Chiew formula at $ds/dse = -1$

This model is capable to evaluate the value of D_s at $T=10^6$ with relatively low error with respect to its measured value. On the other hand, this model does not show enough accuracy for

evaluation of D_s at lower values of dimensionless time. At $T=10^5$ the relative error greater than 25% of the corresponding measured values of D_s is increasing as can be seen.

3.9.2. Oliveto and Hager (2002)

Using similarity arguments and the analogy to flow resistance, an equation for temporal scour evolution is proposed by Oliveto and Hager (2002) in the following form:

$$D_s = 0.068 N \sigma^{-0.5} Fr^{1.5} \log(T) \quad (3.22)$$

Where:

N =shape number and is equal to 1 for circular pier;

Fr = Froude number= $u/(g'd_{50})^{1/2}$;

g' = Reduced gravitational acceleration= $g \cdot \Delta$;

$T_{oliveto}$ =dimensionless time= $\{(g'd_{50})^{1/2}/L_R\} t$;

L_R =Reference length= $b^{2/3} h^{1/3}$;

t = Time;

b = Pier width; and

h = Upstream flow depth.

In this model the temporal scour evolution depends on three main parameters, namely:

1. Reference length $b^{2/3} h^{1/3}$ for pier;
2. Densimetric mixture Froude number $\sigma^{-0.5} u/(g'd_{50})^{1/2}$; and
3. Relative time T involving geometry and sediment characteristics.

In order to compare the Oliveto & Hager formula with the one which is developed in this study, first of all, the criteria of selection of the suitable isolated points and series which is mentioned before (section 3.3.2) are applied to all the valid data. In addition, only the tests with rigorously fully turbulent flow are considered. Then, the selected data are inserted to the plot of figure 3.42 in which the axis are the one proposed by Oliveto & Hager.

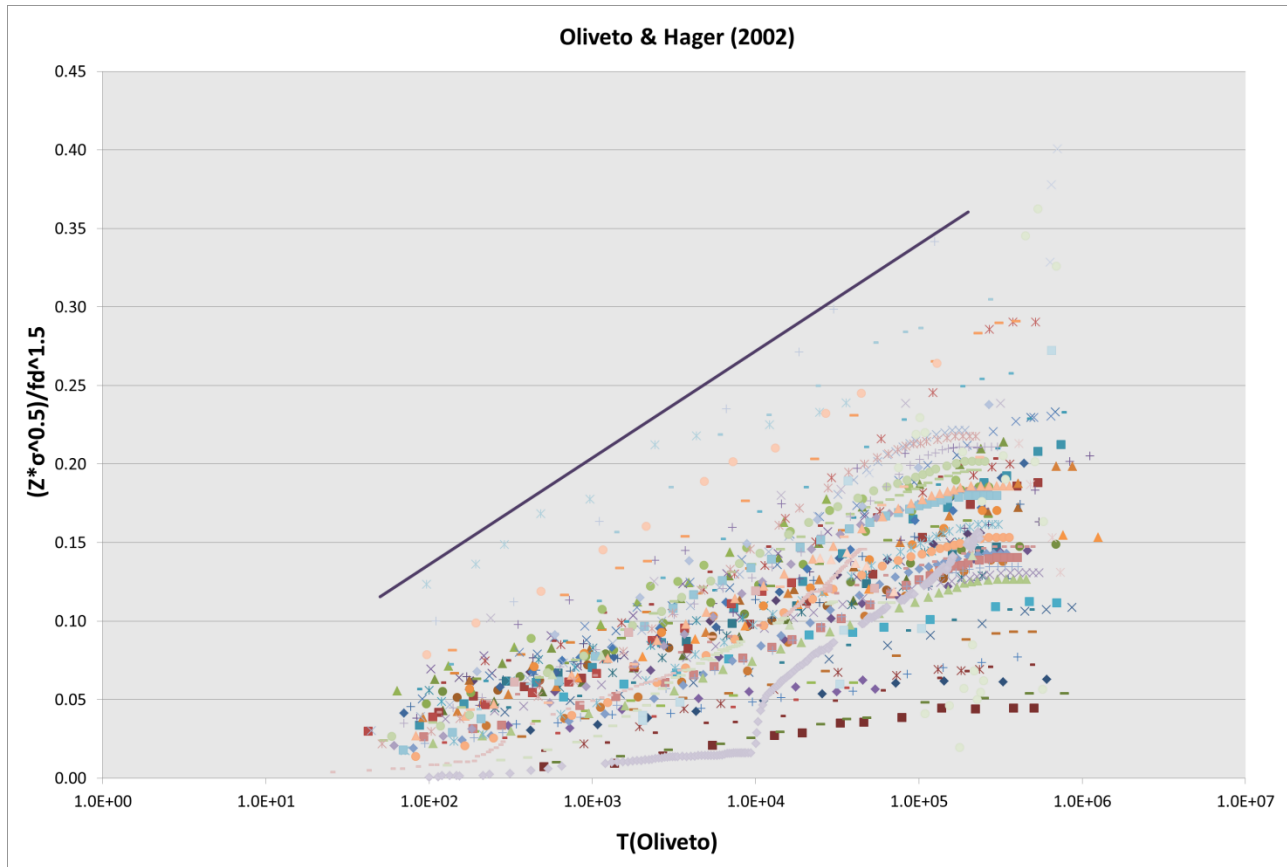


Figure 3.42: Oliveto and Hager formula

3.9.2.1. Comparison at the dimensionless times 10^5 and 10^6

In the previous sections (section 3.8) the efficiency of the developed formula has been evaluated at two dimensionless times (T) 10^5 and 10^6 . Therefore the efficiency of the formula presented by Oliveto & Hager will be checked at the same dimensionless times in order to be able to compare these two formulas.

To this aim, the tests with dimensionless times 10^5 and 10^6 are selected to be compared. Therefore, the efficiency of Oliveto & Hager formula at dimensionless time 10^5 and 10^6 will be investigated in the following.

- **$T = 10^5$**

The values of scour depth at dimensionless times 10^5 are computed by means of Eq.3.22 for all of the valid experiments.

After the selection of the tests which are fitting the test selection criteria, due to plot the measured dimensionless scour depth D_s vs. the computed one at $T=10^5$, firstly, the tests within the range $10^5/K \leq T \leq 10^5 \times K$ (K assumed to be equal to 3) are chosen. Then, the value of D_s is computed for each of these dimensionless times according to Oliveto & Hager formula. Finally, the measured and computed values are plotted as shown in figure 3.43.

In case there is more than one dimensionless time in the mentioned range, the one which has the lowest relative error to 10^5 is selected.

The PDF and CDF of the ratio measured/calculated D_s are also plotted in figure 3.44 and 3.45.

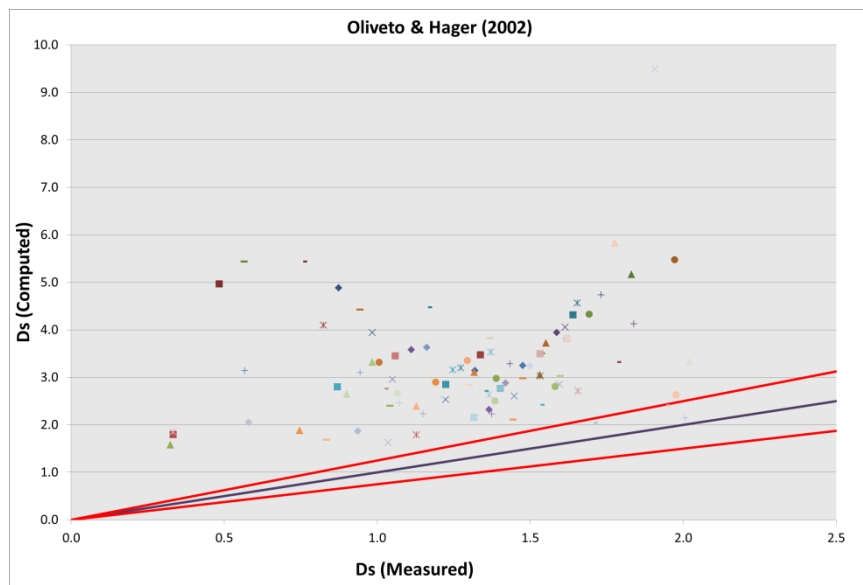


Figure 3.43: Measured vs. Computed value of D_s using Oliveto & Hager formula at $T=10^5$

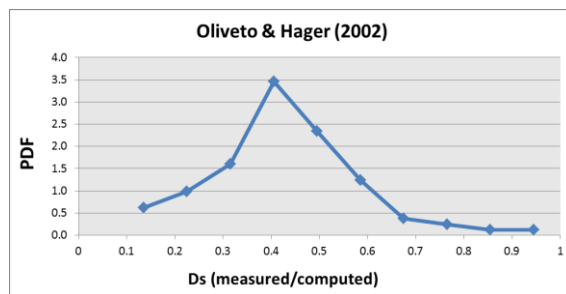


Figure 3.44: PDF of Oliveto & Hager formula at $T=10^5$

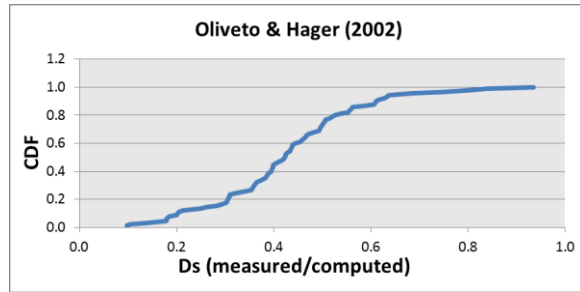


Figure 3.45: CDF of Oliveto & Hager formula at $T=10^5$

- **$T=10^6$**

The same as previous case the tests are selected and among the selected tests the dimensionless times within the range $10^6/K \leq T \leq 10^6 \times K$ (K assumed to be equal to 3) are plotted in figure 3.46.

In case there is more than one dimensionless time in the mentioned range, the one which has the lowest relative error to 10^6 is selected.

Moreover the Pdf and CDF at $T=10^6$ is computed as presented in figure 3.47 and 3.48.

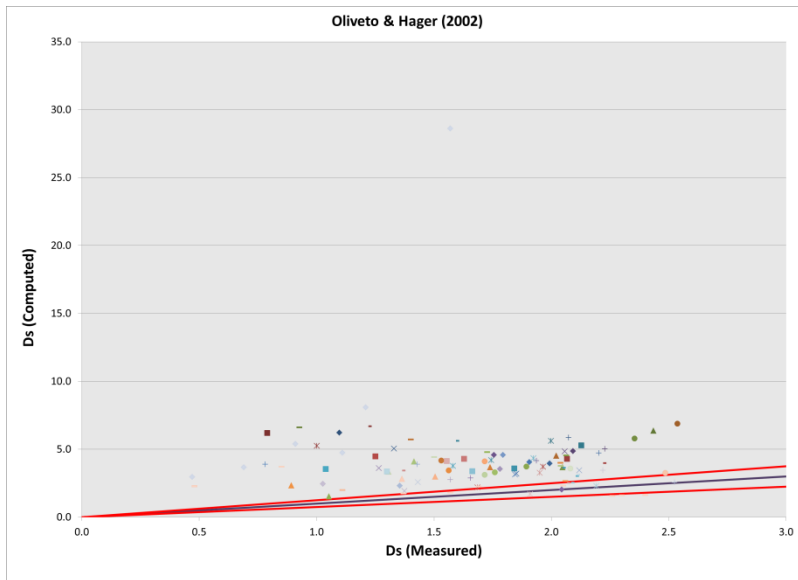


Figure 3.46: Measured vs. Computed value of D_s using Oliveto & Hager formula at $T=10^6$

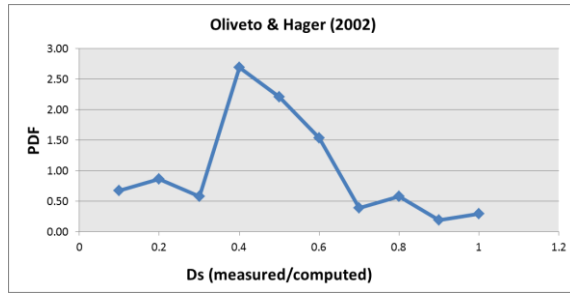


Figure 3.47: PDF of Oliveto & Hager formula at T=10⁶

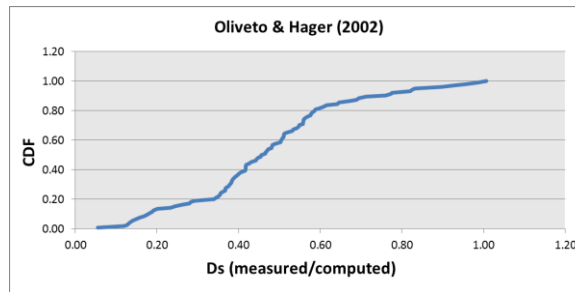


Figure 3.48: CDF of Oliveto & Hager formula at T=10⁶

In conclusion, the proposed formula is not able to produce accurate result in compare to the Melville & Chiew (1999).

Conclusion

Despite big research efforts in recent decades, predictive capabilities for local scour at bridge piers are still not fully satisfactory and formulae proposed by some authors may fail in representing data from others. Therefore, this thesis has been oriented to a comprehensive analysis of literature data for clear-water scour at cylindrical piers in uniform sand beds, in an attempt to calibrate a formula that could perform better than existing ones. A relatively large amount of local scour data has been used for the purpose of the analysis. Laboratory data are derived from experiments that were well documented by the authors. Suitable criteria were used for selection of appropriate tests among all the available experimental results.

The dimensionless framework proved to be beneficial for the evaluation of temporal scour trend and an accurate prediction of scour depth could be obtained. According to the comparison between the proposed equation and some others available in literature it is shown that the proposed formula is able to provide more accurate estimation of the scour depth compared to the mentioned literature ones.

Recommendations for further research

This thesis project has thrown up more questions in need of further investigation. Thus, it is recommended that further research be undertaken in the following areas:

- Considering the isolated points to develop the scour formula. (Although the isolated points are presented in the plots in this study, they are not considered for developing the final equation to predict the scour trend.)
- Quantify the effect of narrowing the ranges of h/b , L_c , σ , d_{50} and T to investigate the results of accepting the values out of the chosen ranges.
- Study the effects of velocity. For example doing the same procedure by using the velocity presented by the author instead of the converted velocities.
- Comparing the results to more existing formula and taking into account the tests in slightly transitional condition.
- Another possible area of future research would be to investigate the effect of flow shallowness (H) on the scour depth evolution. This task needs a wider range of database that includes tests with also flow shallowness less than 2.

References

1. Chabert, J., and Engeldinger, P. (1956), "Etude des affouillements autour des piles des ponts," Laboratoire National d'Hydraulique, Chatou, France.
2. Chang, W.Y, Lai J., S., and Yen C., L. (2004), "Evolution of Scour Depth at Circular Bridge Piers" *J. Hydraul. Eng.*, 130(9), 905-913.
3. Chiew, Y. M. (1995), "Mechanics of Riprap Failure at Bridge Piers", *ASCE Journal of Hydraulic Engineering*, 121(9), 635-643
4. Dey et al. (1999) "Time Variation of Scour in The Vicinity of Circular Piers". *Water Maritime and Energy*, Volume 136, Issue 2, p. 67 –75
5. Dey, S., Bose, S. K., and Sastry, G. L. N. (1995), "Clear Water Scour at Circular Piers", *J. Hydraul. Eng.*, 121(12), 869-876.
6. Ettema, R. (1980). "Scour at bridge piers." Rep. No.216, Scholl of Engrg, University of Auckland, Auckland, New Zealand.
7. Franzetti, S., Larcan, E., and Migonsa, P. (1982), "Influence of Tests Duration on The Evaluation of Ultimate Scour Around Circular Piers", *International conference on Hydraul Modeling of Civil engineering Structure*, Coventry, England , pp. 381-396.
8. Franzetti, S., Larcan, E. and Mignosa P. (1989), "Erosione alla Base di Pile Circolari di Ponte: Verifica Sperimentale di Esistenza di Una Situazione Finale di Equilibrio", *Estratto da idrotecnica*, n. 3 maggio-giugno. Italy.
9. Franzetti, S., Malavasi, S., Piccinin, C. (1994), "Sull'Erosione alla Base delle Pile Di Ponte in Acque Chiare", *XXIV Convegno di Idraulica e Costruzioni Idrauliche*. Napoli, p. 1-13
10. Hager, W. H., Oliveto, G. (2002), "Shields' Entrainment Criterion in Bridge Hydraulics", *Journal of Hydraulic Engineering* 128(5): 538-542.
11. *Hydraulics & Marine Studies* (2013), "Bridge Scour Manual", Queensland, Canada.
12. Lanca, M. R. et al (2013), "Clear-Water Scour at Comparatively Large Cylindrical Piers". *J. Hydraul Eng.*, 139(11), 1117-1125.
13. Melville, B. (1997), "Pier and Abutment Scour: Integrated Approach", *J. Hydraul Eng.*, 123(2), 125-136.
14. Melville, B. W., Coleman, S. E. (2000), "Bridge Scour", *Water Resources Publication*
15. Melville, B., and Chiew, Y. M. (1987), "Local Scour around Bridge Piers", *J. Hydraulic Research*, 125(1), 59-65.

16. Melville, B., and Chiew, Y. M. (1999), "Time Scale for Local Scour at Bridge Piers", *J. Hydraul Eng.*, 125(1), 59-65.
17. Mignosa, P. (1980), "Fenomeni di Erosione Locale alla Base delle Pile del Ponti", Tesi di Laura, Department of hydraulic and Hydraulic structure, Politecnico di Milano. Milan, Italy.
18. National Highway institute (2001), "Evaluating Scour At bridge", Fourth Edition, *Hyd. Eng. Circular No.18*, Publication No. FHWA NHI 01-001, USA.
19. Oliveto, G., and Hager, W. H. (2002), "Temporal Evolution of Clear-Water Pier and Abutment Scour", *J. Hydraul Eng.*, 128(9), 811-820.
20. Raikar, R. V., and Dey, S. (2005), "Clear-water Scour at Bridge Piers in Fine and Medium Gravel Beds" *Canadian Journal of Civil Engineering*, 32 (4), 775-781,
21. Sheppard, D. M, et al (2011) "Scour At Wide Piers and Long Skewed Piers", NCHRP, Report 682
22. Sheppard, D. M. (2003), "Large Scale and Live Bed Local Pier Scour Experiments, Phase 2, Live Bed Experiments", Florida Department of Transportation.
23. Sheppard, D. M., Odeh, M., and Glasser, T. (2004), "Large Scale Clearwater Local Pier Scour Experiment", *J. Hydraul Eng.*, 130(10), 957-963.
24. Sheppard, D., Melville, B., and Demir, H. (2014), "Evaluation of Existing Equations for Local Scour at bridge Pies", *J. Hydraul Eng.*, 140(1), 14-23.
25. Yanmaz, A. M., and Altinbilek H. D. (1991), "Study of Time-Dependent Local Scour around Bridge Piers" *J. Hydraul. Eng.*, 117(10), 1247-1268.